

***IN SILICO* MODELLING OF COMPLEX BIOLOGICAL PROCESSES**

***IN SILICO* MODELLING OF COMPLEX BIOLOGICAL PROCESSES WITH
APPLICATIONS TO ALLERGIC ASTHMA AND CANCER**

By

MARC COLANGELO, B.H.Sc.

A Thesis

Submitted to the School of Graduate Studies

In Partial Fulfilment of the Requirements

For the Degree

Doctor of Philosophy

McMaster University

© Copyright by Marc Colangelo, July 2011

DOCTOR OF PHILOSOPHY (2011)
(Medical Sciences)

McMaster University
Hamilton, Ontario

TITLE: *In Silico* Modelling of Complex Biological Processes
with Applications to Allergic Asthma and Cancer

AUTHOR: Marc Colangelo, B.H.Sc. (McMaster University)

SUPERVISOR: Dr. Manel Jordana

NUMBER OF PAGES: xiii, 161

ABSTRACT

Regardless of their origin or pathology, many, if not all, diseases have long been regarded as complex. Yet, despite the progression in the understanding of complexity and the development of systems biology, the majority of biomedical research has been derived from qualitative principles. In comparison to the ethical, temporal and logistical limitations of human experimentation, *in vivo* animal models have served to provide a more advantageous means to elucidate the underlying disease mechanisms. However, given the additional limitations presented by such models, *in silico* models have emerged as an effective complement, and, in some cases, a replacement for *in vivo* experimentation. The *in silico* models presented in this thesis were developed using mathematical and computational methods to investigate the evolution of two complex, diverse diseases from a systems biology perspective: allergic asthma and cancer.

We generated two novel *in silico* models of allergic asthma aimed at clarifying some dynamic aspects of allergic responses. Experimentally, we utilized an *in vivo* murine model of chronic exposure to the most pervasive aeroallergen worldwide, house dust mite (HDM), for up to 20 weeks, equivalent to at least 20 human years. Using a range of HDM concentrations, experimental data were collected to study local and systemic effects. The first model applied empirical mathematical techniques to establish equations for airway inflammation and HDM-specific immunoglobulins using an iterative approach of

experimentation and validation. Using the equations generated, we showed that the model was able to accurately predict and simulate data. The model also demonstrated the non-linear relationship between HDM exposure and both airway inflammation and allergic sensitization and identified system thresholds.

The second model used mechanistic mathematical techniques to investigate the trafficking of eosinophils as they migrated from bone marrow to the blood and, ultimately, to the lungs. Making use of a limited data set, the model determined the effect of individual processes on the system. We identified eosinophil production, survival and death as having the greatest impacts, while migration played a relatively minor role. Furthermore, the model was used to simulate knockout models and the use of antibodies *in silico*.

In the context of cancer growth and metastasis, we developed a theoretical model demonstrating the spatio-temporal development of a tumour in two-dimensions. The model was encoded to create a computer graphic simulation program, which simulated the effects of various parameters on the size and shape of a tumour. Through simulations, we demonstrated the importance of the diffusion process in cancer growth and metastasis.

Ultimately, we believe the greatest benefit of each *in silico* model is the ability to provide an understanding of each respective disease recognized as dynamic and formally complex, but predominantly studied in reductionist, static or un-integrated approaches.

ACKNOWLEDGEMENTS

Having spent my entire academic career immersed in a collaborative environment, I have been mentored and guided by several influential individuals. This thesis is the culmination of their support, efforts and contributions to my research, to which I must humbly extend my utmost gratitude and appreciation.

To my supervisor, Dr. Manel Jordana, simply put, thank you for everything. You have provided me with invaluable advice and clarity through not only research, but all facets of life. You have been a mentor, a teacher and a friend, and have always had the intuition to know which role is needed when.

To my supervisory committee members, Dr. Miroslav Lovric, Dr. Jonathon Stone and Dr. Delsworth Harnish, thank you for your guidance in shaping me educationally, professionally, and personally.

To all my current and former laboratory colleagues in the Jordana, Stone and Stämpfli labs, thank you all for your input and contributions to my work, and most of all, your support throughout our time together.

To all my colleagues in the Bachelor of Health Sciences (Honours) Program, thank you all for your friendship and support.

To my mom and dad, my sister, and my wife, thank you all for your continuous and unconditional help, patience, love and encouragement. I would not be who I am or where I am without all of you.

TABLE OF CONTENTS

PRELIMINARIES	ii
Abstract	iii
List of Figures and Tables	ix
List of Abbreviations	xi
Declaration of Academic Achievement	xii
CHAPTER 1: Introduction	1
Modelling	4
Biomedical Modelling	5
Mathematical Modelling	6
Context	9
Allergic Asthma	9
From an Immunological Perspective	9
From a Mathematical Perspective	11
Cancer Growth and Metastasis	13
From a Biological Perspective	13
From a Mathematical Perspective	15
Objectives	17
CHAPTER 2: <i>In Vivo</i>-to-<i>In Silico</i> Iterations to Investigate Aeroallergen-Host Interactions	20
Abstract	21
Introduction	21
Methods	22
Results	22
Discussion	28
References	29
Supporting Information	31

CHAPTER 3:	Modelling of House Dust Mite-Induced Chronic Airway Eosinophilia	43
	Abstract	45
	Background	47
	Results & Discussion	50
	Conclusions	60
	Methods	62
	References	68
	Tables and Figures	73
	Additional File	82
CHAPTER 4:	A Mathematical and Computational Model for Simulating Complex Dynamic Cancer Growth and Metastasis	84
	Abstract	86
	Introduction	88
	The Model	92
	Results	98
	Discussion	102
	References	107
	Tables and Figures	110
CHAPTER 5:	Discussion	114
	What did Modelling Reveal?	115
	Future Directions of the Models	119
	House Dust Mite Models	121
	HDM Exposure Model	121
	Eosinophil Trafficking Model	124
	Applicability and Implications	125
	Cancer Model	129
	Applicability and Implications	131
	Concluding Remarks	139

REFERENCES:	(For Chapters 1 and 5)	142
APPENDIX I:	Permission to Reprint Published Materials	157

LIST OF FIGURES AND TABLES

CHAPTER 2

Figure 1	<i>Airway inflammation and systemic immunity in BALB/C mice exposed to HDM for 10 consecutive days.</i>	23
Figure 2	<i>Airway inflammation in BALB/C mice exposed to HDM and subsequent mathematical modelling.</i>	24
Figure 3	<i>2D and 3D models for total cells generated from mathematical equations.</i>	25
Figure 4	<i>Nature of the inflammatory response in mice exposed to HDM and mathematical modelling of eosinophils.</i>	26
Figure 5	<i>Systemic responses in HDM-exposed mice, subsequent mathematical modelling and comparison between inflammation and sensitization.</i>	27
Figure 6	<i>Physiological and structural lung changes in mice exposed to different doses of HDM.</i>	28
Figure S1	<i>Iterations to validate the mathematical model for the inflammatory response.</i>	32

CHAPTER 3

Table 1	<i>List of model rate parameters.</i>	73
Figure 1	<i>Simplified visual model of eosinophil trafficking among compartments.</i>	77
Figure 2	<i>Eosinophil experimental data in BALB/c mice exposed to HDM for up to 14 weeks.</i>	77
Figure 3	<i>Dose- and time-response dynamics of rate processes involved in eosinophil trafficking.</i>	78
Figure 4	<i>Mathematical model simulations over 14 weeks of exposure to saline, 1, 5, and 25 μg of HDM.</i>	79
Figure 5	<i>Relative effects of individual model parameters on eosinophils in the lung at 25 μg of HDM.</i>	80
Figure 6	<i>Sensitivity of individual model parameters on eosinophils in the lung at 25 μg of HDM.</i>	81

CHAPTER 4

Table 1	<i>Default parameter values used for baseline simulations.</i>	110
Figure 1	<i>Potential directions for cancer cell diffusion in two-dimensional space.</i>	110
Figure 2	<i>Various methods used in the cancer cell diffusion process.</i>	110
Figure 3	<i>Simulated tumour growth over time.</i>	111
Figure 4	<i>Effects of variation in model parameters on tumour growth.</i>	111
Figure 5	<i>Simulated tumour growth over time with varying seed sizes.</i>	112
Figure 6	<i>Simulated tumour growth over time for deterministic, mixed and pseudorandom algorithms.</i>	112
Figure 7	<i>Simulated cancer cell distribution von Neumann and Moore neighbourhoods.</i>	113

CHAPTER 5

Figure 1	<i>A graphical representation of iron diffusion.</i>	132
Figure 2	<i>A simple model of angiogenesis.</i>	135
Figure 3	<i>The major variables and processes in an expanded cancer model.</i>	138
Figure 4	<i>Conceptual similarities between allergic asthma and tumour growth.</i>	140

LIST OF ABBREVIATIONS

BIOLOGICAL ABBREVIATIONS		MATHEMATICAL ABBREVIATIONS	
<i>Ab</i>	antibody	<i>B</i>	blood eosinophils
<i>AHR</i>	airway hyperresponsiveness	<i>BM</i>	bone marrow eosinophils
<i>APC</i>	antigen-presenting cell	<i>D</i>	disease
<i>BAL</i>	bronchoalveolar lavage	<i>dX/dt</i>	differentiation of variable X with respect to time, t
<i>CD</i>	cluster of differentiation	<i>E</i>	exposure (dose of HDM)
<i>CGF</i>	chemotactic growth factor	<i>EOS</i>	eosinophils
<i>DNA</i>	deoxyribonucleic acid	<i>f</i> or <i>f_x</i>	unknown mathematical function
<i>GM-CSF</i>	granulocyte-macrophage colony-stimulating factor	<i>F</i>	lung function or dysfunction
<i>HDM</i>	house dust mite	<i>I</i>	inflammation
<i>Ig</i>	immunoglobulin	<i>L</i>	lung (airway) eosinophils
<i>IL</i>	interleukin	<i>LISA</i>	local interaction simulation approach
<i>i.n.</i>	intranasal	<i>MNC</i>	mononuclear cells
<i>KO</i>	knock-out	<i>N</i>	nutrient
<i>MOI</i>	multiplicity of infection	<i>NT</i>	neutrophils
<i>OVA</i>	ovalbumin	<i>R</i>	airway remodelling
<i>PBS</i>	phosphate-buffered saline	<i>R²</i>	linear regression
<i>RNA</i>	ribonucleic acid	<i>S</i>	sensitization
<i>TCN</i>	total cell number	<i>t</i> or <i>T</i>	time
<i>TAF</i>	tumour angiogenic factor	<i>w</i> or <i>wk</i>	week(s)
<i>Th</i>	T helper		

DECLARATION OF ACADEMIC ACHIEVEMENT

In accordance with the *Guide for the Preparation of Theses at McMaster University*, the research documented herein is presented as a “Sandwich” Thesis, including both previously published and prepared material. The articles presented in Chapters 2, 3, and 4 are three independent manuscripts that are connected by the overall theme of this thesis, mathematical and computational modelling of complex biological processes. Given that the manuscripts presented in this thesis are multiply authored, my contributions as first author or co-first author for each have been highlighted below. As of June 2011, each manuscript has been published by or submitted to a peer-reviewed journal.

CHAPTER 2 Llop-Guevara, A.* , Colangelo, M.* , Chu, D.K., Moore, C.L., Stieber, N.A., Walker, T.D., Goncharova, S., Coyle, A.J., Lundblad, L.K.A., O’Byrne, Lovric, M. and Jordana, M. *In Vivo-to-In Silico* Iterations to Investigate Aeroallergen-Host Interactions. *PLoS ONE* **3**(6): e2426, 2008.

This work was conducted over the period of June 2006 – April 2008.

My contributions to this work included:

- Equal responsibility with AL-G for the design, development, analysis and interpretation of all experiments
- Primary responsibility for design and development of the mathematical model (along with AL-G)
- Sole responsibility for the execution of *in silico* simulations
- Equal responsibility with AL-G for the writing, preparation and submission of the manuscript
- Equal responsibility with AL-G for responding to comments from peer-reviewers (along with MJ)

CHAPTER 3 Colangelo, M., Llop-Guevara, A., Fattouh, R., Walker T.D.,
Goncharova, S., Lovric, M. and M. Jordana. Modelling of
House Dust Mite-Induced Chronic Airway Eosinophilia.
Submitted June 2011 to *Biology Direct*. (Submission #
1429158914566452)

This work was conducted over the period of June 2008 – June 2011.

My contributions to this work included:

- Sole responsibility for the design, development, analysis and interpretation of the model
- Sole responsibility for the execution and analysis of bone marrow extraction
- Equal responsibility with AL-G for the execution and analysis of all other *in vivo* experiments (with technical assistance from RF, TDW and SG)
- Sole responsibility for the execution of *in silico* simulations
- Sole responsibility for the writing, preparation and submission of the manuscript (with assistance from ML and MJ)

CHAPTER 4 Colangelo, M., Lovric, M. and J. Stone. A Mathematical and
Computational Model for Simulating Complex Dynamic
Cancer Growth and Metastasis. Accepted for publication
June 2011 in *The International Journal of Computers and
Their Applications*. (Submission #6077)

This work was conducted over the period of September 2005 – June 2006 and
July 2010 – December 2010.

My contributions to this work included:

- Sole responsibility for the design, development, analysis and interpretation of the model
- Sole responsibility for the execution of *in silico* simulations
- Sole responsibility for the writing, preparation and submission of the manuscript (with assistance from ML and JS)

CHAPTER 1

INTRODUCTION

CHAPTER 1

INTRODUCTION

In all areas of scientific research, the development of novel tools and techniques is driven by necessity; the necessity to discover new knowledge, and to do so in a manner that is more effortless, time-efficient, and cost-effective. These methods, whether original or adapted from existing methods, provide an avenue to further our current understanding and acquire information. *Information*, in a biological context, is considered to have an inherent, linear hierarchy, ranging from DNA and RNA, to cellular and tissue networks, to individuals and populations [1]. Biological *processes* within each level of this hierarchy, however, are not linear, nor are they hierarchical. In biological processes, causes and effects are not always proportionate [2]. Rather, biological processes are complex. Collectively, they can be considered as complex systems [3-6].

The field of systems biology seeks to understand observed biological phenomena through the net interactions occurring in a system, as opposed to those exhibited by its components [7]. By definition, a system consists of a series of elements or parts that interact with one another, all of which possess their own individual, diverse behaviours [4]. Based upon the manner of these interactions, systems can be further characterized based on their level of abstractness, linearity and complexity [8]. Through systems biology, this understanding is approached by the study of a system's interactions and behaviours quantitatively

over time [9]. In this context, it has been suggested that the greatest challenge in this approach is not from a biological perspective, but rather from computational and organizational perspectives [7].

The concept of complexity can be both peculiar and intriguing. The description of a process as complex can take on the meaning of complicated [8]. In some instances, it can be used to insinuate difficulty [7]. In mathematical terms, it can refer to non-linearity or chaos [10]. Complex systems can encompass elements from each of these meanings. A particular subset of complex systems, termed complex adaptive systems, is capable of “learning” from experience over time, allowing for the system to modify and adjust to its environment in an advantageous manner. Examples of such systems include health care organizations [11], stock markets [12], education [13], stem cells [14], and the brain [15].

With respect to biological systems, complexity arises from the interactions among signals and processes, creating a network of relationships [4,8]. In order to understand a complex biological system as a whole, it must be systematically simplified through subsystems, which can be represented by *in vitro*, *in vivo*, or more recently, *in silico* models [3,5].

MODELLING

Given their complexity, biological systems cannot be modelled in their entirety. As such, models are used to create a simplification of what occurs in a system [7,16]. Furthermore, models provide a contrivance through which hypotheses can be tested and predictions can be made and validated [17]. In a simple, non-biological context, consider a model train. The model in this case is a scaled down version of the actual representation. Although each individual detail is not captured in the modelled version, the essential components to make the model recognizable and functional are included, such as the shape of the train, the tracks, the cars, the sounds and the motion. The number, importance and accuracy of the components included (i.e. variables) are directly related to the goals of the model. In this instance, the goal is to create a smaller, aesthetic version of a train that is able to travel on a set of tracks.

When modelling a complex system, it becomes difficult to determine what factors are important, and their relative effects on the overall system. If each individual aspect of a system were to be included in a model, then, inherently the purpose of the model would be defeated. This is counteracted by the objective of trying to make the model as realistic as possible. As eloquently stated previously by a former colleague, "*The information an animal model of asthma can provide is therefore very much a reflection of its design, which itself is a reflection of both the research motive and the biological/immunological assumptions that inform it*"

[18]. These same simple principles may be applied to both biomedical and mathematical modelling. Although they share the goals of creating smaller, functional versions of a larger system while maintaining the general properties and important features, they differ in their approach and purposes for research. Deciphering the important features and identifying the desired outcomes dictates the degree of discrepancy and creative freedom these models contain. The information elicited by an *in silico* model is a reflection of the type of model, the purpose of the model, and the underlying biological system in question.

BIOMEDICAL MODELLING

Understanding the origin, evolution and nature of many diseases has come principally through experimentation via *in vitro* and, notably, *in vivo* human and animal models. However, it seems important to recognize that conventional biomedical modelling differs greatly from modelling in other scientific domains such as physics, ecology and economics [4,19,20]. Indeed, biomedical models are designed with a pre-established goal in mind: to mimic a known phenotype. This literally dictates the logic of biomedical modelling such that a given set of variables is manipulated to fabricate a pre-defined outcome. Consequently, little or no attention is dedicated to the array of outcomes (biologic-clinical heterogeneity) that could have emerged from allowing such a set of variables to interact unrestrictedly. Moreover, conventional biomedical experimental approaches have been pervasively aimed at understanding the role of a single

cell, molecule or gene in a given process. To date, experimentation has produced fascinating results, but we have also learned that there are an overwhelming number of molecules that are pleiotropic and often redundant.

The outcome-driven approach has dictated the manner in which experimental models are developed. However, it is evident that an approach driven by the outcome itself is inherently limited in its ability to discover the underlying conditions to achieve such outcome. In fact, research predicated on this approach has taught us little about the nature of the interaction between variables in biomedical systems. More conceptually, we believe that it is important to assert that a good part of our current understanding of biomedical systems is largely teleological, i.e. derived from notions and theories without precise definitions. Understandably, this has influenced the modelling strategies to date: researchers attempt to model what they think is happening, or could happen, rather than what is actually happening.

MATHEMATICAL MODELLING

Using mathematics in biological and health related research is certainly not a new concept. Various biological phenomena, such as genetics and stem cells, have applied mathematics in order to help explain their respective biological premises [20,21]. The use of mathematics and computers in biomedical problems can help in identifying the relationships among different variables within a system. Once the relationships are apparent, models can be

created in order to hypothesize a seemingly infinite number of effects and changes in a system simply by changing parameter values that would otherwise be very difficult, if not impossible to alter in a clinical or lab setting [22,23]. Through simulations generated by these models, we can ultimately strive for a better comprehension of the systems in question and therefore target particular areas of further research with some understanding of what is likely to occur.

Mathematical models vary in their structure and possess many dichotomous properties, such as empirical vs. mechanistic, stochastic vs. deterministic, theoretical vs. experimental. Despite the framework of a mathematical model or the system it models, each model is constructed through a combination of these properties. Empirical models have an inherent simplicity about them. They tend to be based solely on data, which limits their predictive potential [24]. Mechanistic models are initiated using a variety of parameters that are distinct to that particular system in the form of confirmed generalizations, concepts, definitions, facts, and/or laws, and completed in combination with assumptions and hypotheses about the system [17]. As a result, mechanistic models have the ability to generate new knowledge and have better predictive potential [25]. Without the inclusion of any physical, biological, or psychological mechanism that is unique to a system, the process of empirically modelling dynamic systems is considered curve fitting [24].

Along these lines, models may be theoretical in nature, attempting to use general known concepts of a system. On the other hand, models can also be purely based on experimental data. Models can also range on a spectrum from stochastic to deterministic, with the extremes of being completely random or purely deterministic. When analyzing the simulated results from a mathematical model using a set of initial conditions, a stochastic model would return different results each time, whereas a deterministic model should always be the same [26]. The structure and type of model used to characterize a system is not specific to a particular field or discipline, but rather is determined by what is known about the system and the goals of the model.

Mathematics and computer code can be considered distinct languages that can be used to explain biological properties in a different context. Mathematical equations and computer simulations are tools that are used to translate these languages. *In silico* models consider complex biological systems from both mathematical and computational perspectives. The behaviours of the system are interpreted and often described using ordinary and partial differential equations, which are subsequently encoded computationally allowing for simulations or *in silico* experiments to be performed [16,27]. *In silico* models, ideally, should not be used in isolation, nor do they provide the complete story of a system. Rather, they are tools to take information and build upon *in vivo* and *in vitro* biomedical models. In doing so, *in silico* models can be used to explain biological properties in a different context.

CONTEXT

The biological and immunological concepts in this thesis represent two diverse biological systems, each modelled using different mathematical and computational approaches. The first system investigates allergic asthma, due to chronic aeroallergen exposure to HDM, focusing particularly on aspects of inflammation. The second system examines avascular cancer growth and metastasis in two dimensions, with a single nutrient source. Although each represents a complex system, the manner in which they are modelled is affected by the previous research of their respective biological and mathematical backgrounds, as well as the goals and purposes of the models themselves.

ALLERGIC ASTHMA

FROM AN IMMUNOLOGICAL PERSPECTIVE

During the last 30 years, there has been significant progress in understanding the immunological and molecular pathogenesis of allergic asthma. Despite the current level of knowledge, the prevalence of asthma has steadily increased throughout the same time period leading to over 100 million cases worldwide [28]. Recognition of allergic asthma as a complex disease, during this time, has also become apparent. Allergic asthma arises from the interaction between two complex systems, the immune system and the environment containing aeroallergens, both of which are heterogeneous in their own right.

Allergic asthma is a multifaceted disease characterized by chronic inflammation of the airways that is associated with a defined structural-functional phenotype. The chronic airway inflammation is manifested by reversible airway obstruction, infiltration of eosinophils and Th2 (T-helper type 2) cells into airway submucosa, airway hyperresponsiveness (AHR), airway remodelling, and mucus hypersecretion [29]. The immunological response in allergic asthma is a typical input-output biological system. Briefly, upon inhalation of an aeroallergen, antigen-presenting cells (APC) engulf the antigen, present it to naïve CD4⁺ T cells, which then differentiate into Th2 effector cells. The ensuing immune response is a hallmark characteristic of allergic asthma, characterized by the production of cytokines that contribute to manifestations of the allergic disease, principally IL-4, IL-5 and IL-13 [30]. These cytokines lead to the isotype switch to IgE (IL-4), the development of eosinophils (IL-5), and the hypersecretion of mucous (IL-13) [31,32]. The ensuing immune response is deemed excessive in relation to the insidiousness of the antigen, in that cytokines are produced in abundance [33]. The term “endotype” has been recently proposed to encompass differences in allergic asthma presentations in the clinical setting, which may not be explainable by one single mechanism alone, thus strengthening the notion of complexity of the disease [34]. The therapeutic approach for allergic asthma, perhaps due to the associated complexity, has largely concentrated on either non-specific (corticosteroids) and/or symptomatic (bronchodilators) treatments aimed at improving the management of the disease [35].

Despite the simplification of the system with respect to input-output, it would be naïve to consider these parameters in a singular sense. With a plethora of possible contributing factors and outcomes, biomedical models of allergic asthma simplify the system in order to establish the direct relationship of particular inputs with corresponding outputs.

FROM A MATHEMATICAL PERSPECTIVE

An understanding of allergic asthma as a complex disease brings to light the temporal, technical and ethical limitations of *in vivo* research. Indeed, there are many fundamental questions that can be addressed only in experimental systems, yet have been sacrificed through the use of static and punctual models. That is, many *in vivo* models tend to focus on particular time-points and allergen concentrations, as opposed to using a continuum to investigate temporal responses or a range of doses (inputs) [36-39]. As a result, the study of immunological systems using mathematical and computational models has been widely used in a variety of contexts, the focus ranging from genomics, to proteins, to cells, to tissues [40]. With the understanding that insight into the immunological mechanisms will drive disease-based therapy, the quantification of these mechanisms is fundamental to identifying the behavior of the system [41].

Historically, mathematical models have been used extensively in immunology (reviewed in [42]). As computational technology has advanced, the

sophistication, applicability and use of such models has increased [43-48]. While modelling the immune system [49], as well as specific areas of immunology, such as tumour-immune dynamics [50,51], virus-immune dynamics [52-54], immune-receptor signaling [55], and acute inflammation [49,56] have garnered much attention, mathematical analysis of allergic asthma has been explored to a much lesser extent. *In silico* modelling of allergic asthma and, particularly, chronic allergic inflammation, is considered to be best suited for studying the elements leading to chronic disease, testing the efficiency of drug therapies, the responses of cells, and the induction of disease, from a mathematical perspective using simulations (reviewed in [57,58]). In comparison to their *in vitro* and *in vivo* counterparts, *in silico* models have the ability to investigate a larger scope of these experimental aspects in a shorter period of time and with limited experimental data. Of particular note, Entelos Inc. developed a computer-based mathematical model, named Asthma PhysioLab™, as a means to emulate virtual patients with respect to airway structure, airway function, and inflammation [59,60]. Despite the presentation of simulation results using therapeutic interventions, there are no methodologies presented, thereby preventing the critical appraisal of their work. Similarly, although examples in the literature outline asthma as a complex dynamic system, they are not directly supported by a mathematical construct [61-63]. Models focused on allergic asthma using mathematical and/or computational techniques have been concentrated on a particular aspect of the disease, such as airway constriction [64], bronchial

hyperresponsiveness [65] or airway function [66]. No studies to date have focused on basic immune facets of the disease, such as eosinophil inflammation and allergic sensitization.

CANCER GROWTH AND METASTASIS

FROM A BIOLOGICAL PERSPECTIVE

Although different classes of cancer may arise from various instigating causes, they all share the distinguishing feature of the inability to regulate cell proliferation [67]. The evolution of a tumour can be attributed directly to the mutation of proto-oncogenes and tumour suppressor genes. When a proto-oncogene mutates, becoming an oncogene, the internal signalling of a cell deteriorates, primarily causing uncontrolled multiplication [67,68]. Likewise, inactivation of a tumour suppressor gene via mutation can lead to over-activated proliferation [69].

In the case of epithelial cancers, which are the most common and comprise upwards of 85% of all cancers, once an initial tumour cell emerges, additional proliferation and diffusion leads to a small mass, referred to as hyperplasia [69]. Further mutations may ensue, eliciting additional growth. The cancerous mass may exhibit dysplasia, by appearing irregular in shape, following continued proliferation [68,69]. As the tumour continues to grow and spread within the tissue, it is referred to as *in situ* cancer, since it is relatively contained within the tissue boundaries. When, and if, the cancer spreads to neighbouring

tissue, or into the lymph nodes or the bloodstream, it is considered invasive due to the potential metastasis, causing secondary tumours [2,69].

When cancerous cells divide, they consume available resources in the immediate area, resulting in a necrotic core of dead cells in the centre of the tumour [70,71]. The outer layer of cancer cells seeks to migrate to other areas of the tissue in search of nutrients such as iron, glucose and oxygen [72,73]. As the tumour grows in diameter, the necrotic core also becomes larger, due to diminishing regions to which nutrients can potentially diffuse [74]. Since these nutrients are unavailable near the core of the tumour, the adhesive interactions between cancer cells become disrupted. As cells detach, they diffuse to adjacent areas in search of adequate conditions to continue growing [72,73]. It is this movement that can ultimately lead to the deterioration of the body's systems prior to clinical detection, ultimately causing fatality.

Cancerous tumours can be detected clinically with conventional diagnostic tools at a minimum volume equal to approximately 1 millilitre [75,76]. This corresponds to 1 gram or 10^9 cells, which would require more than the 30 cell divisions to achieve, as cancer cells experience high death rates *in vivo* [76]. Assuming a doubling time equal to one-third year, a newly seeded cancerous cell and its daughters would remain undetected for just under one decade before they could be diagnosed (reviewed in [75,76]). Consequently, scant data are available for this initial phase in cancer growth. It may be appreciated that this

initial phase is critical on the basis of publications in which researchers have promoted growing cancer cell populations as complex dynamic systems [75,77-80].

FROM A MATHEMATICAL PERSPECTIVE

In the study of cancer growth and metastasis, there has been a long history of using mathematics to explain the growth patterns and metastatic effects of tumours in given environments [81-84]. As the use of computational and mathematical methods has increased, cancer has been increasingly considered as a complex system [74,85-91]. Such systems are characterised by sensitive dependence on initial conditions, oscillatory behaviour, and exhibiting properties that seem to be unpredictable but are actually deterministic [2,92]. These properties are hallmarks for chaos, a trait common to some complex systems [8,10,93].

Cancer growth can be modelled in multiple ways. A model focussing on the intracellular level would investigate the various components in the cell that lead to cancerous growth, whereas modelling on an intercellular level considers only the cells themselves, their growth and their movement [94]. Several key characteristics of cancer have been identified and proposed, including: growth despite the absence of normal “stop” and “go” signals from neighbouring cells, the ability to initiate angiogenesis, and the capacity to infiltrate surrounding tissues and organs [95]. From a modelling perspective, these characteristics

would be ideal to create an accurate mathematical representation of tumour growth, in terms of the patterns of growth.

For instance, some authors have focused on models to describe nutrient-dependent cancer growth and the phase transitions involved [79,80,96]. In particular, Scalerandi *et al.* (1999) considered variation in a parameter which quantified bound nutrient per cancer cell, and reported that chaotic behaviour was elicited from competition among cancer cells during initial growth stages [96]; and Delsanto *et al.* (2000) considered parameters which quantified the ratio of nutrient availability to nutrient absorbed by cancer cells and nutrient availability in blood vessels, and found attractors in necrotic core volume-cancer tumour volume space [79]. Furthermore, Rasnick (2002) used aneuploidy (imbalance in chromosome number and composition) theory and logistic difference equations to describe cancer growth and showed that the auto-catalysed progression that characterises aneuploidy is comparable to the deterministic laws in chaos theory [76].

Within the many processes involved in cancer growth and metastasis, most two-dimensional cancer models involve some aspect of cell diffusion [74,80,91,97]. Generally, diffusion of individual cancer cells and, thus, the tumour mass, limit the size and speed of a growing tumour [67,69]. The ability for cells to diffuse impacts their acquisition of nutrients, which are necessary to sustain growth in the absence of angiogenesis [98]. As most mathematical models focus

on this avascular stage of tumour growth, the effects of this diffusion can be crucial [74,80,89-91,97]. If the growth pattern of a tumour is known, then it may be possible for researchers to use this information to aid in the development of various treatments [78,88,94,98,99].

OBJECTIVES

Although the content of this thesis is primarily focused on immunological models in a computational context, the overall theme is ~~The Study of~~ complex biological systems and describes how mathematics can be used to portray and further understand biological systems. The research presented in this thesis focuses on the design, development and uses of novel and innovative mathematical and computational models of chronic allergic asthma and airway eosinophilia. The techniques used in these models are juxtaposed and contrasted with earlier research focused on mathematical and computational modelling of tumour growth. In each instance, mathematical models are used to simplify complex biological systems and learn more about them through the testing of various hypotheses, both probable and hypothetical.

The first manuscript, presented in Chapter 2 of this thesis, describes an investigation of the impact of dose and length of aeroallergen exposure of HDM on allergic sensitization and allergic disease outcomes, primarily airway inflammation, from a computational perspective. Using an established, chronic experimental model for allergic asthma we collected *in vivo* data and developed a

mathematical model. Initially, the objective of this study was to develop a computational tool via mathematical equations that would enable the simulation of doses and time-points both within and outside the established experimental protocol. Furthermore, the model allowed for two- and three-dimensional visualizations of the system. In addition to the predictive ability of the model, we identified thresholds for both allergic sensitization and inflammation, represented by doses that elicit changes in system behaviour in HDM-specific IgG₁ and eosinophils, respectively.

The second manuscript, presented in Chapter 3, describes a subsequent mathematical model that builds upon the model in Chapter 2, now focused on a specific cell type (eosinophils) from a mechanistic perspective. In this case, we examined chronic airway eosinophilia in response to HDM exposure over the course of 14 weeks, and modelled the trafficking of eosinophils from the bone marrow to the blood and, ultimately, to the lungs. Using the model, we identified which processes, when altered, were most likely to affect the levels of airway eosinophilia. In doing so, we were also able to test the sensitivity of those processes deemed to have the largest global effect on airway eosinophilia. With respect to their relative importance to airway eosinophilia, we identified eosinophil production, death and survival as having a greater effect in comparison to eosinophil migration. Through *in silico* simulations, the model was able to emulate the effects of both the use of an antibody and a knockout model in order to minimize eosinophilia.

The third manuscript, presented in Chapter 4, investigates tumour growth and metastasis from a mathematical and computational aspect. The model considered the evolution of a tumour within a slab of tissue in an avascular, two-dimensional environment, with a single blood vessel supplying nutrient. Using an approach that incorporates cellular interaction and movement, the initial stages of tumour growth were defined primarily by growth, death and diffusion processes. Each process corresponds to a mathematical equation, which is then encoded into computational software program, creating a computer graphic simulation program. The code is systematically segregated into sub-routines, each corresponding to a specific calculation within the program. The model simulates tumour growth over time, and through the variation of individual parameters, shows the effects on overall tumour size and shape. In particular, the model is distinguished by its ability to vary the number of directions in which cancerous cells are able to diffuse, using von Neumann and Moore diffusional neighbourhoods. By considering the early stages of cancer growth, the model is able to study the interaction among the various cell states and the processes that govern them. Furthermore, the model is able to examine the sensitivity of the overall growth of the tumour to changes in the initial parameter values. Our results showed that while changes in most model parameters affected the overall size and shape of the tumour, changes in the initial size of the tumour had no effect. Ultimately, the most influential parameter in the model was determined to be the manner in which cancerous cell diffusion is calculated.

CHAPTER 2

In Vivo-to-In Silico Iterations to Investigate Aeroallergen-Host Interactions

Alba Llop-Guevara^{1*}, Marc Colangelo^{1*}, Derek K. Chu¹, Cheryl Lynn Moore¹, Nicole A. Stieber¹, Tina D. Walker¹, Susanna Goncharova¹, Anthony J. Coyle^{1,4}, Lennart J. Lundblad⁵, Paul M. O'Byrne², Miroslav Lovric³, and Manel Jordana¹

¹Department of Pathology and Molecular Medicine, Division of Respiratory Diseases and Allergy, Centre for Gene Therapeutics, ²Department of Medicine, ³Department of Mathematics and Statistics, McMaster University, Hamilton, Ontario, Canada, ⁴Department of Inflammation and Autoimmunity, MedImmune Inc., Gaithersburg, Maryland, United States of America, and ⁵Vermont Lung Center, University of Vermont, Burlington, Vermont, United States of America

*Co-first authors

Published in *PLoS ONE*, 3(6): e2426 (2008).

© 2008 Public Library of Science (PLoS)

Reprinted under the Creative Commons Attribution License (CCAL).

See *Declaration of Academic Achievement* for details regarding authorship.

Summary and Central Message: This article aims to capture the multidimensionality, quantitative nature and, ultimately, complexity of the interaction between aeroallergens and the host. We extensively investigated the impact of dose and length of allergen exposure, using house dust mite, on allergic sensitization and airway inflammation in mice, and developed mathematical algorithms that accurately predict actual biological data as well as an extensive array of unknown responses. Our data demonstrate the non-linearity of the relationship between aeroallergen exposure and either allergic sensitization or airway inflammation, identify distinct system thresholds and behaviours for each outcome, and provide a novel computational view of allergens-host interactions.

In Vivo-to-In Silico Iterations to Investigate Aeroallergen-Host Interactions

Alba Llop-Guevara^{1,3}, Marc Colangelo^{1,3}, Derek K. Chu¹, Cheryl Lynn Moore¹, Nicole A. Stieber¹, Tina D. Walker¹, Susanna Goncharova¹, Anthony J. Coyle^{1,2}, Lennart K. A. Lundblad⁵, Paul M. O'Byrne³, Miroslav Lovric⁴, Manel Jordana^{1*}

1 Department of Pathology and Molecular Medicine, Division of Respiratory Diseases and Allergy, Centre for Gene Therapeutics, McMaster University, Hamilton, Ontario, Canada, **2** Department of Inflammation and Autoimmunity, MedImmune Inc., Gaithersburg, Maryland, United States of America, **3** Department of Medicine, McMaster University, Hamilton, Ontario, Canada, **4** Department of Mathematics and Statistics, McMaster University, Hamilton, Ontario, Canada, **5** Vermont Lung Center, University of Vermont, Burlington, Vermont, United States of America

Abstract

Background: Allergic asthma is a complex process arising out of the interaction between the immune system and aeroallergens. Yet, the relationship between aeroallergen exposure, allergic sensitization and disease remains unclear. This knowledge is essential to gain further insight into the origin and evolution of allergic diseases. The objective of this research is to develop a computational view of the interaction between aeroallergens and the host by investigating the impact of dose and length of aeroallergen exposure on allergic sensitization and allergic disease outcomes, mainly airway inflammation and to a lesser extent lung dysfunction and airway remodeling.

Methods and Principal Findings: BALB/C mice were exposed intranasally to a range of concentrations of the most pervasive aeroallergen worldwide, house dust mite (HDM), for up to a quarter of their lifespan (20 weeks). Actual biological data delineating the kinetics, nature and extent of responses for local (airway inflammation) and systemic (HDM-specific immunoglobulins) events were obtained. Mathematical equations for each outcome were developed, evaluated, refined through several iterations involving *in vivo* experimentation, and validated. The models accurately predicted the original biological data and simulated an extensive array of previously unknown responses, eliciting two- and three-dimensional models. Our data demonstrate the non-linearity of the relationship between aeroallergen exposure and either allergic sensitization or airway inflammation, identify thresholds, behaviours and maximal responsiveness for each outcome, and examine inter-variable relationships.

Conclusions: This research provides a novel way to visualize allergic responses *in vivo* and establishes a basic experimental platform upon which additional variables and perturbations can be incorporated into the system.

Citation: Llop-Guevara A, Colangelo M, Chu DK, Moore CL, Stieber NA, et al. (2008) *In Vivo-to-In Silico* Iterations to Investigate Aeroallergen-Host Interactions. PLoS ONE 3(6): e2426. doi:10.1371/journal.pone.0002426

Editor: Jacques Zimmer, Centre de Recherche Public-Santé, Luxembourg

Received: April 24, 2008; **Accepted:** May 3, 2008; **Published:** June 11, 2008

Copyright: © 2008 Llop-Guevara et al. This is an open-access article distributed under the terms of the Creative Commons Attribution License, which permits unrestricted use, distribution, and reproduction in any medium, provided the original author and source are credited.

Funding: This research was supported by the Canadian Institutes for Health Research (CIHR) and MedImmune Inc. AL-G holds a LaCaixa-ICCS scholarship (Spain) and MC is supported by an Ontario Graduate Scholarship. MJ is a Senior Canada Research Chair.

Competing Interests: The authors have declared that no competing interests exist.

* E-mail: jordanam@mcmaster.ca

These authors contributed equally to this work.

Introduction

Allergic asthma emerges from the interaction between two complex dynamic systems, the immune system and the environment, where aeroallergens exist. These systems are intricate, comprise multiple parts which are subject to many interactions and feedback loops and, consequently, contain a broad array of outputs. The interaction between these already complex systems generates an even higher degree of complexity. Thus, deciphering the conditions under which allergic disease evolves would benefit from the elaboration of models that can explain and/or predict the potential outputs of that interaction.

Advances in the understanding of disease processes have come in great measure through experimentation using *in vitro* and, notably, *in vivo* human and animal models. A detailed appreciation of the

immunopathology of asthma, along with the explosion in molecular immunology has prescribed the modeling strategies to recapitulate the asthmatic phenotype, particularly in mice. It should be noted that conventional biomedical modeling greatly differs from modeling in other scientific domains, such as ecology or economics in that biomedical models are conceived with a pre-established goal in mind: to establish a known phenotype. While such an approach has produced conspicuous benefits, it has inherently prevented an unbiased, global understanding of the consequences of the interaction between allergens and the immune system.

Although it is generally thought that there is a reasonable correlation between early allergen exposure and sensitization [1,2,3,4] or sensitization and disease [1,5,6], the connection that may exist between exposure and disease is less clear [1]. The intrinsic constraints of these clinical and epidemiological studies

preclude achieving both a longitudinal and quantitative understanding of these relationships. Yet, it seems intuitive that such knowledge is essential to gain further insight into the origin, evolution and nature of allergic disease.

The strategy that we followed to investigate the relationship between aeroallergen exposure, allergic sensitization and allergic disease embraces a computational conception of immune responsiveness [7]. In this conception, the view is *synthetic* rather than *analytical* and, therefore, the focus is on system behaviors rather than specific components, i.e. the complex molecular networks underlying the outcomes that we measured. We surmise that this strategy is justified *ad interim* given the current state of knowledge in systems biology *in vivo*. We present data delineating the kinetics and dose-responses for local (total inflammation and eosinophilia) and systemic (HDM-specific immunoglobulins (Ig) G₁ and E) events elicited in mice by extended exposure to house dust mite (HDM). We developed and refined algorithms defining the behavior of each outcome that were subsequently used to conduct *in silico* simulations to guide new biological experiments and visualize an extensive array of unknown responses. We propose that the iterative approach applied to construct the model exhibits considerable fidelity to the biological structure of the process.

Methods

Animals

Female BALB/C mice (6 to 8 weeks old) were purchased from Charles River Laboratories. The mice were housed in a specific pathogen-free environment under 12 h light-dark cycle. All experiments described in this report were approved by the Animal Research Ethics Board of McMaster University.

Protocol of respiratory mucosal sensitization

House dust mite extract (Greer Laboratories) was resuspended in saline (0.9% NaCl Irrigation Solution, Baxter) and serial dilutions were done to obtain the desired concentrations. This suspension was delivered to isoflurane-anaesthetized mice intranasally in a 10 μ l volume. Mice were exposed daily to HDM for either 10 consecutive days (short-term protocol) or 5 consecutive days a week followed by 2 days of rest for a total of 1, 2, 3, 5, 7, 10, 14 and 20 weeks (long-term protocol).

Sample collection

At various time-points, always 72 hours after the last HDM exposure, mice were sacrificed. Blood was collected by retro-orbital bleeding. Blood smears were prepared and serum was obtained by centrifugation of whole blood. Bronchoalveolar lavage (BAL) was performed as previously described [8,9]. Briefly, the lungs were dissected, the trachea was cannulated with a polyethylene tube (BD Biosciences) and two lavages were done with PBS (0.25 ml followed by 0.2 ml). Total cell counts were then determined using a hemocytometer and smears were prepared by cytocentrifugation. Protocol Hema 3 stain set (Fisher Scientific) was used to stain blood and BAL smears and differential cell counts (≥ 500 leukocytes) were determined according to a previously established protocol [9]. The right lobe of the lung was inflated and fixed in 10% formalin for histological analysis.

HDM-specific Ig measurements

Levels of HDM-specific IgE and IgG₁ in serum were measured using ELISA techniques as previously described in detail [10]. Optical density (OD) was read at 405 nm. HDM-specific IgE titres (in OD units) were calculated by subtracting from each sample OD the average OD value of 20 zero standard replicates plus two

standard deviations. HDM-specific IgG₁ titers (in relative units) were calculated using the formula $1/(x/ODx*0.05)$, where x equals the dilution factor closest to but greater than double the average OD value of 20 zero standard replicates, and ODx is the OD reading of x .

Determination of airway responsiveness

Mice were anesthetized with nebulized isoflurane (3% with 1 L/min of O₂), paralyzed with pancuronium bromide (1 μ g i.p.), tracheostomized with a blunted 18-gauge needle, and mechanically ventilated with a small animal computer-controlled piston ventilator (flexiVent, SCIREQ Inc.) [11]. Mice received 200 breaths per minute and a tidal volume of 0.25 ml; the respiratory rate was slowed during nebulization (10 seconds) to provide 5 large breaths of aerosol at a tidal volume of 0.8 ml. The response to nebulized saline and increasing doses (3.125, 12.5 and 50 mg/ml) of methacholine (MCh, Sigma-Aldrich) was measured. A positive-end-expiratory pressure of 3 cm of H₂O was applied by submerging the expiratory line in water. Respiratory impedance was determined from 3 second broadband volume perturbations ranging from 1 to 20.5 Hz every 10 seconds during approximately 2 minutes following each dose of MCh. The data was fitted with the constant phase model and model parameters (airway resistance (R_n), tissue dampening (G), tissue elastance (H) and hysteresivity, a measure of lung heterogeneity ($\eta = G/H$)) were calculated [12]. Model fits that resulted in a coefficient of determination less than 0.8 were excluded.

Histology and morphometric analysis

Lung tissue was embedded in paraffin and cut at a thickness of 3 μ m. Sections were stained with hematoxylin and eosin for evaluation of the severity and the nature of leukocyte infiltration in the lungs by light microscopy. Additional sections were stained with Picro Sirius red to demonstrate the presence of collagen in the extracellular matrix. Images of main airways were captured with OpenLab (Improvision) via a Leica camera and microscope attached to a computer. Analysis was performed on a custom computerized image analysis system (Northern Eclipse software, Empix Imaging) as previously described [13]. Briefly, morphometric quantification involved calculation of the percentage of tissue area that was positively stained within a 40 μ m-thick area from the basement membrane extending into the airway lumen.

Mathematical and computational modeling

All the equations for the mathematical models and analyses were generated using curve-fitting techniques within FindGraph software (UNIPHIZ Lab) for each outcome. (All equations and additional detail on the validation analysis of the model is provided in an online data supplement)

Data analysis

Data are expressed as means \pm standard error of the mean (s.e.m.). Statistical analysis was performed with GraphPad Prism (GraphPad Software). Results were interpreted by analysis of variance (one-way ANOVA) followed by the Dunnett *post hoc* test to compare HDM exposed groups versus the saline control group. Differences were considered statistically significant when p values were less than 0.05.

Results

Dose-response to short-term HDM exposure

We have previously shown that mice exposed intranasally to HDM at a concentration of 25 μ g/day for 10 consecutive days develop acute airway inflammation [14], and that exposure to 25 μ g/day for up to 7 weeks establishes chronic airway

inflammation associated with remodeling [15]. These static conditions, fixed times and concentrations, were selected to achieve desired specific outcomes, thus neglecting the dynamic nature of a living system. Hence, we initially carried out a dose-response experiment using a 10,000-fold range, from 0.01 to 100 µg/day, for 10 days. As shown in Figure 1A, the response in terms of total cell numbers (TCN), eosinophils (EOS) and HDM-specific serum IgG₁ followed a logistic pattern with an incipient response observed with 1 µg and a plateau after 25 µg. Based upon these findings, we chose doses of 1 (incipient), 7.5 (moderate) and 25 µg/day (submaximal) for subsequent experiments utilizing longer exposure periods.

Modeling the inflammatory response to long-term HDM exposure

We investigated the impact of exposing mice to those three concentrations of HDM for up to 14 weeks. As shown in Figure 2A, repeated allergen exposure initially elicited airway inflammation in a near-exponential manner that was both dose- and time-dependent. At 2 weeks, 7.5 and 25 µg led to a distinct peak in inflammation; from then on, 25 µg maintained a stable level of maximal inflammation. A similar plateau was also achieved with 7.5 µg only after 7 weeks. Interestingly, exposure to 1 µg of HDM even for such a protracted period of time did not elicit significant airway inflammation suggesting that a threshold of responsiveness for this outcome must be above this concentration.

Once experimental data were collected and analyzed, a *bottom-up* model was constructed using mathematical and computational methods to accurately portray the data and the ensuing dynamics. Although identical methodology was used for all outcomes (TCN, EOS and immunoglobulins), detailed steps (Figure 1B) are presented for only TCN for brevity.

The initial equation was encoded to be used iteratively to simulate and predict output responses given inputs of dose and time. Figure 2B shows a *retrodiction* of the model in which simulations were compared to actual data and proved to fit fairly well. Given that lower doses (saline and 1 µg) exhibited a seemingly different behavior compared to higher doses (7.5 and 25 µg), an intermediate dose of 5 µg was selected to further assess the model. In this evaluation, a *prediction*, or interpolation, of a 5 µg dose was performed and compared to actual data (Figure S1A). Figure 2C depicts a refined model that incorporates these new experimental data.

An additional evaluation of the model was also carried out by extrapolating data up to 20 weeks (Figure S1B). Following comparison to actual data, the model was further refined to include all experimental data (Figure 2D), resulting in a final equation generated from 5 doses and 9 time-points. Equation 1 describes total inflammation (*y*) as a function of time (*t*) and dose (*x*), while each of the respective co-efficients (*x_{a1}, x_{b1},...*) represent dose-dependent quantities (see Methods S1, equations 1.1 to 1.21):

$$y = f_C^{TCN}(x, t) = \begin{cases} x_{a1} + x_{b1} \sin(z_1(x, t))^2 & , 0 \leq t \leq 3 \\ x_{a2} + x_{b2} e^{z_2(x, t)} + x_{g2} t + x_{h2} t^2 & , 3 \leq t \leq 7 \\ x_{a3} + x_{b3} e^{z_3(x, t)} + x_{g3} e^{z_4(x, t)} & , t \geq 7 \end{cases} \quad (1)$$

While the model visually fit the experimental data, accuracy was verified and quantified mathematically. Using linear regression, the initial equation, the revised equation (including the 5 µg data), and the final equation (including both the 5 µg and 20 week data) yielded R² values of 0.987, 0.987 (not shown), and 0.990, respectively (Figure 2E). Furthermore, 95% confidence intervals (CI) and global validation metrics were calculated (see online data supplement and Figure 2F). The latter accounts for experimental uncertainty, error and chance [16,17,18], and confirmed that not only the model accurately predicts actual responses but also that an additional dose in the model did not enhance the accuracy of the system, while the integration of a further time-point had only a minimal effect.

This *complex* model accurately mimics varying system dynamics. However, in order to facilitate the visualization of responses, we developed a *simple* model (see online data supplement), represented by Equation 2, which captures the general features of the system:

$$y = f_S^{TCN}(x, t) = \frac{x_a + x_b t + x_c t^2}{1 + x_d t + x_g t^2} \quad (2)$$

To visualize the dynamics of the system, simulations were performed with both *complex* and *simple* models to emulate the response between 0 and 25 µg, in sequential 0.5 µg increments over a 20 week period (Figure 3A–B). Further extrapolations were performed doubling both the highest dose and latest time-point used to construct the model. Figure 3C shows simulations in three-dimensions up to 40 weeks (approximately 50% of the lifespan of a

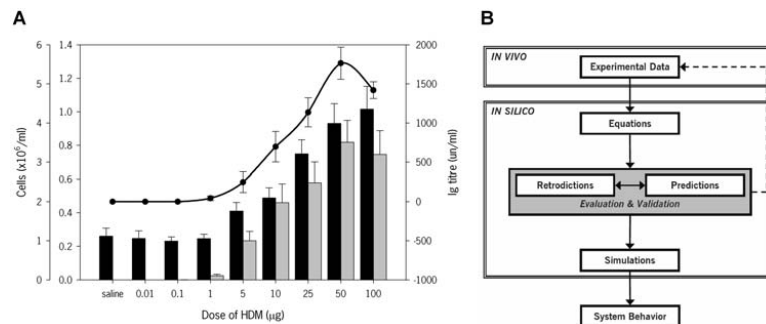


Figure 1. Airway inflammation and systemic immunity in BALB/C mice exposed to HDM for 10 consecutive days. (A) Dose-response: total inflammation (black bars), eosinophilia (grey bars) and serum HDM-specific IgG₁ (solid circles and solid line). Results for cells (n=5–19 mice/group) and IgG₁ (n=2–6 mice/group) are expressed as means±s.e.m. (B) Schematic of the steps followed to develop the mathematical models. doi:10.1371/journal.pone.0002426.g001

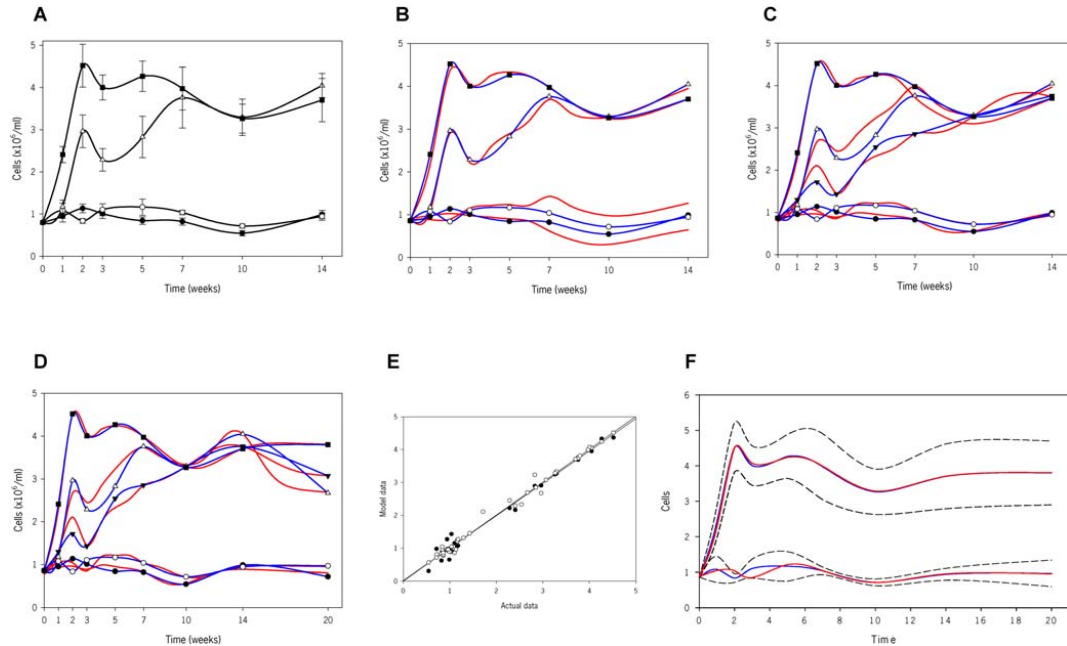


Figure 2. Airway inflammation in BALB/C mice exposed to HDM and subsequent mathematical modeling. (A) Inflammatory response in the BAL. Mice were exposed intranasally to either saline (solid circles) or HDM, 1 µg (open circles), 7.5 µg (open triangles up) or 25 µg (solid squares) for up to 14 weeks (5 days of exposure and 2 days of rest per week). Cell numbers are expressed as mean ± s.e.m (n=6–12 mice/group). (B) Mathematical modeling of the inflammatory response. A mathematical equation was developed from the experimental results (blue lines) based on dose and length of exposure to HDM. Simulations (red lines) for each of the doses studied experimentally were generated. (C) Results of the first iteration. Predictions using the first mathematical model were generated for 5 µg of HDM (see Figure S1) and were subsequently evaluated experimentally. Then, the new 5 µg experimental data (solid triangles down) was used to readjust the previous equation and refine the model. Actual data (blue lines) and virtual simulations (red lines) are shown for saline, 1, 5, 7.5 and 25 µg of HDM up to 14 weeks. (D) Results of the second iteration. Predictions using the second mathematical model were generated for all doses studied at 20 weeks of exposure (not shown) and were subsequently evaluated experimentally. Then, the new 20 week data was used to readjust the previous equation and further refine the model. Actual data (blue lines) and virtual simulations (red lines) are shown for saline, 1, 5, 7.5 and 25 µg of HDM up to 20 weeks. (E) Regression analysis to evaluate the accuracy of the mathematical models. Deterministic validation metrics were performed to mathematically measure the agreement between computational predictions and experimental results. For the line $y = x$, where y is model data and x is actual data, the coefficient of determination R^2 in the first model is 0.987 (solid circles) and 0.990 in the last one (open circles). (F) Confidence intervals (CI) to evaluate the accuracy of the mathematical models. Non-deterministic validation metrics were also used to account for experimental and computational uncertainties and errors. The 95% CI for each point depicts uncertainty due to experimental variability. Model data for 25 µg (top) and 1 µg (bottom) accurately predict actual data, and fall within the 95% CI band. doi:10.1371/journal.pone.0002426.g002

mouse) and 50 µg to further enhance the visualization of the dose-time-response relationship. The *complex* model predicts actual data with slightly greater accuracy than the *simple* model, as indicated by an approximate 0.05 increase in the R^2 value and an 8.5% increase in the 95% CI (data not shown and Figure 3D). Such simulations epitomize visual and numerical information that can only be derived mathematically and computationally.

Analysis of global inflammation was followed by an evaluation of airway eosinophilia, a typical hallmark of allergic inflammation. As illustrated in Figure 4A, eosinophils initially increase in a dose- and time-dependent fashion but later dramatically decrease to a level of 6–9% of total cells at 20 weeks of exposure. These findings are supported by a histopathological assessment (Figure 4E). As shown in the top panels, inflammation at 2 weeks is minimal in mice exposed to 1 µg of HDM and severe in those exposed to 25 µg. A graded level of inflammation was evident after exposure to 5, 7.5 and 25 µg (data not shown). Figure 4E (bottom panels) depicts a

comparison of acute versus chronic exposure revealing stable inflammation over time but a relative decrease in tissue eosinophilia at later time-points. To note, we also observed a similar decrease in eosinophils in peripheral blood (data not shown). At variance with these findings, neutrophils and, particularly, mononuclear cells increased throughout the entire duration of allergen exposure, numerically compensating for the decrease of eosinophils and, hence, maintaining the overall degree of inflammation (Figure 4F). Again, exposure to 1 µg of HDM for up to 14 weeks did not elicit any significant changes in eosinophils (Figure 4A), or mononuclear cells and neutrophils (data not shown).

Using the aforementioned methods, *complex* and *simple* models were constructed for eosinophils, eliciting the equations:

$$y = f_C^{EOS}(x, t) = \begin{cases} x_{a1} + x_{b1} e^{-1(x,t)} + x_{g1} e^{-2(x,t)} & , 0 \leq t \leq 7 \\ x_{a2} + x_{b2}t + x_{c2}t^2 + x_{d2}t^3 & , t \geq 7 \end{cases} \quad (3)$$

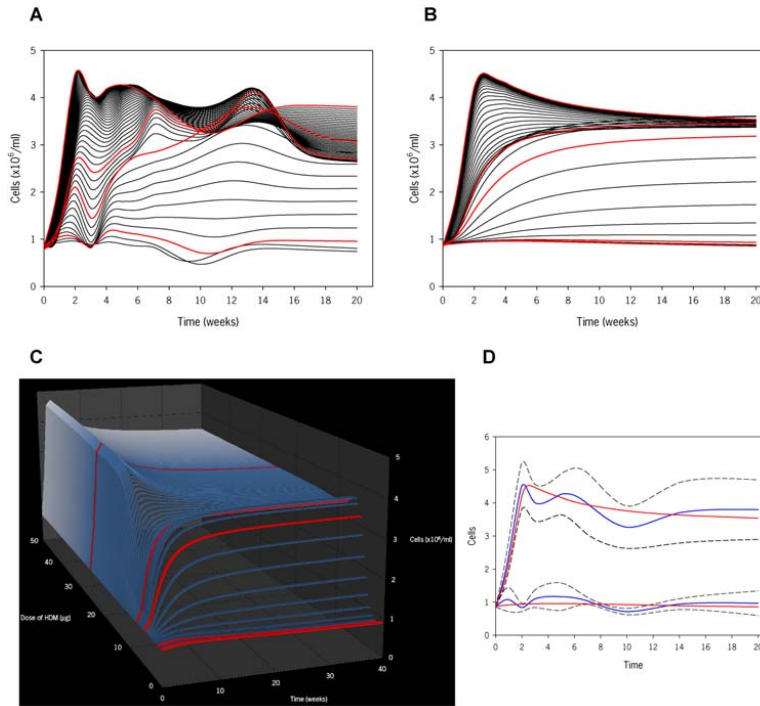


Figure 3. 2D and 3D models for total cells generated from mathematical equations. In panels **A**, **B** and **C**, the simulations for the doses of HDM used experimentally are highlighted in red. **(A)** Simulations based on dose of HDM (range from 0 to 25 µg at 0.5 µg intervals) and length of exposure (0 to 20 weeks) using the final mathematical model (Figure 2D). **(B)** Simplified mathematical model for the total cell number. **(C)** 3D simulations generated from the simplified mathematical model including predictions up to 50 µg and 40 weeks of HDM exposure. **(D)** Confidence intervals to evaluate the accuracy of the simple mathematical model. Visual inspection shows that the simple model falls within the 95% CI, while quantification of the simple TCN model accuracy was calculated to be $89.03 \pm 22.42\%$ with 95% confidence. Thus, the simple TCN model has similar fidelity to the complex model.
doi:10.1371/journal.pone.0002426.g003

$$y = f_S^{EOS}(x, t) = \left| \frac{t + x_a}{x_b + x_c(t + x_a) + x_d(t + x_a)^2} \right| \quad (4)$$

Although Equations 3 and 4 represent different functions, they both maintain relatively high and similar predictive value, yielding R^2 values of 0.968 and 0.938, respectively. Using these equations, we performed computer simulations in two- and three-dimensions (Figure 4B–D). These images illustrate that the decrease in airway eosinophilia occurs throughout the entire range of exposures, and that is not dependent on eosinophilia reaching an absolute level; moreover, it is also evident that the higher the eosinophil level, the sooner the downturn begins. This suggests that part of the program of the immune-inflammatory response elicited by chronic allergen exposure may contain an inherent controlling mechanism to prevent persistent eosinophilia in the lung.

Modeling allergic sensitization to long-term HDM exposure

Allergic sensitization is a crucial event in allergic asthma. Hence, we investigated the effect of allergen exposure on defining

features of B cell immunity, namely serum levels of HDM-specific immunoglobulins. As shown in Figure 5A–D, IgG₁ and IgE serum levels follow a logistic-like behavior similar to that identified for total airway inflammation. However, there are kinetic differences; indeed, serum immunoglobulins are detected after 2–3 weeks of allergen exposure at a time where the inflammatory response has already reached its peak. Given the nature of the immunoglobulin response, *simple* models for both IgE and IgG₁ were constructed and proved to be accurate (R^2 values of 0.900 and 0.985, respectively). Equations 5 and 6 depict the values of IgE and IgG₁:

$$y = f_S^{IgE}(x, t) = \frac{x_a t^{x_d}}{x_c^{x_d} + t^{x_d}} \quad (5)$$

$$y = f_S^{IgG_1}(x, t) = x_a + \frac{x_b - x_a}{1 + \left(\frac{t}{x_c}\right)^{x_d}} \quad (6)$$

Relationship between allergic sensitization and airway inflammation

Airway inflammation and allergic sensitization were compared using two different approaches. First, we considered the *threshold* of

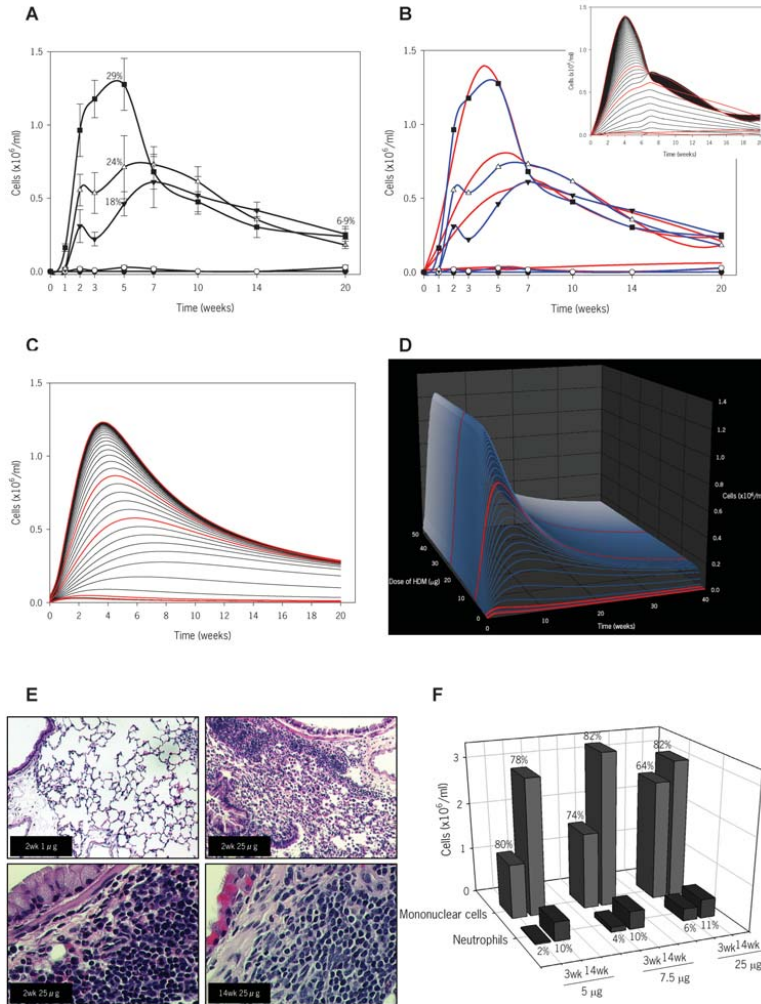


Figure 4. Nature of the inflammatory response in mice exposed to HDM and mathematical modeling of eosinophils. In panels **B insert**, **C** and **D**, the simulations for the doses of HDM used experimentally are highlighted in red. **(A)** Eosinophilic response in the BAL fluid. Mice were exposed to either saline (solid circles) or HDM, 1 µg (open circles), 5 µg (solid triangles down), 7.5 µg (open triangles up) or 25 µg (solid squares) for up to 20 weeks. Eosinophil numbers are expressed as mean \pm s.e.m (n = 6–12 mice/group); percentage of eosinophils at 5 and 20 weeks are inserted in the graph. **(B)** Final mathematical model for eosinophils. The equation to obtain these predictions (red lines) was developed from the experimental results (blue lines) based on dose and length of exposure to HDM. The *insert* shows simulations based on dose of HDM (range from 0 to 25 µg at 0.5 µg intervals) and length of exposure (0 to 20 weeks) using the final mathematical model. **(C)** Simplified mathematical model for eosinophils. **(D)** 3D simulations generated from the simplified mathematical model including predictions up to 50 µg and 40 weeks of HDM exposure. **(E)** Light photomicrograph of lung sections stained with hematoxylin and eosin. Top left: after 2 weeks of exposure to 1 µg of HDM ($\times 10$ magnification); top right: after 2 weeks of exposure to 25 µg of HDM ($\times 10$); bottom left: after 2 weeks of exposure to 25 µg of HDM ($\times 40$); bottom right: after 14 weeks of exposure to 25 µg of HDM ($\times 40$). **(F)** Cellular profile in the BAL fluid. Absolute numbers and percentage of mononuclear cells (light grey bars) and neutrophils (dark grey bars) after continued exposure to 5, 7.5 and 25 µg of HDM for either 3 or 14 weeks. Bars represent mean of cells (n = 6–12 mice/group).
doi:10.1371/journal.pone.0002426.g004

responsiveness, understood here as the lowest dose of allergen that elicits a measurable response. To address this, we calculated areas under the curve (AUC) for all modeled responses and determined that a threshold would be the point at which there was an

apparent change in behavior. The lowest dose of allergen required to elicit an eosinophilic response is 2 µg, whereas that required to induce an IgG₁ response is 0.5 µg. (Figure 5E). Of interest, these doses elicit responses that are approximately 20% of the maximal

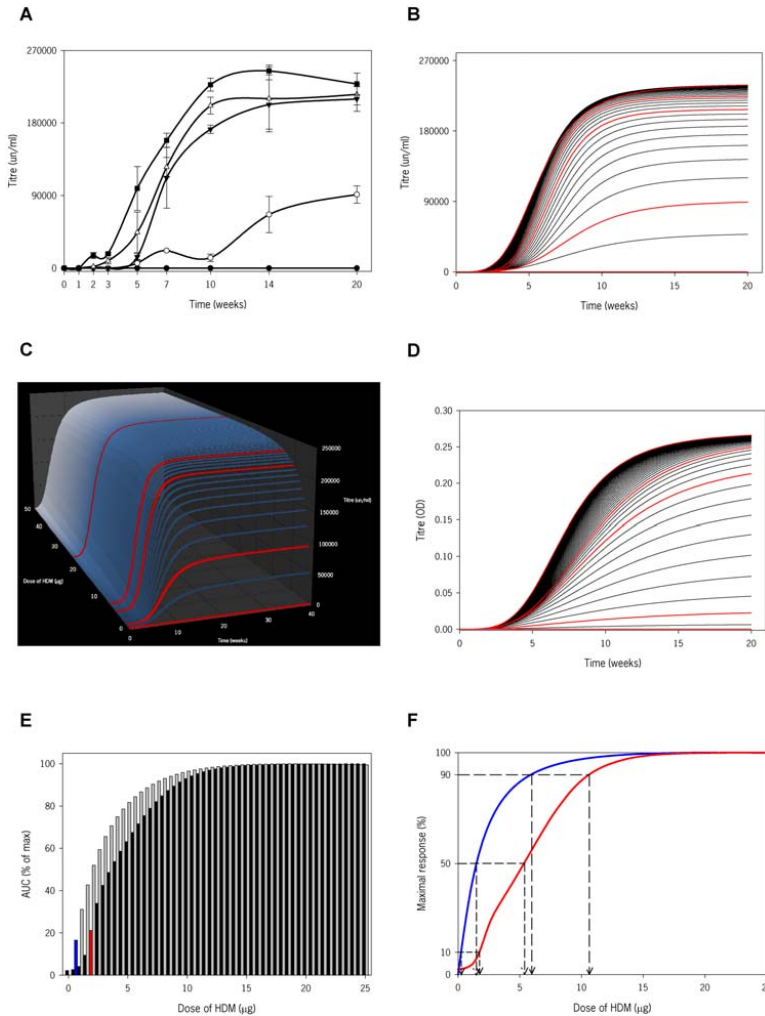


Figure 5. Systemic responses in HDM-exposed mice, subsequent mathematical modeling and comparison between inflammation and sensitization. In panels **B**, **C** and **D**, the simulations for the doses of HDM used experimentally are highlighted in red. **(A)** Serum levels of HDM-specific IgG₁. BALB/C mice were exposed to either saline (solid circles) or HDM, 1 µg (open circles), 5 µg (solid triangles down), 7.5 µg (open triangles up) or 25 µg (solid squares) for up to 20 weeks. Data represent mean ± s.e.m. (n = 2–9 mice/group). **(B)** Mathematical model for HDM-specific IgG₁. A simple mathematical model was developed and IgG₁ levels over time and at doses ranging from 0 to 25 µg of HDM, in 0.5 µg increments, were predicted. **(C)** 3D representation of HDM-specific IgG₁ responses, including predictions up to 50 µg and 40 weeks of HDM exposure. **(D)** Mathematical model for HDM-specific IgE. A simple mathematical model based on serum measurements was developed and IgE levels were simulated over time and at doses ranging from 0 to 25 µg of HDM in 0.5 µg increments. **(E)** Area under the curve (AUC) of the maximal number of eosinophils (black bars) and level of HDM-specific IgG₁ (grey bars). The lower dose showing a change in the behavior of the curve (threshold dose), is identified for HDM-specific IgG₁ (blue bar, 0.5 µg) and eosinophilia (red bar, 2 µg). The results are based on computer simulations. **(F)** Maximal responses for HDM-specific IgG₁ (blue line) and eosinophilia (red line) at a range of doses of HDM. The 90% of the maximal inflammatory or immunoglobulin response (long dashed line) is reached when given about 11 or 6 µg of HDM, respectively; approximately 2 and 5 µg of HDM are required to elicit 50% of the maximal inflammatory and immunoglobulin responses (medium dashed line), and <1 and 2 µg to induce 10% of these responses (short dashed line).
doi:10.1371/journal.pone.0002426.g005

inducible response. It is clear that the pattern of the areas under each curve for IgG₁ and eosinophils are similar; however, the latter is shifted to the right indicating that the amount of allergen required to elicit not only the lowest response but all responses is

different. To better visualize this, and to standardize measurements, we plotted each outcome as a percentage of the maximal response. As shown in Figure 5F, any level of sensitization is achieved with about half the amount of allergen required to

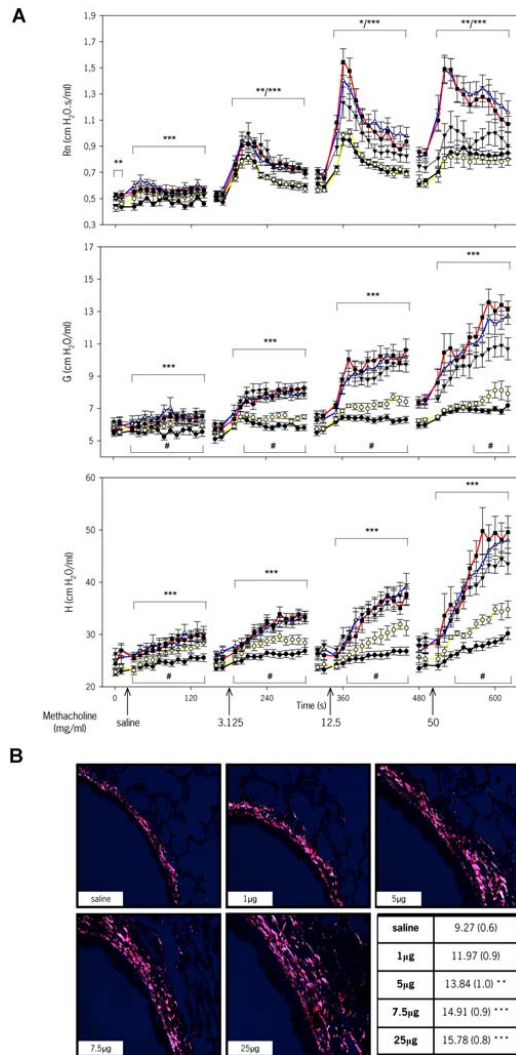


Figure 6. Physiological and structural lung changes in mice exposed to different doses of HDM. (A) Analysis of airway responsiveness to methacholine (MCh) in mice exposed to HDM for 3 weeks. Airway resistance (Rn), tissue dampening (G) and tissue elastance (H) were determined in BALB/C mice exposed to either saline (solid circles, black line) or HDM, 1 µg (open circles, yellow line), 5 µg (solid triangles down, grey line), 7.5 µg (open triangles up, blue line) or 25 µg (solid squares, red line). A time-course of 2 baseline measurements prior to nebulization of increasing doses of MCh (0, 3.125, 12.5 and 50 mg/ml) followed by 12 consecutive measurements is shown. Data represent mean ± s.e.m. (n = 5–12 mice/group). *, ** and *** indicate $p < 0.05$, < 0.01 and < 0.001 , respectively, in mice exposed to 5, 7.5 and 25 µg compared to saline; # indicates $p < 0.05$ in mice exposed to 1 µg compared to saline. (B) Airway remodeling after 7 weeks of HDM exposure. Picro Sirius red-stained lung sections visualized under polarized light ($\times 20$) and morphometric analysis show increased subepithelial accumulation of collagen in HDM exposed mice. Data represent the mean of the percentages of stained area of interest

(± s.e.m.). ** indicates $p < 0.01$ and ***, $p < 0.001$ versus saline exposed mice (n = 7–12 mice/group). doi:10.1371/journal.pone.0002426.g006

achieve the same level of eosinophilic inflammation. Higher IgG₁ responses are not only induced by the same amount of allergen but also greater changes in IgG₁ are observed at lower doses of allergen. Similar observations were made for TCN and IgE (data not shown).

Lung function and remodeling

Airway dysfunction, notably airway hyperreactivity (AHR), is a hallmark of allergic asthma. Preliminarily, we have evaluated lung function to a range of doses after 3 weeks of HDM exposure, a time-point where there is prominent inflammation but no airway remodeling [15]. As shown in Figure 6A, airway resistance (Rn), tissue dampening (G) and elastance (H) increase dose-dependently, being severe in mice exposed to 7.5 and 25 µg of HDM. Most of the peripheral effects observed at these doses of allergen exposure, as measured by G and H, can be explained as airway closure with some elements of lung heterogeneity, as assessed by hysteresivity (η , data not shown) [19]. Rn in mice exposed to 1 µg of HDM was not significantly different than that in saline-treated animals. Interestingly, G and H seemed to be increased in these mice suggesting incipient functional abnormalities occurring prior to detectable inflammation. To note, mice exposed to 5, 7.5 and 25 µg of HDM had a significantly higher baseline Rn compared to the 1 µg and saline groups, indicating a degree of permanent narrowing of the conducting airways. A comprehensive clarification of the variables that influence airway function in this system will require not only the acquisition of an extensive set of functional data but also of additional data including mucous production, permeability and airway structural changes, i.e. remodeling. In specific regard to the later, Figure 6B shows that subepithelial collagen deposition increases in a dose-dependent manner after 7 weeks of allergen exposure; changes in mice exposed to 1 µg of HDM were not significant compared to saline. Clearly, a quantitative delineation of the relationships between tissue and functional variables with inflammatory and immune variables is a major computational challenge beyond the scope of the research presented here.

Discussion

Understanding immune responsiveness will benefit from accepting the multidimensionality and quantitative nature of immunological phenomena [20]. Here, we have engaged this precept to investigate immune-inflammatory responses following repeated HDM exposure in mice. The computational analysis we have performed allows for the identification of rules and parameters that define the system. Principal rules are that relationships between time and infiltrating total cells, as well as mononuclear cells and neutrophils, and serum immunoglobulins follow a logistic-like curve; in sharp contrast, the eosinophil response over time follows a bell shaped-like curve. These rules presuppose a dynamic behavior with at least one significant implication: the lung cellular effector profile quite drastically changes depending on dose and length of exposure to allergen. These multiple possible outcomes may be mathematically viewed as a demonstration of heterogeneity.

The distinct behavior of eosinophils is intriguing. The underlying immunological explanation is unknown at this time; however, it seems intuitive that if allergen exposure is considered as an input, persistent deliverance of such an input will stress the

system and instigate reactive responses. From this perspective, the decrease of eosinophils and the increase in mononuclear cells are likely to be mechanistically related. Flow cytometric analysis delineating the changes in the dynamics of subsets of mononuclear cells (T cells and monocyte/macrophages) over the entire protocol will be informative and suggest future venues of research.

Several parameters define the behavior of the system. First, we have identified a threshold dose at approximately 0.5 μg of HDM for sensitization and 2 μg for inflammation. In fact, exposure to 2.5 μg of HDM elicits a detectable eosinophilic inflammatory response (data not shown). Second, responsiveness for all constituents is dependent on the strength of the initial dose of allergen; moreover, the greater the input, the steeper the initial slope of the response. Third, the system has an inherently limited capacity to respond, at least to the same allergen. This maximal responsiveness is achieved at a dose between 10 and 15 μg , and further increases in dose or length of exposure do not result in greater responses. Fourth, there is an entire range of responses between the threshold and the maximum; mathematically, however, the model reveals that the distribution of responses is non-linear. Lastly, a comparative analysis of inflammation and sensitization outputs reveals that the development of the latter is more sensitive to allergen than the induction of airway inflammation. That the relationships between exposure and either sensitization or inflammation are non-linear intimates that the relationship between sensitization and inflammation is non-linear as well. It is tempting to speculate that these findings may contribute to explain the difference between the prevalence of atopy (~40%) and asthma (5–10%) in humans [21,22,23,24].

The question of how the concentrations of allergen used here compare to human exposure is elusive because the terms of reference are precarious (reviewed in [25]). Many studies have examined the amount of mite allergen present in homes. However, the numbers vary extraordinarily. Not only is there a plethora of environmental variables influencing the concentration of mite allergens in the household but there are also several collection and measurement techniques [3,26,27,28]. In addition, the relationship between the micrograms of allergen measured in a dust sample and the amount of allergen that is airborne, inspired, and reaches the lower airway is enigmatic. Indeed, the inability to precisely determine mucosal HDM exposure in humans frustrates the justifiable desire to formulate a rigorous interspecies comparison of exposures. Perhaps such a straightforward comparison is an ill-conceived goal; arguably, numbers may not be translated between species but behaviors likely can.

Many issues have not been addressed here. For example, experiments were conducted in BALB/C mice. While we know that C57BL/6 mice respond to HDM even more vigorously in terms of inflammation, it definitely cannot be assumed that the behavior of these two strains, or others, is identical. Similarly, these experiments were performed in female mice and, thus, a direct application to male mice is unadvisable. In addition, we cannot presume that the behaviors described for HDM apply to other aeroallergens. With these limitations, our research furnishes a conceptual foundation and operating tools for the evaluation of other variables or system perturbations of a pharmacological, environmental or genetic nature. Based on the present research,

References

- Lau S, Ili S, Sommerfeld C, Niggemann B, Bergmann R, et al. (2000) Early exposure to house-dust mite and cat allergens and development of childhood asthma: a cohort study. Multicentre Allergy Study Group. *Lancet* 356: 1392–1397.
- Wahn U, Lau S, Bergmann R, Kulig M, Forster J, et al. (1997) Indoor allergen exposure is a risk factor for sensitization during the first three years of life. *J Allergy Clin Immunol* 99: 763–769.
- Platts-Mills TA, Vervloet D, Thomas WR, Aalberse RC, Chapman MD (1997) Indoor allergens and asthma: report of the Third International Workshop. *J Allergy Clin Immunol* 100: S2–24.
- Sporik R, Squillace SP, Ingram JM, Rakes G, Honsinger RW, et al. (1999) Mite, cat, and cockroach exposure, allergen sensitisation, and asthma in children: a case-control study of three schools. *Thorax* 54: 675–680.

future analysis of immune responses exploring these variables may not require the generation of entire data sets but of selected experiments to generate comparative algorithms to re-define the overall behavior of the system.

There has been a considerable interest by engineers, mathematicians and computer scientists in the application of their skills to modeling biological processes. Over the last few years, biologists have shown an increasing attraction to join in this enterprise. Arguably, the catalyst underlying this initiative has been the recognition that biological processes are, formally, complex processes. As such, efforts to incorporate new conceptual and experimental stratagems must be made to better comprehend them. The development of mathematical modeling based upon research, primarily *in vitro*, examining hemopoiesis and stem cell renewal [29], models of virus-immune dynamics [30] and cancer cell propagation [31] typify these efforts. Particularly in the area of inflammation, agent-based and equation-based models have been established to provide insight into the complex dynamics of this process [32,33,34,35,36,37]. However, the research presented in this manuscript is, to our knowledge, the first to investigate the interaction between aeroallergens and the immune system *in vivo* from a computational perspective.

Supporting Information

Figure S1 Iterations to validate the mathematical model for the inflammatory response. (A) A mathematical equation was developed based on the responses to saline, 1, 7.5 and 25 μg of HDM up to 14 weeks (blue lines). Simulations (red lines) for these doses studied were generated. Then, the equation was used to predict the response to 5 μg , which was subsequently evaluated experimentally (blue line, triangles down). (B) A refined mathematical equation was developed based on the responses to saline, 1, 5, 7.5 and 25 μg of HDM up to 14 weeks (blue lines). Simulations (red lines) for these doses were generated. Then, responses for all doses at 20 weeks were predicted, and these were subsequently evaluated experimentally.

Found at: doi:10.1371/journal.pone.0002426.s001 (1.50 MB TIF)

Methods S1 Supplementary methods, including elaboration of mathematical Equations 1 to 6.4 used in the models, validation analysis and area under curves.

Found at: doi:10.1371/journal.pone.0002426.s002 (0.11 MB PDF)

Acknowledgments

The authors gratefully thank R. Fattouh, N.G. Midence and M.A. Korzeniowski for technical help; M. Serra-Julιά for input into the mathematical modeling; Drs. N.S. Greenspan and J. Gaudie for critical review of the manuscript; and M. Kiriakopoulos for secretarial assistance.

Author Contributions

Conceived and designed the experiments: MJ AL MC. Performed the experiments: AL MC DC CM NS TW. Analyzed the data: MJ AL MC LL ML. Wrote the paper: MJ AL MC. Other: Contributed writing the paper: AC ML PO LL. Analyzed biological samples: SG AL.

5. Sporik R, Holgate ST, Platts-Mills TA, Cogswell JJ (1990) Exposure to house-dust mite allergen (Der p I) and the development of asthma in childhood. A prospective study. *N Engl J Med* 323: 502-507.
6. Martinez FD, Wright AL, Taussig LM, Holberg CJ, Halonen M, et al. (1995) Asthma and wheezing in the first six years of life. The Group Health Medical Associates. *N Engl J Med* 332: 133-138.
7. Cohen IR (2007) Modeling immune behavior for experimentalists. *Immunol Rev* 216: 232-236.
8. Stampfli MR, Wiley RE, Neigh GS, Gajewska BU, Lei XF, et al. (1998) GM-CSF transgene expression in the airway allows aerosolized ovalbumin to induce allergic sensitization in mice. *J Clin Invest* 102: 1704-1714.
9. Ohkawara Y, Lei XF, Stampfli MR, Marshall JS, Xing Z, et al. (1997) Cytokine and eosinophil responses in the lung, peripheral blood, and bone marrow compartments in a murine model of allergen-induced airways inflammation. *Am J Respir Cell Mol Biol* 16: 510-520.
10. Fattouh R, Midence G, Arias K, Johnson JR, Walker TD, et al. (2008) TGF- β Regulates House Dust Mite-induced Allergic Airway Inflammation but not Airway Remodeling. *Am J Respir Crit Care Med*.
11. Schuessler TF, Bates JH (1995) A computer-controlled research ventilator for small animals: design and evaluation. *IEEE Trans Biomed Eng* 42: 860-866.
12. Hantos Z, Daroczy B, Suki B, Nagy S, Fredberg JJ (1992) Input impedance and peripheral inhomogeneity of dog lungs. *J Appl Physiol* 72: 168-178.
13. Leigh R, Ellis R, Wattie J, Southam DS, De Hoogh M, et al. (2002) Dysfunction and remodeling of the mouse airway persist after resolution of acute allergen-induced airway inflammation. *Am J Respir Cell Mol Biol* 27: 526-535.
14. Cates EC, Fattouh R, Wattie J, Inman MD, Goncharova S, et al. (2004) Intranasal exposure of mice to house dust mite elicits allergic airway inflammation via a GM-CSF-mediated mechanism. *J Immunol* 173: 6384-6392.
15. Johnson JR, Wiley RE, Fattouh R, Swirski FK, Gajewska BU, et al. (2004) Continuous exposure to house dust mite elicits chronic airway inflammation and structural remodeling. *Am J Respir Crit Care Med* 169: 378-385.
16. Anderson AE, Ellis BJ, Weiss JA (2007) Verification, validation and sensitivity studies in computational biomechanics. *Comput Methods Biomech Biomed Engin* 10: 171-184.
17. Oberkampf WL, Trucano TG, Hirsch C (2002) Verification, validation, and predictive capability in computational engineering and physics. Foundations for verification and validation in the 21st century workshop. Johns Hopkins University, Laurel, Maryland.
18. Oberkampf WLB, FM (2006) Measures of agreement between computation and experiment: validation metrics. *Journal of Computational Physics* 217: 5-36.
19. Lundblad LK, Thompson-Figueroa J, Allen GB, Rinaldi L, Norton RJ, et al. (2007) Airway hyperresponsiveness in allergically inflamed mice: the role of airway closure. *Am J Respir Crit Care Med* 175: 768-774.
20. Greenspan NS (2007) Conceptualizing immune responsiveness. *Nat Immunol* 8: 5-7.
21. Holt PG, Thomas WR (2005) Sensitization to airborne environmental allergens: unresolved issues. *Nat Immunol* 6: 957-960.
22. Sporik R, Platts-Mills TA (2001) Allergen exposure and the development of asthma. *Thorax* 56 Suppl 2: ii58-63.
23. Pleis JR, Lethbridge-Cejku M (2006) Summary health statistics for U.S. adults: National Health Interview Survey, 2005. *Vital Health Stat* 10: 1-153.
24. Masoli M, Fabian D, Holt S, Beasley R (2004) The global burden of asthma: executive summary of the GINA Dissemination Committee report. *Allergy* 59: 469-478.
25. Cates EC, Fattouh R, Johnson JR, Llop-Guevara A, Jordana M (2007) Modeling responses to respiratory house dust mite exposure. *Contrib Microbiol* 14: 42-67.
26. Tovey ER, Mitakakis TZ, Sercombe JK, Vanlaar CH, Marks GB (2003) Four methods of sampling for dust mite allergen: differences in 'dust'. *Allergy* 58: 790-794.
27. Custis NJ, Woodfolk JA, Vaughan JW, Platts-Mills TA (2003) Quantitative measurement of airborne allergens from dust mites, dogs, and cats using an ion-charging device. *Clin Exp Allergy* 33: 986-991.
28. Sakaguchi M, Inouye S, Sasaki R, Hashimoto M, Kobayashi C, et al. (1996) Measurement of airborne mite allergen exposure in individual subjects. *J Allergy Clin Immunol* 97: 1040-1044.
29. Kirkland MA (2004) A phase space model of hemopoiesis and the concept of stem cell renewal. *Exp Hematol* 32: 511-519.
30. Perelson AS (2002) Modelling viral and immune system dynamics. *Nat Rev Immunol* 2: 28-36.
31. Deisboeck TS, Mansury Y, Guiot C, Degiorgis PG, Delsanto PP (2005) Insights from a novel tumor model: Indications for a quantitative link between tumor growth and invasion. *Med Hypotheses* 65: 785-790.
32. Vodovotz Y, Clermont G, Chow C, An G (2004) Mathematical models of the acute inflammatory response. *Curr Opin Crit Care* 10: 383-390.
33. Reynolds A, Rubin J, Clermont G, Day J, Vodovotz Y, et al. (2006) A reduced mathematical model of the acute inflammatory response: I. Derivation of model and analysis of anti-inflammation. *J Theor Biol* 242: 220-236.
34. Vodovotz Y, Chow CC, Bartels J, Lagoa C, Prince JM, et al. (2006) In silico models of acute inflammation in animals. *Shock* 26: 235-244.
35. Day J, Rubin J, Vodovotz Y, Chow CC, Reynolds A, et al. (2006) A reduced mathematical model of the acute inflammatory response II. Capturing scenarios of repeated endotoxin administration. *J Theor Biol* 242: 237-256.
36. An G (2001) Agent-based computer simulation and sirs: building a bridge between basic science and clinical trials. *Shock* 16: 266-273.
37. Chow CC, Clermont G, Kumar R, Lagoa C, Tawadrous Z, et al. (2005) The acute inflammatory response in diverse shock states. *Shock* 24: 74-84.

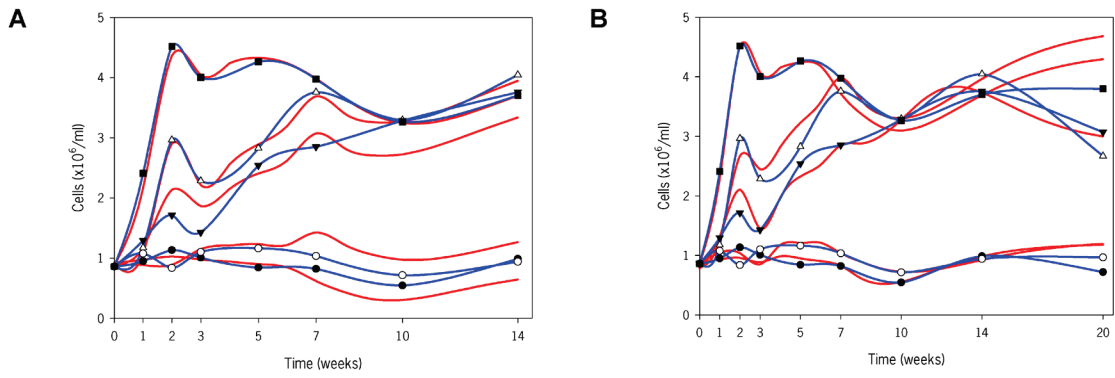
CHAPTER 2

In Vivo-to-In Silico Iterations to Investigate Aeroallergen-Host Interactions

Alba Llop-Guevara^{*}, Marc Colangelo^{*}, Derek K. Chu, Cheryl Lynn Moore, Nicole A. Stieber, Tina D. Walker, Susanna Goncharova, Anthony J. Coyle, Lennart J. Lundblad, Paul M. O'Byrne, Miroslav Lovric, and Manel Jordana

Supporting Information

Figure S1



Methods S1 (Supporting Information)

Mathematical and computational modeling

Outcomes were analyzed by individual doses over specific time periods, deriving a general equation for all doses and all times. Within each equation, numerical coefficients were analyzed based on dose, establishing dose-dependent equations. In some cases, equations were subsequently re-adjusted manually. In order to capture all of the characteristics for a given outcome, *complex* models were derived based on the dynamics of the experimental data. In the case of TCN and EOS, equations were sectioned in parts according to time intervals where it was visually apparent that the curvature of the responses changed; the time-points of 3, 5, and 7 weeks were selected for TCN, and EOS was split at 7 weeks. Through the incorporation of data from additional doses and time-points, the model proved to be modular, i.e. the inclusion of new data did not require the derivation of a new equation, but rather only re-adjustment of the existing model. After performing simulations with the *complex* models, it was determined that *simple* models would yield the general characteristics of each outcome with more clarity and conciseness. Such *simple* models were generated for TCN, EOS, IgG₁ and IgE using a single equation for all time-points, as opposed to defining dose-responses piecewise. 2D comparison of actual data and simulated data was visualized in SigmaPlot software (Systat Software Inc.), while 3D simulation images were generated using Microsoft Excel 2007.

The following sets of equations describe the dynamics of each measured outcome (y) in the context of dose (x , in μg of HDM) and time (t , in weeks).

TCN (Complex)

$$y = f_C^{TCN}(x, t) = \begin{cases} x_{a1} + x_{b1} \sin(z_1(x, t))^2 & , 0 \leq t \leq 3 \\ x_{a2} + x_{b2} e^{z_2(x, t)} + x_{g2} t + x_{h2} t^2 & , 3 \leq t \leq 7 \\ x_{a3} + x_{b3} e^{z_3(x, t)} + x_{g3} e^{z_4(x, t)} & , t \geq 7 \end{cases} \quad (1)$$

where,

$$z_1 = \frac{\pi(t - x_{c1})}{x_{d1}} \quad (1.1)$$

$$z_2 = -0.5 \left(\frac{t - x_{c2}}{x_{d2}} \right)^2 \quad (1.2)$$

$$z_3 = -0.5 \left(\frac{t - x_{c3}}{x_{d3}} \right)^2 \quad (1.3)$$

$$z_4 = - \left(\frac{t - x_{h2}}{x_{k2}} \right) \quad (1.4)$$

$$x_{a1} = 1.172 - 0.516 e^{-0.5 \left(\frac{x - 12.955}{12.284} \right)^2} \quad (1.5)$$

$$x_{b1} = -0.245 + \frac{4.171}{\left(1 + 10^{-0.103(x + 0.252)} \right)^{3.802}} \quad (1.6)$$

$$x_{c1} = 0.029 + 0.377 \sin \left(\pi \left(\frac{x - 0.066}{24.889} \right) \right)^2 \quad (1.7)$$

$$x_{d1} = \frac{3.361 + 0.289x + 0.004x^2 - 0.178x^3}{1 + 0.280x + 0.0002x^2 - 0.037x^3} \quad (1.8)$$

$$x_{a2} = \begin{cases} 0.996 - 0.056x + 0.049(0.377^x) & , 0 \leq x \leq 5 \\ 5.338 \left(1 - e^{-\left(0.065(x-4.382)^{0.606}\right)} \right) & , x > 5 \end{cases} \quad (1.9)$$

$$x_{b2} = \begin{cases} -0.055 + 0.229x - 0.007x^2 & , 0 \leq x \leq 5 \\ -0.039 + \frac{0.958}{1 + \left(\frac{x-5.050}{10.092}\right)^{0.167}} & , x > 5 \end{cases} \quad (1.10)$$

$$x_{c2} = \begin{cases} \frac{x + 0.157}{0.006 + 0.220(x + 0.157) - 0.005(x + 0.157)^2} & , 0 \leq x \leq 5 \\ 5.208 - \frac{9.888}{x} + \frac{47.078}{x^2} & , x > 5 \end{cases} \quad (1.11)$$

$$x_{d2} = \begin{cases} 1.166 + \frac{0.948}{1 + \left(\frac{x}{2.152}\right)^{0.438}} & , 0 \leq x \leq 5 \\ \frac{x - 4.562}{0.103 + 0.401(x - 4.562) + 0.013(x - 4.562)^2} & , x > 5 \end{cases} \quad (1.12)$$

$$x_{g2} = \begin{cases} 0.014 + 0.002x + 0.0001x^2 & , 0 \leq x \leq 5 \\ 0.149 - \frac{3.067}{x} + \frac{12.508}{x^2} & , x > 5 \end{cases} \quad (1.13)$$

$$x_{h2} = \begin{cases} -0.007 + 0.004x + 0.0006x^2 & , 0 \leq x \leq 5 \\ 0.039 + 0.002x^{0.524} - 0.0004x^{1.478} & , x > 5 \end{cases} \quad (1.14)$$

$$x_{a3} = \begin{cases} \frac{0.298 + 0.657x - 0.020x^2}{x - 4.749} & , 0 \leq x \leq 5 \\ \frac{-0.024 + 0.423(x - 4.749) - 0.008(x - 4.749)^2}{x - 4.749} & , x > 5 \end{cases} \quad (1.15)$$

$$x_{b3} = \begin{cases} -0.455 - 0.216\sqrt{x} + 0.347x & , 0 \leq x \leq 5 \\ -5.056 + 6.237e^{\frac{-(\ln(x)-2.075)^2}{3.487}} & , x > 5 \end{cases} \quad (1.16)$$

$$x_{c3} = \begin{cases} \frac{9.212 + 5.586x}{1 + 0.431x - 0.013x^2}, & 0 \leq x \leq 5 \\ 3.101 + 10.475e^{-\frac{(\ln(x)-2.033)^2}{3.914}}, & x > 5 \end{cases} \quad (1.17)$$

$$x_{d3} = \begin{cases} \frac{4.064 + 1.785e^{-\frac{x}{1.797}} - 2.582e^{-\frac{x}{5.497}} - 1.547e^{-\frac{x}{6.004}}}{x - 4.505}, & 0 \leq x \leq 5 \\ \frac{-0.194 + 0.808(x - 4.505) - 0.016(x - 4.505)^2}{x - 4.505}, & x > 5 \end{cases} \quad (1.18)$$

$$x_{g3} = \begin{cases} 0.019 - 0.066x + 0.739(0.246^x), & 0 \leq x \leq 5 \\ -0.316 + 6.708e^{-\frac{(x-5.078)}{9.779}} \left(1 - e^{-\frac{(x-5.078)}{13.719}} \right)^{0.489}, & x > 5 \end{cases} \quad (1.19)$$

$$x_{h3} = \begin{cases} 4.527 - 1.986e^{-\frac{x}{0.213}} + 3.123e^{-\frac{x}{9.057}}, & 0 \leq x \leq 5 \\ 1.127 \left(\frac{x}{-3.863 + x} \right) + 3.257 \left(\frac{x}{28.574 + x} \right) + 0.178x, & x > 5 \end{cases} \quad (1.20)$$

$$x_{k3} = \begin{cases} 5.291 + 30.559e^{-3.157x}, & 0 \leq x \leq 5 \\ 7.844 + \frac{-2.847}{1 + \left(\frac{x-4.997}{9.340} \right)^{0.269}}, & x > 5 \end{cases} \quad (1.21)$$

TCN (Simple)

$$y = f_S^{TCN}(x, t) = \frac{x_a + x_b t + x_c t^2}{1 + x_d t + x_g t^2} \quad (2)$$

where,

$$x_a = 0.989 + 0.046 \left(\frac{0.665}{1 + 10^{0.407(x-6.214)}} \right) + 0.045 \left(\frac{1 - 0.665}{1 + 10^{-0.097(x-18.773)}} \right) - 1.4 \quad (2.1)$$

$$x_b = 0.187 + 1.091 \left(\frac{0.978}{1 + 10^{-0.571(x-6.389)}} \right) + 1.091 \left(\frac{1 - 0.978}{1 + 10^{-0.081(x-18.780)}} \right) \quad (2.2)$$

$$x_c = 0.378 + 1.137e^{-0.5 \left(\frac{x-7.548}{0.595} \right)^2} - 0.239e^{-\left(\frac{x-0.876}{12.035} \right)} \quad (2.3)$$

$$x_d = 0.009 + 1.995 \left(\frac{1}{1 + e^{-\frac{x-0.638}{0.273}}} \right) \left(1 - \frac{1}{1 + e^{-\frac{x-0.638}{41.471}}} \right) \quad (2.4)$$

$$x_g = 0.142 + 0.473e^{-0.5\left(\frac{x-7.155}{1.063}\right)^2} + 0.050e^{-\left(\frac{x-0.326}{12.839}\right)} \quad (2.5)$$

EOS (Complex)

$$y = f_C^{EOS}(x, t) = \begin{cases} x_{a1} + x_{b1}e^{z_1(x,t)} + x_{g1}e^{z_2(x,t)} & , \quad 0 \leq t \leq 7 \\ x_{a2} + x_{b2}t + x_{c2}t^2 + x_{d2}t^3 & , \quad t \geq 7 \end{cases} \quad (3)$$

where,

$$z_1 = -0.5 \left(\frac{t - x_{c1}}{x_{d1}} \right)^2 \quad (3.1)$$

$$z_2 = -0.5 \left(\frac{t - x_{h1}}{x_{k1}} \right)^2 \quad (3.2)$$

$$x_{a1} = \frac{-0.018 + 0.106x - 0.145x^2 - 0.005x^3}{1 + 0.096x - 0.151x^2 - 0.005x^3} \quad (3.3)$$

$$x_{b1} = \frac{0.057x^{1.633}}{1 + 0.036x^{1.633}} \quad (3.4)$$

$$x_{c1} = 2.595 - 2.021e^{\frac{-x}{10.062}} + 2.935e^{\frac{-x}{32.085}} \quad (3.5)$$

$$x_{d1} = \frac{7.088 + 0.903x - 0.199x^2}{1 + 0.048x - 0.113x^2} \quad (3.6)$$

$$x_{g1} = \frac{0.045x^{2.665}}{1 + 0.031x^{2.665}} \quad (3.7)$$

$$x_{h1} = 10.578 + 0.234x - 0.019x^2 + 0.0004x^3 \quad (3.8)$$

$$x_{k1} = 7.078 - 0.097\sqrt{x} + 0.076x \quad (3.9)$$

$$x_{a2} = -0.233 \left(\frac{x}{0.553 + x} \right) + 0.508 \left(\frac{x}{4.993 + x} \right) + 0.176x \quad (3.10)$$

$$x_{b2} = \begin{cases} -0.066 + \frac{0.110}{1 + 10^{0.232x - 0.109}} & , \quad 0 \leq x \leq 5 \\ 0.335 - 0.019x & , \quad x > 5 \end{cases} \quad (3.11)$$

$$x_{c2} = \frac{x}{512.820 + 205.158x + 324.354\sqrt{x}} \quad (3.12)$$

$$x_{d2} = 2.590E^{-06} - 1.509E^{-05}x + 5.980E^{-07}x^2 \quad (3.13)$$

EOS (Simple)

$$y = f_S^{EOS}(x, t) = \left| \frac{t + x_a}{x_b + x_c(t + x_a) + x_d(t + x_a)^2} \right| \quad (4)$$

where,

$$x_a = -0.047 - 0.019 \ln(x + 0.081) \quad (4.1)$$

$$x_b = 3.737 + 46.203e^{\frac{-(x-0.180)}{2.148}} \left| 1 - e^{\frac{-(x-0.180)}{12.861}} \right|^{0.145} \quad (4.2)$$

$$x_c = -0.615 + 5.029e^{-0.987x} \quad (4.3)$$

$$x_d = 0.200 + \frac{7.909}{1 + 10^{1.439x - 1.389}} \quad (4.4)$$

IgE (Simple)

$$y = f_S^{IgE}(x, t) = \frac{x_a t^{x_d}}{x_c^{x_d} + t^{x_d}} \quad (5)$$

where,

$$x_a = 0.272 \left(1 - e^{(-0.297(x-0.015))^{1.819}} \right) \quad (5.1)$$

$$x_c = 6.737 + 70.018 \left(\frac{20.601}{4(x - 1.682)^2 + 20.601^2} \right) \quad (5.2)$$

$$x_d = \frac{17.942 + 9.965x^{1.562}}{9.111 + x^{1.562}} \quad (5.3)$$

IgG₁ (Simple)

$$y = f_S^{IgG_1}(x, t) = x_a + \frac{x_b - x_a}{1 + \left(\frac{t}{x_c}\right)^{x_d}} \quad (6)$$

where,

$$x_a = \frac{x}{1.06E^{-05} + 4.583E^{-06}x - 4.237E^{-06}\sqrt{x}} \quad (6.1)$$

$$x_b = \frac{-244.738x}{1.527 + x} \quad (6.2)$$

$$x_c = 5.752 + \frac{4.489}{1 + 10^{0.855(x-1.261)^{0.182}}} \quad (6.3)$$

$$x_d = 2.133 + \frac{7.243x}{1.915 + x} + \frac{-8.133x}{16.102 + x} \quad (6.4)$$

*Note: All numerical coefficients above are given to 3 decimal places for brevity, however all equations were computed using the full coefficients as derived by the model.

Validation analysis

Linear regression analysis and 95% CI were used to validate the mathematical models since they are deterministic and non-deterministic approaches, respectively [1]. *Deterministic validation metric:* Actual data was plotted against model data and linear regression performed with the condition that the regression line must pass through (0,0). The possible goodness of fit statistic, R^2 (coefficient of determination), was calculated. An R^2 of 1 would mean that all values of actual data and model data are equal and thus lie upon the line $y=x$. *Non-deterministic validation metric:* 95% CIs were created using the

appropriate t probability distribution ($t_{0.05, df}$), depending on the number of degrees of freedom (number of mice sacrificed minus 1) at each time (t) and dose (x) with an α of 0.05. In addition, as proposed by Oberkampff, *et al.* [2], global validation metrics to quantify overall model accuracy were calculated as follows:

$$\text{Average Relative Accuracy of Model} = 1 - \left[\frac{1}{x_{\max}} \int_0^{x_{\max}} \frac{1}{t_{\text{final}}} \int_0^{t_{\text{final}}} \left| \frac{\bar{y}_a - y_m}{y_a} \right| dt dx \right]$$

where y_a is the actual mean (obtained from experiment), y_m is the predicted mean (virtual data). Definite integrals, estimated by trapezoidal Riemann sum, are used instead of straight summation in order to be able to assess predictive (interpolation) capabilities of each model. A similar method is applied to calculate the confidence indicator (half-width 95% CIs are averaged over both time and dose):

$$\text{Confidence Indicator} = \left[\frac{1}{x_{\max}} \int_0^{x_{\max}} \frac{1}{t_{\text{final}}} \int_0^{t_{\text{final}}} \frac{SD}{\sqrt{n_{t,x}}} \frac{t_{0.05,df}}{y_a} dt dx \right]$$

The average relative accuracy of the model, in line with assessment using linear regression, respectively calculated our initial, second and final *complex* TCN models to be $94.23 \pm 21.55\%$, $95.49 \pm 22.67\%$ and $97.50 \pm 22.42\%$ accurate (to a maximum of a 100%) with 95% confidence. Comparing between *complex* and *simple* TCN models, the *complex* TCN model again provides slightly more accurate predictions than the *simple* model, $97.50 \pm 22.42\%$ versus $89.03 \pm 22.42\%$ accuracy with 95% confidence. Further, our models (both *simple* and *complex*) fall within the 95% CI band meaning that there is a high probability for our model

to be able to predict real responses. Comprehensive non-deterministic analysis supports our findings from linear regression and allows for inferences to be made about our models' predictive capabilities.

Area under curves

For each outcome (IgG₁ and EOS), equations that represented each increment of 0.5µg HDM, dose-response curves were exported into Wolfram Mathematica software (Wolfram Research Inc.) to calculate the definite integral from 0 to 20 weeks of each equation.

REFERENCES:

1. Anderson AE, Ellis BJ, Weiss JA. Verification, validation and sensitivity studies in computational biomechanics. *Comput Methods Biomech Biomed Engin* 2007;10:171-184.
2. Oberkampf WLB, M.F. Measures of agreement between computation and experiment: Validation metrics. *Journal of Computational Physics* 2006;217:5-36.

CHAPTER 3**Modelling of House Dust Mite-Induced
Chronic Airway Eosinophilia**

Marc Colangelo¹, Alba Llop-Guevara¹, Ramzi Fattouh¹, Tina D. Walker¹,
Susanna Goncharova¹, Miroslav Lovric², and Manel Jordana¹

¹Department of Pathology and Molecular Medicine, Division of Respiratory Diseases and Allergy, Centre for Gene Therapeutics, and ²Department of Mathematics and Statistics, McMaster University, Hamilton, Ontario, Canada

Submitted June 2011 to *Biology Direct*.

(Submission # 1429158914566452)

Reprinted under the Creative Commons Attribution License (CCAL).

See *Declaration of Academic Achievement* for details regarding authorship.

Summary and Central Message: This article extends the work presented in the previous chapter. Here, we sought to further investigate the behaviour and pattern exhibited by airway eosinophils, in response to HDM exposure. We developed a mechanistic mathematical model, representing the trafficking of eosinophils between the bone marrow, the blood and the lung (airways). The regulation and movement of eosinophils between compartments was represented by various processes, including eosinophil production, migration, death and survival. The model demonstrated that eosinophil production, death and survival had the greatest relative impact on airway eosinophilia, while migration elicited a minor role in comparison. Moreover, the model was able to simulate the effects changes in these processes, corresponding to the use of using knock-out models and antibodies. These findings further demonstrated that production and death would be the most suitable factors to be targeted in reducing levels of airway eosinophils.

Modelling of House Dust Mite-Induced Chronic Airway Eosinophilia

Marc Colangelo¹, Alba Llop-Guevara¹, Ramzi Fattouh¹, Tina D Walker¹, Susanna Goncharova¹, Miroslav Lovric² & Manel Jordana^{1§}

¹Department of Pathology and Molecular Medicine, Division of Respiratory Diseases and Allergy, Centre for Gene Therapeutics, McMaster University, Hamilton, Ontario, Canada

²Department of Mathematics and Statistics, McMaster University, Hamilton, Ontario, Canada

[§]Corresponding author

Email addresses:

MC: colangmp@mcmaster.ca

AL-G: llopa@mcmaster.ca

RF: ramzi.fattouh@sickkids.ca

TDW: twalker@mcmaster.ca

SG: goncharo@mcmaster.ca

ML: lovric@mcmaster.ca

MJ: jordanam@mcmaster.ca

Abstract

Background

Allergic asthma is a complex disease of the airways that develops as a consequence of an aberrant immune-inflammatory response to allergen exposure, with the distinct feature of eosinophilic inflammation in the lung. Importantly, knowledge on this disease has progressed largely from qualitative principles. We surmise that enhanced understanding may be achieved through the incorporation of mathematical approaches. Previously, we *empirically* modelled the evolution of immune-inflammatory responses, namely eosinophils, in the lung of mice exposed to a range of house dust mite (HDM) concentrations and showed that the relationship between allergen exposure and airway inflammation is nonlinear. While early (increasing) responses appeared to be dependent on the dose and length of exposure, later (decreasing) responses converged to similar levels. This observation presupposes a dynamic behaviour with the implication that the dynamics of the eosinophilic response may be influenced by additional factors other than dose and length of exposure.

Results

Here, we developed a *mechanistic* mathematical model to investigate the evolution of the eosinophilic response to continuous allergen exposure, using biological observations combined with mathematical assumptions. The model considers a simplified system in which eosinophils are present in three compartments: bone marrow, blood and lungs. In addition, we assume that the

number of eosinophils within each compartment varies according to rates that depend on production, migration and regulation (death, loss and survival).

Conclusions

The model identified eosinophil production, survival and death as having a prime importance in the dynamics of the response, while migration elicited a small influence. Interestingly, although production and survival exhibit dose-dependent patterns, death remains constant suggesting that fluctuations in the overall response are largely governed by changes in production and survival factors. This synergistic approach using immunological data and mathematical analysis provides a mechanistic description of airway eosinophilia dynamics and insight into areas that may be targeted for future experimentation.

Background

Allergic asthma, like other immune-inflammatory diseases, is a complex disease whereby exposure to antigens triggers an immune response that results in different degrees of inflammation severity. The complexity of the disease has been largely referred to as a means to illustrate the complicated nature of the extensive number of events of the immunological response [1, 2]. However, when analyzing this immunological response from a mathematical perspective, this complexity can adopt additional meanings including the sensitivity to initial system conditions or the tendency of the response to attract to particular values [3, 4]. This approach may provide quantitative principles to explain and understand the dynamics of the inflammatory response in the lung.

One of the distinctive hallmarks of allergic asthma is the presence of eosinophilic inflammation in the lung (airway) [5]. Understanding the dynamics of the eosinophil response over time will help to delineate factors initiating and regulating the response and thus, inform about the relative potential of distinct therapeutic targets. The identification of specific areas for experimentation and subsequent treatment through mathematical modelling advise experiments and, ultimately, expedite the research. From a qualitative perspective, the biological sequence of events in eosinophil trafficking, from their production in the bone marrow to their release into the circulation and recruitment and accumulation into the airways has been well documented [6-10]. Cellular trafficking and signaling has been mathematically modelled for a variety of other cell types, including

neutrophils [11, 12], basophils [13] and dendritic cells [14, 15], in several diseases but not in the context of asthma. Indeed, the dynamics of the eosinophil response in allergic asthma have yet to be studied using mathematical approaches.

Previously, our laboratory established an *in vivo* model of chronic allergic asthma in mice using house dust mite (HDM), the most pervasive aeroallergen worldwide [16]; subsequently, we employed an empirical mathematical approach to quantitatively analyze lung inflammation including eosinophilia [17]. This analysis showed that chronic allergen exposure and airway inflammation exhibit a nonlinear relationship; particularly interesting was the pattern of airway eosinophilia in that it followed a bell shaped-like curve. The data showed that early responses increased exponentially to a maximal value, which was dependent on both the dose and length of aeroallergen exposure. Later responses, following the peak response, converged downward to a residual plateau. This observation presupposes a dynamic behaviour intimating that the dynamics of the lung eosinophilic response is influenced by a number of intermediate factors.

While a number of different processes and key mediators affecting the dynamics of eosinophilia have been identified, their relative importance has yet to be quantitatively investigated in a system that takes into account dynamic interactions. Here, a model of extended eosinophilia involving up to 14 weeks of exposure to HDM in mice was used to evaluate the changes in eosinophils in

several compartments over time. Then, we developed a *mechanistic* mathematical model to examine changes in key compartments and processes based on a limited set of experimental data points. In this case, we use the term “*limited*” in reference to the various doses and time-points that would typically be used in our *in vivo* chronic exposure experiments. Data are collected at multiple time-points, in some cases at 1, 2, 3, 5, 7, 10, 14 and 20 weeks of exposure and multiple doses [17]. In this respect, our model used a relatively *limited* data set in comparison. This approach captured the complex nature of the system and permitted the simulation of various hypothetical scenarios. Furthermore, mathematical modelling identified the relative importance of the parameters governing the dynamics of the system in a way that would be exceedingly difficult using conventional immunological approaches.

Results & Discussion

Compartmentalized eosinophil responses

To develop a mathematical representation that accurately depicted the dynamics of eosinophils between compartments, a platform of experimental data was first established (Figure 2). Given our prior experience with *in vivo* models of allergic asthma using HDM exposure [5, 16, 18, 19], an important objective was to make use of a data set that was limited but sufficient to capture the complex nature of the system [17]. The expectation was that by using a combination of *in vivo* and *in silico* methods, relevant features of the system could be identified.

The dose-response dynamics in both short-term and long-term exposure to HDM has been previously characterized [5,16,19-21]. The system achieved a sub-maximal response at 25 $\mu\text{g}/\text{day}$ of HDM, while 7.5 $\mu\text{g}/\text{day}$ and 1 $\mu\text{g}/\text{day}$ elicited intermediate and minimal responses, respectively [17]. Thus, these doses were chosen, with the exception of the intermediate dose, in which 5 $\mu\text{g}/\text{day}$ was used instead of 7.5 $\mu\text{g}/\text{day}$ to maintain five-fold increases. In addition, experimental time-points were also selected based upon our previous experience. At a dose of 25 $\mu\text{g}/\text{day}$, airway eosinophils initially increase in a dose- and time-dependent manner to a maximal value after approximately 3 weeks of exposure. Following this peak, the response subsequently decreases considerably up to 14 weeks of exposure, with a further slow decline up to 20 weeks of exposure; the response does not resolve completely, but rather remains elevated at a smaller magnitude [17]. Consequently, time-points were

selected corresponding to the initial conditions (0 weeks), the zenith (2-3 weeks) and the nadir (14 weeks) of the system.

As shown in Figure 2A, bone marrow eosinophils increased throughout the entire duration of allergen exposure, ultimately approaching a plateau and, hence, maintaining the global amount of eosinophils produced and input into the system, particularly evident at 25 μg of HDM. In Figure 2B, blood eosinophils across all doses exhibited an initial increase and a subsequent decreasing trend up to 14 weeks of exposure following their peak response, with the exception of 5 μg . At 5 μg of HDM, the peak response occurred at a later time-point and remained elevated at a similar value of the 25 μg response at 14 weeks. This observation may explain the converging values of eosinophils in the lung for these doses at 14 weeks of exposure. Figure 2C shows that airway eosinophils at 25 μg peaked at 4 to 5 weeks, and then decreased up to 14 weeks. Interestingly, as shown by the 5 μg data peaking at 7 weeks, the magnitude of the peak response was dose-dependent, while the time at which the peak was achieved exhibited an inverse relationship to the dose.

Analysis of rates

Using the experimental data from each compartment, the hypothesized processes were determined mathematically through the model equations, to provide information on how each process would behave over time, at varying doses. Given that these processes were unknown with no corresponding experimental data, they were calculated as rates (at static time points) and

normalized (between 0 and 1), which represented the degree at which a process occurred. For example, a production rate of 1 would represent maximum production of eosinophils, whereas a production rate of 0 would signify minimal or no production.

As shown in Figure 3A, eosinophil production for all doses exhibited similar trends with an initial increase, followed by a plateau. This general pattern mimicked the dynamics of eosinophils in the bone marrow, which was expected given that eosinophils are produced in this compartment. As shown in Figures 3B and 3C, both the rates of migration from the bone marrow to the blood and from the blood to the lungs, respectively, did not appear to have any dose or time related patterns. Similarly, loss from the bone marrow and blood did not have any consistent trends among the dose of HDM (Figures 3D & 3E, respectively). These findings suggested that these processes may not have a direct contribution to global changes in airway eosinophilia in relation to the amount of HDM delivered to the system. Throughout the construction of the model, eosinophil survival and death were modelled as separate processes, given that various biological signals distinctively impact one of these processes, but not necessarily the other. Consequently, we assumed that these processes are mutually exclusive and both survival and death may be both independently and simultaneously regulated at any time. Figure 3F shows that the rate of eosinophil survival increased slightly with respect to dose. Contrastingly, as shown in Figure 3G, death remained largely consistent across all doses of HDM, suggesting that

the rate of eosinophil death, presumably apoptosis, is an inherent feature that does not depend on the amount of allergen introduced into the system.

The model identified eosinophil production, survival and death as having a greater influence, in comparison to migration and loss between compartments in the extent of lung eosinophilia. The significance of these findings would be that future *in vivo* experiments should preferentially target these processes for therapeutic effects. Indeed, eosinophil migration overall between the compartments appeared to have a less substantial effect in contrast to other processes. The various mechanisms contributing to eosinophil migration have been investigated, but not fully identified to the extent of eosinophil production, survival and death. Tissue eosinophilia was observed in experimental models with mice despite a deficiency in the prominent eosinophil chemokine eotaxin [20]. This model, however, in connection to our model, used a significantly different protocol (single challenge) involving a different antigen (OVA), strain (129SvEv). Further studies have shown lung eosinophils are present in the absence of CCR3, a receptor on eosinophils that recognizes chemokines, including eotaxin [21]. These findings collectively suggest that factors contributing to eosinophil migration play a less substantial role in the development of eosinophilia as compared to production, survival and death factors.

Simulating eosinophil responses

Simulations were performed for each compartment at all of the experimentally used doses to test the accuracy of both the equations and rate values generated by the model. In this case, simulations were confined to the time-points corresponding to the data set used to build the model, although the model would be able to simulate additional points upon the interpolation of the rates. Figures 4A and 4B, exposure to saline and 1 μg , respectively, show that the model was able to accurately capture the dynamics of the eosinophil response to low doses of HDM in the bone marrow, blood and lungs. In Figure 4C, exposure to 5 μg , eosinophils in the lung first exhibited an elevated response, with an initial increase to a peak value, followed by a decline. The 3-week time point, which was initially used in the model to represent the peak response, did not correspond to the peak response in the lungs for doses between 1 and 5 μg (data not shown). Thus, the model was expanded to include a fourth data point (5 weeks of exposure) to perform simulations at 5 μg . This inclusion allowed for a clear improvement in the fit of the model at this dose. As shown in Figure 4D, the modelled data 25 μg of HDM was able to capture the trends of the initial increases in the response, to the peak of the response, and either a maintenance (in the case of the bone marrow) or decrease to a plateau (in the case of the blood and lungs). The simulated data from the model fit the experimental data well, and captured the dynamics of within each compartment over 14 weeks of exposure.

Simulating changes in rates

Having previously performed simulations on the dose-response dynamics over time and determined the dose that leads to a maximal response in the system [17], subsequent *in silico* experiments in this model were limited to the dose of 25 $\mu\text{g}/\text{day}$ of HDM. To assess the precise global impact that each process has on the level of airway eosinophilia, simulations were performed. Although each process was not associated with a single biological signal (i.e. cytokine or chemokine), each was assumed to effectively represent a major component involved in the system at large. As each rate was changed, all other rates were held constant, thereby obtaining a response that could be attributed to that specific change.

A baseline simulation was identified as the simulation of lung eosinophilia at 25 μg of HDM (Figure 3D), and the values of the corresponding rates. Based upon their dose-response over time, changes in the eosinophil production, survival and death rates were initially changed by $\pm 100\%$ of the baseline values. Although some simulations may not have direct biological significance, given that 25 μg of HDM has shown to elicit a maximal response in the system, each scenario was considered in order to investigate the mathematical properties of the equations (i.e. would an increase and decrease in a rate by the same amount elicit equal changes in magnitude from baseline?). The area under the curve (AUC) for each simulation was calculated and compared to baseline, thus resulting in an overall percentage change. This value represented the global

change in airway eosinophils over 14 weeks of exposure. As shown in Figure 5A, increases in the production, migration (from *B* to *L*) and survival rates resulted in the most significant increases in the lung eosinophils (+81.8%, +181.4% and +126.4% change, respectively), whereas a decrease in the production rate and increase in the death rate resulted in the greatest reductions (-81.8% and -94.7% change, respectively).

Given the dose-response trends of each rate (Figure 3), and that a decrease in the migration (from *B* to *L*) rate elicited a non-determinable response, temporal simulations were only performed with the production, survival and death rates, as they showed the greatest overall changes. Of these three rates, Figure 5B shows that only changes (both positive and negative) in the production rate elicited the same absolute change from baseline. In other words, the difference from baseline simulating a +100% change was equal to the difference when simulating a -100% change. With respect to the survival rate, as shown in Figure 5C, a greater change from the baseline simulation occurred when simulating a +100% change, as opposed to a negative change. Interestingly, as illustrated in Figure 5D, positive and negative changes in the death rate showed great impacts in the simulations, both eliciting low levels of airway eosinophilia. The contrasting differences that occurred when altering these rates, both positively and negatively, informs about the distinct sensitivity of the system to various biological processes. In this case, sensitivity was defined as the system's responsiveness to changes in a given rate, specifically the

overall change in airway eosinophilia when simulated over 14 weeks with an altered rate.

This sensitivity was analyzed in greater detail through simulations ranging from baseline values to a 100% reduction, decreasing at 10% intervals. In the case of eosinophil production in Figure 6A, as the reduction in the rate increased, the level of eosinophils in the lung reduced at equal intervals at week 3. As shown in Figure 6D, this observation was further confirmed numerically, as indicated by the consistent distance between simulated curves. At week 14, simulations reduced equally also, although at a smaller magnitude. On the other hand, both eosinophil survival and death exhibited different trends. For both rates, at lower percentages of reduction, the distance between simulations at week 3 were larger, and decreased as the reductions continued to increase (Figures 6B & 6C, respectively). Survival and death did differ in behaviour at 14 weeks. Figure 6B shows that as the survival rate decreased, the simulated responses maintained equidistant differences. On the other hand, as shown in Figure 6D, decreases in the death rate resulted in simulations that maintained the same pattern as they did at 3 weeks. In addition, the values of each response in each simulation approached similar values at 14 weeks (Figure 6E). This suggests that despite any variations in the parameters, the system is attracted to particular values after 14 weeks of exposure, at approximately 0.1×10^6 cells.

Simulations involving a change in these processes were used to hypothesize and perform *in silico* experiments that would be representative of

potential *in vivo* experiments. Although each rate was not directly associated with a single molecular signal, there was an inherent association between each rate (process) and a mechanistic component of the system. For example, eosinophil production in the bone marrow is driven by several factors, principally interleukin (IL)-5 [2, 7, 22, 23]. As such, simulating a complete reduction in the production rate would likely be synonymous to using an IL-5 knockout experimental model, whereas varying degrees of reduction would equate to IL-5 antibody treatments using anti-IL-5. As shown in Figures 5B and 6A, reductions in the production rate resulted in significant decreases, although not a complete resolution, in the overall airway eosinophil response over 14 weeks, of eosinophilia.

Despite varying protocols, particularly the use of an alternative allergen ovalbumin (OVA), the model simulations generated exhibited trends that are consistent with *in vivo* experiments in the literature. In one study using IL-5 knockout (KO) mice, results showed that lung eosinophils were virtually eradicated up to approximately four weeks following the initial exposure to allergen [24]. This mimics the decrease shown in the simulations involving a complete reduction in the eosinophil production parameter. Furthermore, the decrease shown in IL-5 KO mice occurred at a similar time-point at which eosinophilia in our experimental model achieves a peak response (Figure 2). Interestingly, another model, despite using combined gene transfer of both IL-5 and eotaxin in IL-5 KO mice, found that the addition of eotaxin failed to induce a significant increase in eosinophilia as compared to control IL-5 KO mice [25]. The

results of this study suggest that indeed the effects of eosinophil production may be of greater relevance to eosinophilia, in comparison to migration. Studies in which IL-5 antibody was administered also showed decreases in eosinophils for both human [26] and animal [27, 28] models. Using an anti-IL-5 antibody, one study was able to show a 79% mean decrease in BAL eosinophils in humans [28]. When varying amounts of antibody were used in mice, the magnitude of the decrease exhibited by anti-IL-5 antibody was amplified as the quantity of antibody was increased [27]. Likewise, our simulations showed that as eosinophil production was gradually reduced, eosinophils decreased as well. A further study made use of IL-3, IL-5 and granulocyte-macrophage colony-stimulating factor (GM-CSF) antibodies, both individually and in combination [29]. While IL-3 and GM-CSF antibodies partially reduced the number of lung eosinophils, IL-5 antibody was more effective. With the understanding that GM-CSF may promote eosinophil survival [18], these findings are aligned with our simulations showing that decreases in eosinophil production exhibit lower levels of eosinophilia compared to decreases in eosinophil survival (Figures 6A and 6B).

Conclusions

The eosinophil is thought to be a central mediator in the pathogenesis of allergic asthma [10]. However, which process in the sequence leading to lung eosinophilia is best suited as a therapeutic target remains to be fully elucidated [20, 29-31]. Here, we have presented a mechanistic model for the development of airway eosinophilia in response to the most pervasive aeroallergen worldwide, house dust mite. We have investigated the dynamics of the eosinophilic response in the bone marrow, blood and lungs mathematically in order to reveal information on the system dynamics. Using 3 to 4 data points per dose, we found that the model was able to encapsulate the experimental data and provide a representation of the patterns among each compartment, particularly in the bone marrow and the blood (Figure 4). In the lungs, however, the dose-response trends did benefit from an additional data point, as shown by the 5 μg data. Importantly, the model revealed which processes involved in the development of airway eosinophilia have the greatest relative impact on the system as a whole (Figure 5). Through these simulations, eosinophil death was the most sensitive to changes, while eosinophil production and survival showed substantial but slightly less sensitivity when changed (Figure 6). In comparison, eosinophil migration between compartments showed no consistent patterns between each of the doses used, as well as insignificant effects on the system as a whole. Although HDM is certainly not the only allergen that elicits eosinophilia, it is likely that other models of eosinophilia would share similar dynamics and compartmentalization,

as well as regulation by the same processes investigated herein. Through mathematical analysis of the development of airway eosinophilia, future experimentation may not require extensive data sets, but rather development of the system model. Such analysis could identify which rates showing the greatest effects in minimizing eosinophilia, as well as determining optimal therapeutic strategies.

Methods

Mathematical Model

With the understanding that the eosinophilic response in the airway is influenced by the production, migration and regulation of eosinophils between and within compartments, the model accounts for these events in a simplified system, as illustrated in Figure 1. Eosinophils are considered to be present in three compartments: bone marrow (*BM*), blood (*B*) and lungs (*L*). The number of cells within each compartment varies according to the dose of HDM (*E*) and rates representing the range of cellular processes involved in each compartment. As outlined in Table 1, seven processes are represented in the model. The number of eosinophils in each compartment varies according to the general equation:

$$\frac{dCells}{dt} = \text{Input} - \text{Output} \pm \text{Regulation}$$

where *input* represents production of new eosinophils or immigration of eosinophils to a compartment and *output* considers eosinophil death or emigration of eosinophils from a compartment. The final term, *regulation*, represents the death, loss or survival, of eosinophils between compartments given that the system is not contained (i.e. the number of eosinophils produced will not be maintained throughout the flow of the system). The number of eosinophils within each compartment is described by a set of ordinary differential equations:

Bone Marrow Eosinophils

Bone marrow eosinophils represent the initial input of cells in the system, given that eosinophils are produced solely in this compartment. The change in the number of eosinophils in the bone marrow over time (t) is described by the equation:

$$\frac{dBM(E,t)}{dt} = k_P - k_E \cdot BM(E,t) - k_A \cdot BM(E,t)$$

where k_P represents the rate of eosinophil production, k_E is the rate of bone marrow eosinophil migration to the blood, and k_A is the rate of loss as bone marrow eosinophils migrate and/or die.

Blood Eosinophils

Following production in the bone marrow, eosinophils then migrate into the blood circulation, from where they may eventually migrate into the lungs. The rate of change in the number of eosinophils in the blood is given by the equation:

$$\frac{dB(E,t)}{dt} = k_E \cdot BM(E,t) - k_I \cdot B(E,t) - k_B \cdot B(E,t)$$

where k_E represents the rate of bone marrow eosinophils immigrating into the blood, k_I represents the number of blood eosinophils emigrating to the lungs, and k_B is the rate of loss as blood eosinophils migrate to other tissues and/or die.

Lung Eosinophils

Lastly, the change in the number of eosinophils in the lungs with respect to time is represented as:

$$\frac{dL(E,t)}{dt} = k_I \cdot B(E,t) - k_D \cdot L(E,t) + k_S \cdot L(E,t)$$

where k_I represents the rate of blood eosinophils immigrating into the lungs, k_D represents the rate of lung eosinophil death, and k_S is the rate of lung eosinophil survival.

Parameter Estimation

In order to determine the parameter values, experimental data were used to solve the set of equations at a given dose and time-point. Initially, holding the dose of HDM constant, the general solution of $BM(t)$ was solved for all possible combinations of k_P , k_E and k_A , at a given dose, that fell within $\pm 20\%$ of the mean experimental data, thus yielding a set of solutions. The $\pm 20\%$ range was chosen arbitrarily to limit the solutions within an acceptable variance of the experimental data. This set was tested to solve for combinations of k_I and k_B that satisfied the same requirements for $B(t)$. This refined set was, then, further tested to determine the combinations of k_D and k_S that satisfied $L(t)$. Therefore, the resulting set consisted of parameter values that satisfied $BM(t)$, $B(t)$ and $L(t)$. Lastly, this set was further refined to include only the parameter values that elicited solutions within a $\pm 5\%$ range of the mean experimental data. In some instances, there were unique solutions for a given dose and time. In the event of multiple solutions, the average of the solutions was taken. This process was repeated for each dose used in the experimental protocol (saline, 1, 5, or 25 μg HDM).

Equation Solving

All equations were encoded in Mathematica 6.0.2.1 (Wolfram, Chicago, IL), in order to solve for $BM(t)$, $B(t)$ and $L(t)$. Unknown parameters were initially solved for using the set of differential equations and three experimental data points for each compartment (0, 3 and 14 weeks). Although eosinophils in each compartment and at each dose had varying number of experimental data-points, only 3 to 4 time-points were used to determine the rates computationally and perform simulations. The resulting equations were then used to simulate cell quantities over time. Areas under the curve were calculated using Mathematica through the integration of each equation over the specified time intervals. For the general and equilibrium solutions for all model equations, see additional file 1: Equation solutions.

Experimental Methods

Animals

Female BALB/c mice (6 to 8 weeks old) were purchased from Charles River Laboratories (Ottawa, ON). The mice were housed in a pathogen-free environment under a 12 hour light-dark cycle. The Animal Research Ethics Board of McMaster University approved all experiments described.

Protocol of Respiratory Mucosal Sensitization

House dust mite was prepared and delivered to mice as previously described [17]. Mice were exposed intranasally to 10 μ l of saline or HDM (1, 5, or

25 µg) daily for 5 consecutive days per week followed by 2 days of rest, for 1, 2, 3, 5, 7, 10 or 14 weeks.

Collection of Samples

For all experimental time-points, mice were sacrificed 72 hours following the final HDM exposure. Eosinophils from the bone marrow, blood and lungs were collected. For bone marrow eosinophils, the femurs from each mouse were excised and opened at both ends. A 25-gauge needle was inserted to collect the bone marrow by flushing each femur with 2 ml of phosphate-buffered saline (PBS). Blood and lung eosinophils were collected, and total cell and eosinophil counts were determined for each compartment as previously reported [17, 32, 33].

Competing interests

The authors declare that they have no competing interests.

Authors' contributions

MC conceived, designed and performed the experiments, analyzed the data, developed the mathematical model, and drafted the manuscript. AL-G conceived, designed and performed the experiments, analyzed the data, and participated in the analysis of biological samples. RF participated in performing the experiments and the analysis of biological samples. TDW participated in performing the experiments. SG performed the analysis of biological samples. ML participated in the development of the mathematical model and helped to draft the manuscript. MJ participated in the study design, analyzing the data, and helped to draft the manuscript.

Acknowledgements

The authors gratefully acknowledge D. Harnish, K. Arias and A. Al-Garawi for critical review of the manuscript; M. Serra-Julià, R. Eftimie and G. Wolkowicz for input on the mathematical modelling; and M. Colbert for secretarial assistance. MC is supported by an Ontario Graduate Scholarship and AL-G is supported by Fundación Caja Madrid (Spain). MJ holds a Senior Canada Research Chair. The funders had no role in study design, data collection and analysis, decision to publish, or preparation of the manuscript.

References

1. Denburg JA, Keith PK: **Eosinophil progenitors in airway diseases: clinical implications.** *Chest* 2008, **134**:1037-1043.
2. Radinger M, Lotvall J: **Eosinophil progenitors in allergy and asthma - do they matter?** *Pharmacol Ther* 2009, **121**:174-184.
3. Higgins JP: **Nonlinear systems in medicine.** *Yale J Biol Med* 2002, **75**:247-260.
4. Rickles D, Hawe P, Shiell A: **A simple guide to chaos and complexity.** *J Epidemiol Community Health* 2007, **61**:933-937.
5. Cates EC, Fattouh R, Johnson JR, Llop-Guevara A, Jordana M: **Modeling responses to respiratory house dust mite exposure.** *Contrib Microbiol* 2007, **14**:42-67.
6. Johansson AK, Sergejeva S, Sjostrand M, Lee JJ, Lotvall J: **Allergen-induced traffic of bone marrow eosinophils, neutrophils and lymphocytes to airways.** *Eur J Immunol* 2004, **34**:3135-3145.
7. Adamko D, Lacy P, Moqbel R: **Eosinophil function in allergic inflammation: from bone marrow to tissue response.** *Curr Allergy Asthma Rep* 2004, **4**:149-158.
8. Kariyawasam HH, Robinson DS: **The eosinophil: the cell and its weapons, the cytokines, its locations.** *Semin Respir Crit Care Med* 2006, **27**:117-127.

9. Rosenberg HF, Phipps S, Foster PS: **Eosinophil trafficking in allergy and asthma.** *J Allergy Clin Immunol* 2007, **119**:1303-1310; quiz 1311-1302.
10. Rothenberg ME, Hogan SP: **The eosinophil.** *Annu Rev Immunol* 2006, **24**:147-174.
11. Orr Y, Wilson DP, Taylor JM, Bannon PG, Geczy C, Davenport MP, Kritharides L: **A kinetic model of bone marrow neutrophil production that characterizes late phenotypic maturation.** *Am J Physiol Regul Integr Comp Physiol* 2007, **292**:R1707-1716.
12. Takumi K, Garssen J, de Jonge R, de Jong W, Havelaar A: **Release kinetics and cell trafficking in relation to bacterial growth explain the time course of blood neutrophils and monocytes during primary Salmonella infection.** *Int Immunol* 2005, **17**:85-93.
13. Wald JA, Salazar DE, Chen HY, Jusko WJ: **Two-compartment basophil cell trafficking model for methylprednisolone pharmacodynamics.** *J Pharmacokinet Biopharm* 1991, **19**:521-536.
14. Klink DJ, 2nd: **An age-structured model of dendritic cell trafficking in the lung.** *Am J Physiol Lung Cell Mol Physiol* 2006, **291**:L1038-1049.
15. Marino S, Pawar S, Fuller CL, Reinhart TA, Flynn JL, Kirschner DE: **Dendritic cell trafficking and antigen presentation in the human immune response to Mycobacterium tuberculosis.** *J Immunol* 2004, **173**:494-506.

16. Johnson JR, Wiley RE, Fattouh R, Swirski FK, Gajewska BU, Coyle AJ, Gutierrez-Ramos JC, Ellis R, Inman MD, Jordana M: **Continuous exposure to house dust mite elicits chronic airway inflammation and structural remodeling.** *Am J Respir Crit Care Med* 2004, **169**:378-385.
17. Llop-Guevara A, Colangelo M, Chu DK, Moore CL, Stieber NA, Walker TD, Goncharova S, Coyle AJ, Lundblad LK, O'Byrne PM, et al: **In vivo-to-in silico iterations to investigate aeroallergen-host interactions.** *PLoS One* 2008, **3**:e2426.
18. Cates EC, Fattouh R, Wattie J, Inman MD, Goncharova S, Coyle AJ, Gutierrez-Ramos JC, Jordana M: **Intranasal exposure of mice to house dust mite elicits allergic airway inflammation via a GM-CSF-mediated mechanism.** *J Immunol* 2004, **173**:6384-6392.
19. Johnson JR, Swirski FK, Gajewska BU, Wiley RE, Fattouh R, Pacitto SR, Wong JK, Stampfli MR, Jordana M: **Divergent immune responses to house dust mite lead to distinct structural-functional phenotypes.** *Am J Physiol Lung Cell Mol Physiol* 2007, **293**:L730-739.
20. Tomkinson A, Duez C, Cieslewicz G, Gelfand EW: **Eotaxin-1-deficient mice develop airway eosinophilia and airway hyperresponsiveness.** *Int Arch Allergy Immunol* 2001, **126**:119-125.
21. Humbles AA, Lu B, Friend DS, Okinaga S, Lora J, Al-Garawi A, Martin TR, Gerard NP, Gerard C: **The murine CCR3 receptor regulates both the role of eosinophils and mast cells in allergen-induced airway**

- inflammation and hyperresponsiveness.** *Proc Natl Acad Sci U S A* 2002, **99**:1479-1484.
22. Kay AB: **The role of eosinophils in the pathogenesis of asthma.** *Trends Mol Med* 2005, **11**:148-152.
23. Vodovotz Y, Csete M, Bartels J, Chang S, An G: **Translational systems biology of inflammation.** *PLoS Comput Biol* 2008, **4**:e1000014.
24. Foster PS, Hogan SP, Ramsay AJ, Matthaei KI, Young IG: **Interleukin 5 deficiency abolishes eosinophilia, airways hyperreactivity, and lung damage in a mouse asthma model.** *J Exp Med* 1996, **183**:195-201.
25. Mould AW, Matthaei KI, Young IG, Foster PS: **Relationship between interleukin-5 and eotaxin in regulating blood and tissue eosinophilia in mice.** *J Clin Invest* 1997, **99**:1064-1071.
26. Flood-Page PT, Menzies-Gow AN, Kay AB, Robinson DS: **Eosinophil's role remains uncertain as anti-interleukin-5 only partially depletes numbers in asthmatic airway.** *Am J Respir Crit Care Med* 2003, **167**:199-204.
27. Nagai H, Yamaguchi S, Inagaki N, Tsuruoka N, Hitoshi Y, Takatsu K: **Effect of anti-IL-5 monoclonal antibody on allergic bronchial eosinophilia and airway hyperresponsiveness in mice.** *Life Sci* 1993, **53**:PL243-247.
28. Shardonofsky FR, Venzor J, 3rd, Barrios R, Leong KP, Huston DP: **Therapeutic efficacy of an anti-IL-5 monoclonal antibody delivered**

- into the respiratory tract in a murine model of asthma.** *J Allergy Clin Immunol* 1999, **104**:215-221.
29. Tomaki M, Zhao LL, Sjostrand M, Linden A, Ichinose M, Lotvall J: **Comparison of effects of anti-IL-3, IL-5 and GM-CSF treatments on eosinophilopoiesis and airway eosinophilia induced by allergen.** *Pulm Pharmacol Ther* 2002, **15**:161-168.
30. Uller L, Persson CG, Erjefalt JS: **Resolution of airway disease: removal of inflammatory cells through apoptosis, egression or both?** *Trends Pharmacol Sci* 2006, **27**:461-466.
31. Vignola AM, Chiappara G, Gagliardo R, Gjomarkaj M, Merendino A, Siena L, Bousquet J, Bonsignore G: **Apoptosis and airway inflammation in asthma.** *Apoptosis* 2000, **5**:473-485.
32. Ohkawara Y, Lei XF, Stampfli MR, Marshall JS, Xing Z, Jordana M: **Cytokine and eosinophil responses in the lung, peripheral blood, and bone marrow compartments in a murine model of allergen-induced airways inflammation.** *Am J Respir Cell Mol Biol* 1997, **16**:510-520.
33. Stampfli MR, Wiley RE, Neigh GS, Gajewska BU, Lei XF, Snider DP, Xing Z, Jordana M: **GM-CSF transgene expression in the airway allows aerosolized ovalbumin to induce allergic sensitization in mice.** *J Clin Invest* 1998, **102**:1704-1714.

Tables

Table 1 - List of model rate parameters

The mathematical model considers the dynamics of eosinophils between three main compartments: bone marrow (BM), blood (B) and lungs (L). The quantity of cells within each compartment varies according to seven major processes outlined above. Both death and survival are considered to be independent active processes and, as such, are modelled separately. In other words, these processes are not mutually exclusive and both death and survival may be promoted simultaneously at any given time.

NAME	DESCRIPTION
k_P	Rate of eosinophil production (in BM)
k_E	Rate of eosinophil migration (from BM to B)
k_A	Rate of eosinophil loss (in BM)
k_I	Rate of eosinophil migration (from B to L)
k_B	Rate of eosinophil loss (in B)
k_S	Rate of eosinophil survival (in L)
k_D	Rate of eosinophil death (in L)

Figures

Figure 1 - Simplified visual model of eosinophil trafficking among compartments

Eosinophils are considered within three main compartments (BM, B and L), and increase and decrease based on seven major rates. The rate parameters used in the model are described in Table 1.

Figure 2 - Eosinophil experimental data in BALB/c mice exposed to HDM for up to 14 weeks

Mice were exposed intranasally to either saline (solid circles) or HDM, 1 μg (open circles), 5 μg (solid triangles) or 25 μg (open triangles) for up to 14 weeks. Eosinophils were collected in **(A)** bone marrow, **(B)** blood and **(C)** lungs. Cell numbers are expressed as means (n = 6-12 mice/group)

Figure 3 - Dose- and time-response dynamics of rate processes involved in eosinophil trafficking

Based on the experimental data, simulated rates were determined for saline (solid circles) or HDM, 1 μg (open circles), 5 μg (solid triangles) or 25 μg (open triangles) for up to 14 weeks, and normalized. **(A)** Eosinophil production for all doses exhibits similar trends with an initial increase, followed by a plateau. **(B)** and **(C)** Migration rates (from both the BM and B compartments showed no apparent dose or time related patterns. **(D)** and **(E)** Similarly, the rates of loss in

both the BM and B compartments showed no dose- or time-dependent dynamics. **(F)** The level of eosinophil survival increases slightly with respect to dose, with the exception of saline. **(G)** Contrastingly, death remains consistent across all doses of HDM, suggesting that eosinophil apoptosis occurs at a fixed rate and does not depend on the amount of allergen present in the system.

Figure 4 - Mathematical model simulations over 14 weeks of exposure to saline, 1, 5, and 25 μg of HDM

Simulations (red lines) were performed and compared to experimental data (black lines) over 14 weeks of exposure to **(A)** saline, **(B)** 1, **(C)** 5, and **(D)** 25 μg of HDM. In this case, simulations were confined to using time-points corresponding to the experimental data set used to build the model (0, 2/3, and 14 weeks). The simulated data was able to capture the trends of the initial increases in the responses, with the peak of the response, and either a maintenance or decrease to a plateau.

Figure 5 - Relative effects of individual model parameters on eosinophils in the lung at 25 μg of HDM

(A) Numerical analysis of simulated changes in model parameters at 25 μg of HDM. Changes in eosinophil production (k_P), survival (k_S), and death (k_D) rates were simulated at $\pm 100\%$ of the baseline simulation and the area under the curve (AUC) was calculated and compared to baseline values (*N.D. – Non-

Determinable). *In silico* experiments were performed to simulate increasing (small dashed lines) and decreasing (large dashed lines) the production, survival and death rates by $\pm 100\%$ of their original values, and compared to the baseline (red lines) lung eosinophil response. **(B)** Positive and negative changes in the production rate elicit the same absolute change from baseline. **(C)** A greater change from baseline occurred when simulating a +100% change in the survival rate, as opposed to a negative change. **(D)** Both positive and negative changes in the death rate elicit decreases in airway eosinophilia.

Figure 6 - Relative effects of individual model parameters on eosinophils in the lung at 25 μg of HDM

The system's sensitivity to production, survival and death rates is evident through simulations (black lines) ranging from baseline values (red lines) to a 100% change, decreasing, for **(A)** and **(B)**, or increasing, for **(C)**, at 10% intervals. **(A)** When altering production, eosinophils in the lung reduce at equal intervals at both week 3 and 14. **(D)** For both survival and death rates, the distance between simulations at week 3 decreases as the intervals increase, while the production rate maintains equal distances. **(E)** At 14 weeks, survival rate simulations remain equidistant, while survival and death rate simulations converge.

Figure 1

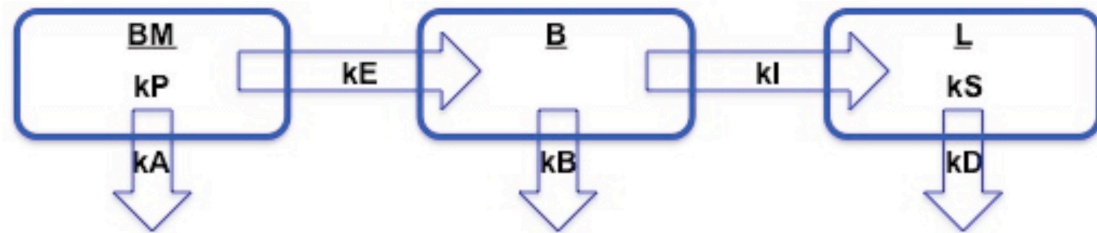


Figure 2

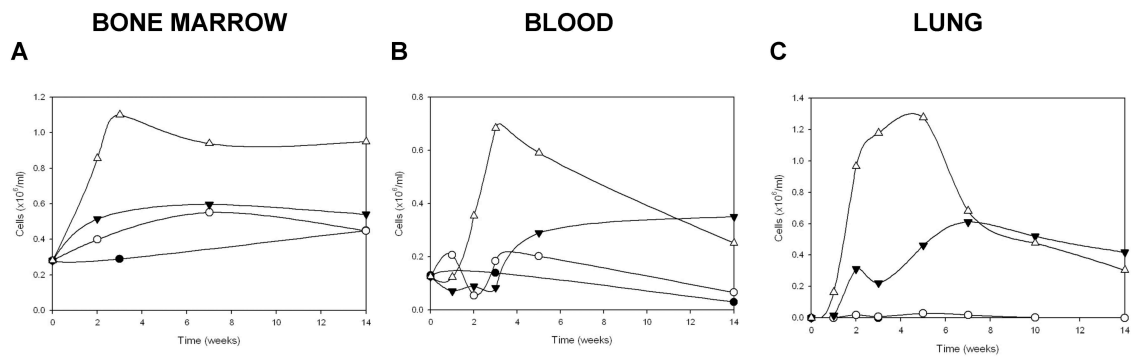


Figure 3

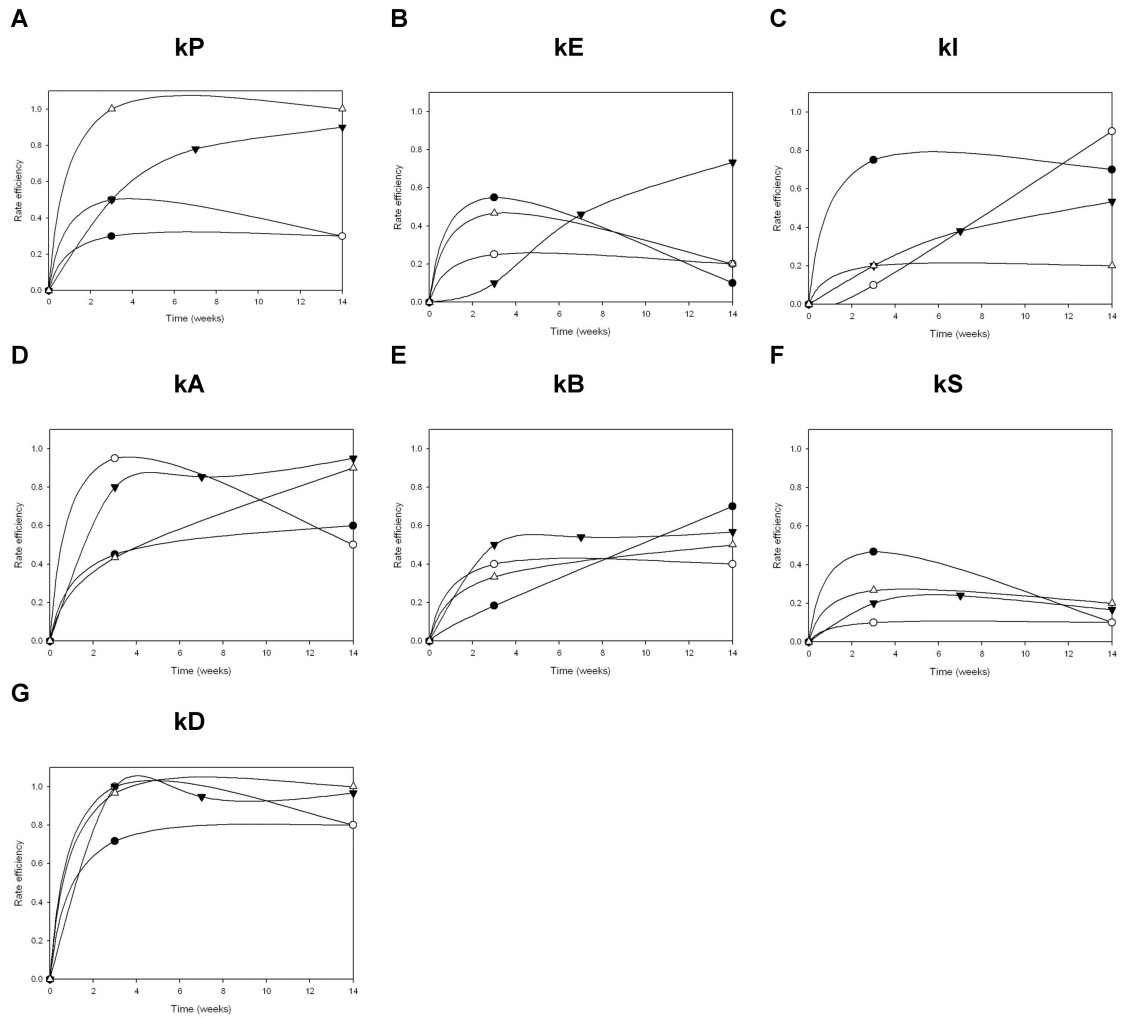


Figure 4

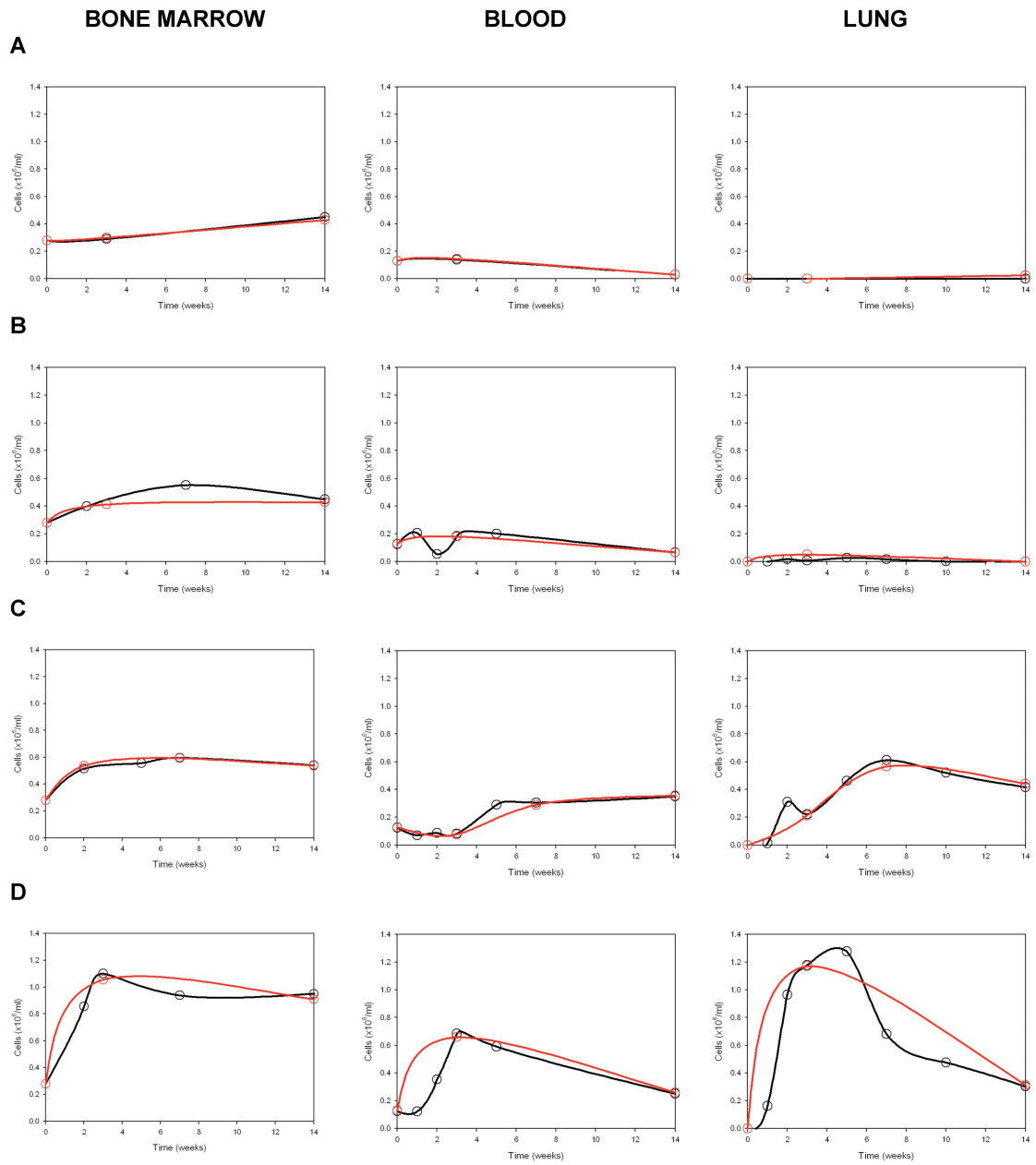
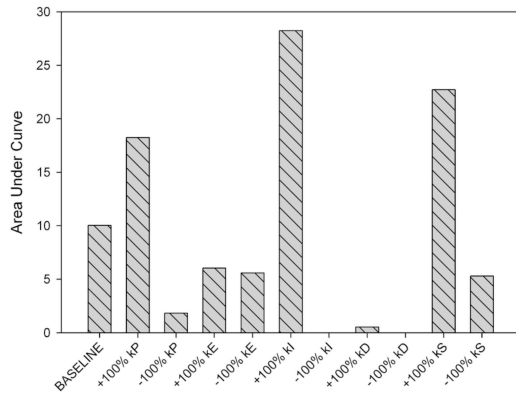


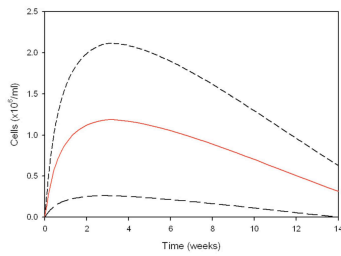
Figure 5

A

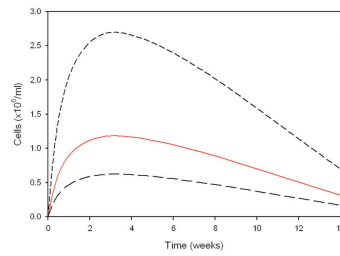


	AUC	% Change
Baseline	10.04	-
+ 100% k_P	18.25	81.8%
- 100% k_P	1.83	-81.8%
+ 100% k_E	6.05	-39.8%
- 100% k_E	5.59	-44.3%
+ 100% k_I	28.24	+181.4%
- 100% k_I	N.D.	N.D.
+ 100% k_D	0.53	-94.7%
- 100% k_D	0	-100%
+ 100% k_S	22.72	126.4%
- 100% k_S	5.30	-47.2%

B



C



D

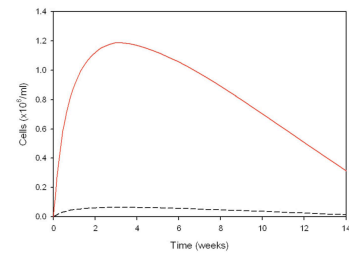
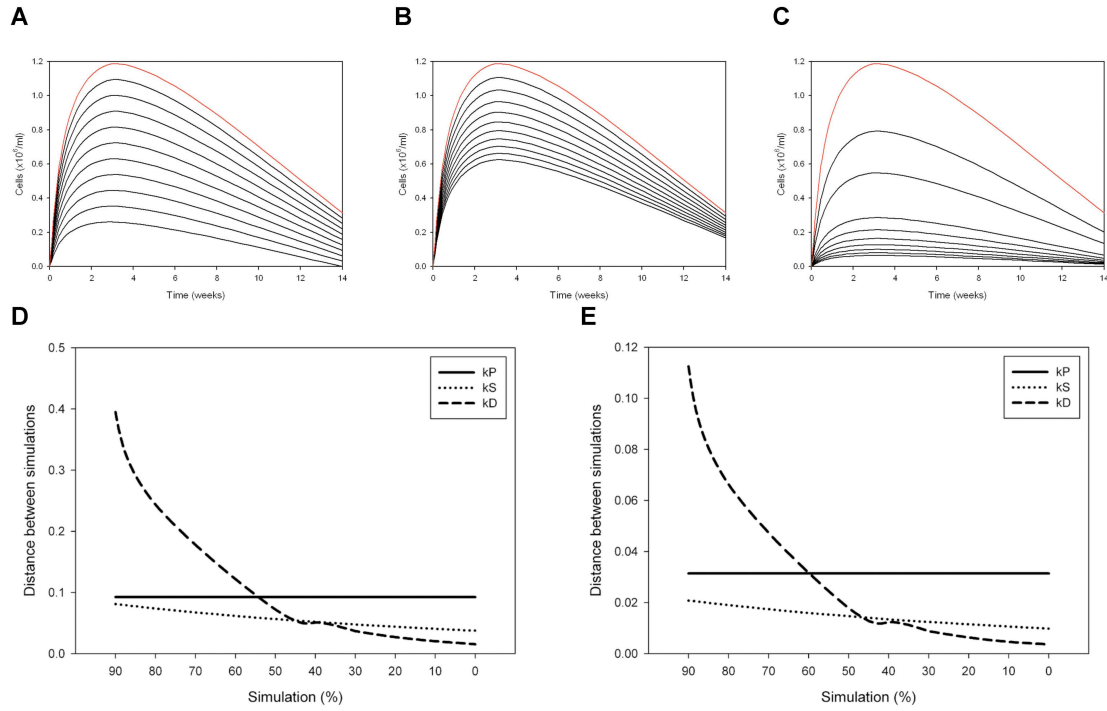


Figure 6



CHAPTER 3

Modelling of House Dust Mite-Induced Chronic Airway Eosinophilia

Marc Colangelo, Alba Llop-Guevara, Ramzi Fattouh, Tina D. Walker,
Susanna Goncharova, Miroslav Lovric, and Manel Jordana

Additional File

General solutions:

$$BM(E,t) = C_1 \frac{k_I + k_B - k_E - k_A}{k_E} e^{-(k_E + k_A)t} + \frac{k_P}{k_E + k_A}$$

$$B(E,t) = C_1 e^{-(k_E + k_A)t} + C_2 e^{-(k_I + k_B)t} + \frac{k_E k_P}{(k_E + k_A)(k_I + k_B)}$$

$$L(E,t) = C_1 \frac{-k_I}{k_E + k_A - k_D - k_S} e^{-(k_E + k_A)t} + C_2 \frac{-k_I}{k_I + k_B - k_D - k_S} e^{-(k_I + k_B)t} \\ + C_3 e^{-(k_D + k_S)t} + \frac{k_E k_I k_P}{(k_E + k_A)(k_I + k_B)(k_D + k_S)}$$

At equilibrium:

$$\frac{dBM(E,t)}{dt} = \frac{k_P}{k_E + k_A}$$

$$\frac{dB(E,t)}{dt} = \frac{k_E k_P}{(k_E + k_A)(k_I + k_B)}$$

$$\frac{dL(E,t)}{dt} = \frac{k_E k_I k_P}{(k_E + k_A)(k_I + k_B)(k_D + k_S)}$$

CHAPTER 4

A Mathematical and Computational Model for Simulating Complex Dynamic Cancer Growth and Metastasis

Marc Colangelo¹, Miroslav Lovric², and Jonathon R. Stone³

¹Department of Pathology and Molecular Medicine, Division of Respiratory Diseases and Allergy, Centre for Gene Therapeutics, ²Department of Mathematics and Statistics, and ³Department of Biology and The Origins Institute, McMaster University, Hamilton, Ontario, Canada

Accepted June 2011 in *The International Journal of Computers and Their Applications*.
(Submission # #6077)

Reprinted with permission under the ISCA Copyright Agreement.
See *Declaration of Academic Achievement* for details regarding authorship.

Summary and Central Message: We developed a mathematical model and computer simulation program to provide an extensive examination of avascular tumour growth and metastasis and simulate different outcomes. We established rules that mimic disease progression, using a local interaction simulation approach (LISA). These “rules” correspond to mathematical equations, embedded within which are parameters with values that can be altered, which were then encoded using *Mathematica* (a technical computing environment software application). Among the distinguishing features of the model was the ability to test the effects of different diffusional neighbourhoods, and the capability to apply both deterministic calculations and pseudo-random algorithms. We determined that the manner in which cancer cells diffuse has the greatest impact on the overall size and shape of a tumour, and is likely a combination of deterministic and stochastic processes.

**A Mathematical and Computational Model for Simulating Complex Dynamic
Cancer Growth and Metastasis**

Marc Colangelo¹, Miroslav Lovric² and Jonathon R. Stone³

¹Department of Pathology and Molecular Medicine, Division of Respiratory Diseases and Allergy, Centre for Gene Therapeutics, ²Department of Mathematics and Statistics, and ³Department of Biology and The Origins Institute, McMaster University, Hamilton, Ontario, Canada

ABSTRACT

Mathematical and computational models have emerged as effective complements and, in some cases, alternatives to *in vitro* and *in vivo* research. Particularly in the area of cancer research, such models allow for testing of a diverse combination of parameters and variables via simulation, some of which would not be possible to examine experimentally. One of the most-common criticisms of mathematical and computational models is the extent to which they can accurately mimic, and subsequently predict, actual biological events. Given that many complex biological processes involve multiple independent but simultaneous events, portraying these processes computationally is difficult, because they must be emulated sequentially *in silico*. Herein, we elaborate a non-linear, dynamic, mathematical model for cancer growth, which involves iron requirements of cells. The model simulates malignant tumour growth, including cancerous cell diffusion and death (apoptosis), allowing for movement in all directions in two-dimensional space according to rule-based mathematical algorithms. To visualize the model, we developed a computer graphic simulation program and used it to demonstrate the effects of varying parameters and various diffusion patterns. We applied the Local Interaction Simulation Approach (LISA) and obtained graphical and numerical results using different diffusional neighbourhoods. Our results show that the growth of a simulated tumour over time is dependent on the availability of its hypothetical nutrient source. Furthermore, we illustrate the effects of changing a variety of model parameters,

and show the influence that is imparted by the diffusion process on the overall shape and growth of the tumour.

Keywords: Cancer Growth, Computer Simulation, Decision-Making Algorithm, Cell Migration, Cell Diffusion, Mathematical Model

INTRODUCTION

Cancer is a condition encompassing over 200 diseases that share uncontrolled cellular proliferation as a diagnostic feature and constitutes the second leading cause-of-death in the western hemisphere [1]. The pathogenesis of cancer has been associated with a variety of origins, including DNA-damaging radiation, stress-inducing mutations, inherited genes, and viral infections [2]. Regardless of its origin, the most recognizable hallmark of cancer growth is the inability to regulate cell replication. As cells divide in an unregulated manner, cellular masses accumulate within tissues or around organs, preventing normal physiological function and causing pathologies that lead eventually to death [1]. Although cancer cells may not respond to normal cellular regulatory signals, they require a constant supply of energy and essential nutrients for continual growth.

When cancerous cells divide, they utilize the available resources in the immediate area, eventually creating a necrotic core of dead cells in the centre of a growing tumour [2]. The outer layer of cancerous cells will seek to migrate to other areas of the tissue or elsewhere in search of nutrients such as iron, glucose and oxygen. As the tumour grows in diameter, the necrotic core also becomes larger, correspondingly in diminishing areas to which nutrients can potentially diffuse [3]. Since these nutrients are unavailable near the core of the tumour, the adhesive interactions between cancerous cells become disrupted. As cells detach, they diffuse to adjacent areas in search of adequate conditions to

continue growing [1, 3]. Diffusion often leads cancerous cells to blood vessels, where they enter the blood stream and metastasize to other areas of the body in search of nutrient sources. Metastasis usually results in cancer cells adhering preferentially to bone marrow, liver, lungs, and other organs. This pattern corresponds with the high prevalence of cancerous tumours in these organs [4]. It is this movement which eventually can lead to the deterioration and death [2].

Pescarmona *et al.* [5] developed a mathematical model for studying cancer growth and tumour metastasis. Their model emphasized the requirement of iron (Fe) during cancerous cell proliferation. In particular, their model utilized the behaviour that cancerous cells exhibit when local Fe-levels become depleted: they migrate to neighbouring areas in search of new Fe-sources [5]. As with many complex biological phenomena, linear mathematical models provide inadequate descriptions for the dynamics that are involved in cancerous cell migration. Thus, the temporal sequences of events involved in cancer growth were considered discretely and analyzed in a manner that concerned only local environmental conditions, the local interaction simulation approach (LISA) [5-8].

Their model attempted to account for the biological pathway of Fe-uptake and consumption, and included four major assumptions [5]:

- a. Fe uptake will be dependent on local Fe concentrations and relatively minimal and constant in the neighbouring, quiescent and non-cancerous cells.
- b. Fe availability and concentrations are dependant on proximity to local blood flow.
- c. Cancerous cell diffusion is represented but limited to 4 directions, corresponding to nearest neighbour nodes in a two-dimensional coordinate grid.
- d. If no adequate Fe-sources are located, then these cells undergo apoptosis. The proportion of cancerous cells that die in any time interval is random (i.e., determined using a pseudorandom number generator).

To create an accurate mathematical depiction of biological events described by a model, it becomes necessary to take into account the diverse relationships among the processes that are emulated therein [9]. Biological processes can be relatively complex in nature, given the many entwined variables that may be interrelated, with multiple simultaneous events occurring constantly [10]. Understanding the diffusion and movement patterns of tumours may allow future therapies to target only cancerous cells, themselves, and also attempt to predict where cancer may spread to and prevent secondary tumours.

Herein, we elaborate on the pioneering work in modelling cancer growth and metastasis by Pescarmona *et al.* [5]. Most notably, we reformulate the equations and refine the decision-making algorithms. We incorporated these equations and algorithms into a computer graphic simulation program to create a computational model with which we consider diffusion of cells in both von Neumann and Moore neighbourhoods (Figure 1) and emulate cancer growth, death and diffusion, using both deterministic calculations and pseudo-random algorithms.

THE MODEL

In our computer graphic simulation program, a two-dimensional coordinate grid (with i and j denoting rows and columns) is initialized with user-defined parameters, and one node within the grid is 'seeded' to represent the initiation of cancer growth. Each node contains proportions of healthy, cancerous, and dead cells (H_{ij} , C_{ij} , and D_{ij}), which for simplicity, are normalized so that their proportions sum to one. The representation that is generated by the computer graphic simulation program represents fluctuations in the values of these three cell states, as well as concentrations of nutrient (e.g. Figures 3-7). These fluctuations are determined by a variety of parameters that affect operations representing cellular processes, which metaphorically affect the manner in which the cancer 'seed' grows and potentially metastasizes.

Nutrient Diffusion

The nutrient concentrations at grid nodes initially are determined by the location of blood vessels in relation to the grid. All simulation results that are reported herein involve a single blood vessel along the top of the grid, which creates a gradient in nutrient concentration by diffusion, with highest concentrations closest to the blood vessel and diminishing with distance. The change in density of free-nutrient (p_{ij}) at node (i,j) with respect to time t is determined by the equation:

$$\frac{dp_{ij}}{dt} = \alpha \left(\sum_{ij} p_{ij} - \eta p_{ij} \right) - \beta p_{ij} \quad (1)$$

where α represents the free-nutrient diffusion rate across tissues; the subscript ij indexes the nearest neighbours, the coefficient η accounts for the nodes that neighbour (i.e., surround) node (i,j) ; and β represents the rate at which nutrient is absorbed by healthy cells at each node. Depending on the location of the node, η may become 3, in the case of corner nodes, 5, in the case of edge nodes, or 8 for all other nodes in the grid. To ensure that a proper nutrient-gradient is established, Equation 1 is calculated over a user-determined number of iterations prior to formally initiating a simulation to establish equilibrium nutrient concentrations.

Feeding

Feeding acts to transform free-nutrient (p_{ij}) to bound-nutrient (q_{ij}) at cancerous node (i,j) . The amount of nutrient that is transformed is given by the equation:

$$\frac{dq_{ij}}{dt} = -\frac{dp_{ij}}{dt} = \gamma p_{ij} \quad (2)$$

where γ represents the rate of free-nutrient uptake by cancerous cells. This equation ensures that the amount of free-nutrient that becomes bound to cancerous cells at a given node is proportional to the amount of nutrient available at that node.

Consumption

Consumption determines the amount of bound-nutrient that is used by cancerous cells. It is proportional to the intrinsic rate of nutrient consumption by cancerous cells (λ) and occurs in a non-linear manner:

$$\frac{dq_{ij}}{dt} = \lambda(1 - e^{-q_{ij}}) \quad (3)$$

Mitosis/Apoptosis

Cell mitosis and apoptosis are determined by thresholds. If, at any time during a simulation, the ratio bound-nutrient:cancerous cells falls below a specified threshold, Q_D , then cancerous cells undergo apoptosis. Conversely, if the ratio bound-nutrient:cancerous cells rises above a specified threshold, Q_M , then cancerous cells proliferate. The proportion of cancerous cells that will undergo proliferation or apoptosis is determined by:

$$\frac{dC_{ij}}{dt} = \left[(1 - \rho_m) \cdot \left(\frac{q_{ij}}{Q_M} - C_{ij} \right) + (\rho_m C_{ij}) \right] - \left[(1 - \rho_d) \cdot \left(C_{ij} - \frac{q_{ij}}{Q_D} \right) + (\rho_d C_{ij}) \right] \quad (4)$$

The proportions of cells perishing or dividing are determined mathematically so that the elevated or diminished bound-nutrient:cancerous cell ratio is related to Q_M or Q_D . The parameters ρ_d and ρ_m determine how apoptosis and mitosis are emulated (0 for completely deterministic or 1 for pseudo-random) in the respective nodes.

Diffusion

If, at any time, the ratio free-nutrient:cancerous cells falls below a specified threshold, P_D , then cancerous cells will migrate to surrounding nodes in a free-nutrient concentration-dependent manner in search for richer nutrient-sources. The amount of cancerous cells that will migrate is given by the equations:

$$\frac{dC_{ij}^o}{dT} = -(1 - \rho_D) \left(\frac{p_{ij}}{P_D} - C_{ij} \right) - \rho_D C_{ij} \quad (5)$$

$$\frac{dC'_{i \neq 0,1, j \neq 0,1}}{dT} = (1 - \rho_D) C_{ij}^o \cdot \left(\frac{p_{i \neq 0,1, j \neq 0,1}}{\sum_{ij} p_{ij}} \right) + \rho_D C_{ij}^o \quad (6)$$

Equations 5 and 6 represent the concentrations of cancerous cells migrating *out* of a central node and *into* neighbouring nodes, respectively. These equations are analogous to those for the cell mitosis and death processes in that sufficient cells will diffuse to bring the free-nutrient:cancerous cell ratio back to the threshold P_D . Migrating cells are distributed in a ‘weighted’ manner, depending on the richness of the neighbouring nutrient-sources (Equation 6). The parameter ρ_D represents a parameter that allows the model to vary from deterministic ($\rho_D = 0$) to stochastic ($\rho_D = 1$), or any situation in between.

Neighbourhoods

We incorporate the effects of two common neighbourhoods used to describe diffusion in two dimensions. In this context, a ‘neighbourhood’ is defined

as the set of nodes surrounding a given node in a square grid (Figure 1). The mathematical definitions of von Neumann and Moore neighbourhoods, respectively, are described as [11]:

$$N_{(x_0, y_0)}^V = \{(x, y) : |x - x_0| + |y - y_0| \leq 1\} \quad (7)$$

$$N_{(x_0, y_0)}^M = \{(x, y) : |x - x_0| \leq 1, |y - y_0| \leq 1\} \quad (8)$$

Given that our model calculates the process of cellular diffusion based on the attainment of a threshold value, we disregard the originating node as a potential neighbour for diffusion. In other words, we consider neighbours to be potential nodes to which cancerous cells may migrate to, although when this threshold is not met, cells will remain in the originating node.

Simulations

All equations were encoded in Mathematica 6.0.2.1 (Wolfram, Chicago, IL) in order to perform simulations over time, with specified parameter values. All simulations, unless otherwise noted, were performed using the values specified in Table 1. During each iteration in a simulation, cellular processes were calculated for each node in the grid. In previous versions of the model, simulated tumours shifted to the right within the grid despite an equal and symmetrical distribution of nutrient [12, 13]. The main loop function in the computer graphic simulation program had been encoded to perform calculations starting in the upper left corner of the grid and continuing from left to right, top to bottom,

ultimately finishing in the bottom right corner (Figure 2A). To circumvent this shift, the model was adjusted to reverse the direction of the calculations in alternating iterations (Figure 2B). For odd-numbered iterations, calculations are performed left to right, top to bottom, whereas, for even-numbered iterations, calculations are performed bottom to top, right to left. Also in previous versions of the model, as cancerous cells diffused to the outer edges of the grid, migrating cells had been provided only with the option to diffuse to neighbouring nodes, creating a border effect caused by the boundaries of the grid. To alleviate this effect, the diffusion process was altered to allow for cancerous cells to migrate beyond the limits of the grid. At each iteration, when the calculations for cancerous cell diffusion are performed, an outer “ring” of nodes is added to the grid, allowing for cancerous cells to migrate to these nodes (Figure 2C). Following this step, the outer “ring” is removed, leaving the original grid with updated values and ready for the next iteration.

The selection for the type of neighbourhood to use during a simulation occurs in the initialization of a simulation, followed by the iterative process for diffusion. Using the selected number of neighbours for either a von Neumann (4) or Moore (8) neighbourhood, the surrounding co-ordinates for each node are calculated and stored. These co-ordinates are used to allow the computer graphic simulation program to move cancerous cells according to the concentrations of free nutrient available at each target node.

RESULTS

Baseline Simulations

Simulations involving default parameter values (Table 1) were run to show that under these conditions, cancer continued to grow and metastasize to neighbouring nodes over time (Figure 3A). As cell populations at each node increased, the consumption of nutrient by cancerous cells overtook the deposition of new free-nutrient by nearby vessels, and thus, the total free-nutrient-source diminished correspondingly (Figure 3B). As nutrient-levels at a given node became depleted, cells not supplied with nutrient underwent apoptosis, which produced the characteristic necrotic core (Figure 3C). Quantitatively, growing and spreading cancerous cells reached the nutrient-source (blood vessel) after approximately 125 iterations; the cancerous and dead cell populations exhibited sigmoidal patterns of growth and death (data not shown). The upper-bound for these two patterns seems to result from space and nutrient limitations; the time needed for these cell populations to plateau is most likely correlated with grid dimensions.

Varying Parameter Values

To illustrate how each parameter affected tumour size and shape, simulations were performed varying each individual parameter. Because the feeding rate (γ) of cancer cells positively regulates the concentration of bound-nutrient and, in turn, cell growth at a given time, increasing γ led to an increase in

rates of cellular proliferation rates (Figure 4A); decreasing γ significantly prevented nutrient-binding and cellular nutrient usage and thus, inhibited growth. Altering the consumption rate (λ) of nutrient by cancer cells yielded similar but inversely proportional patterns (Figure 4B). Decreasing the rate of nutrient-turnover allowed high nutrient-levels to persist for longer time periods and thus, remain available for tumour growth.

As expected, the cancer growth rate and tumour size were dependent on the mitotic threshold, Q_M , in an inversely proportional manner (Figure 4C). The death threshold, Q_D , also affected system dynamics in an inversely proportional manner but showed very unique and interesting patterns (Figure 4D). By decreasing cell sensitivity to death (decreasing Q_D), the formation of a ring so commonly manifested in necrotic cores was delayed and the amount of cancerous cells (and corresponding tumour size) increased slightly, as cells were able to survive with very low levels of bound-nutrient. The metastatic threshold, P_D , elicited proportional changes in both the rate of cancer growth and tumour size. (Figure 4E). Interestingly, as P_D increased, tumours typically developed an octagonal shape.

Varying Seed Sizes

To account for the potential sensitivity of initial cancer 'seed' size in relation to overall tumour size, simulations were performed by varying seed sizes

from 0.2 to 1.0 units, in 0.2 increments. Visually, at both $T=50$ and $T=100$, no differences in tumour size were apparent when increasing the seed size (Figure 5A). Numerically, over the first 100 iterations, each simulation growth curve yielded similar trends (Figure 5B). Magnification of the first 10 iterations revealed that, in fact, slight variations during the initial growth phase had occurred, particularly during the first 2 iterations (Figure 5C).

Comparing 'Random' vs. Fixed Simulations

Simulations involving changes to values for the parameters ρ_m , ρ_d and ρ_D were run to assess how results that were obtained using mathematically precise decision-making algorithms (Figure 6A) compared with results that were obtained using combinations of precise and pseudorandom algorithms (Figure 6B), and a strictly pseudorandom number generator (Figure 6C). Differences in tumour size and shape were apparent qualitatively (Figure 6). The mathematically precise decision-making algorithm generated a more-circular pattern with a higher concentration of cancer cells near richer nutrient-sources (i.e. the blood vessel running along the top of the grid). Although differences in proportions of surviving cells were initially quite small, they accumulated rapidly and dramatically. For example, cumulative survival at 100 iterations was almost two-fold higher in the deterministic compared to the pseudorandom simulations.

Comparing Diffusional Neighbourhoods

To assess differences in diffusion neighbourhoods on the evolution of a simulated tumour over time, simulations were carried out using diffusion processes in 4 and 8 directions. With the objective of analyzing the overall shape and growth pattern of the simulated tumour, run analyses were restricted to the presence and number of cancerous nodes overall. Thus, each node in the grid was recognized as either cancerous or non-cancerous, with no associated amount of cancerous cells. Using a von Neumann neighbourhood (i.e. 4 neighbours) and deterministic algorithms, cancer cells occupied a diamond-shaped pattern over time (Figure 7A). Over the course of such simulations, tumours eventually spread to all areas of invaded tissue. When simulations were carried out using a Moore neighbourhood (i.e. 8 neighbours) and deterministic algorithms, the tumour grew in a square pattern over time (Figure 7B). Ultimately, when using a Moore neighbourhood, the tumour spread to all areas of the tissue in approximately half the time required when using a von Neumann neighbourhood (Figure 7).

DISCUSSION

Using equations and decision-making algorithms to describe the various biological processes, we encoded a computer graphic simulation program to create a computational model to emulate cancerous cell growth, diffusion, and apoptosis using different diffusional neighbourhoods. Cell movements were simulated within various areas of a virtual tissue, the overall diffusion patterns being characterized by a wide variety of parameter values.

As expected, tumours typically evolved throughout tissues, and showed biased growth and diffusion in the direction of the nutrient source. During growth, the available free nutrients became expended, causing a necrotic core to develop in the centre of the tumour. Varying parameter values greatly affected the manner with which tumours typically grew and spread. For example, decreasing the feeding rate γ prevented mitosis, increased cell death, and prevented cancer cell migration. This observation shows how such models can be used to accelerate testing various experimental hypotheses.

The factors that can be influenced in reality are limited. Although some parameters can be increased or decreased experimentally or clinically, others represent fixed physiological thresholds that are constrained from changing substantially. For instance, the amount of nutrient that is needed to realise cell division is a fixed quantity and so, increasing Q_M would represent an impractical

therapeutic approach. Similarly, altering P_D and Q_D may be considered untenable practically. Despite increases in initial cancer seed size, simulations remained essentially unchanged over time. This observation indicates that the biological processes considered in the model limit the initial growth of the tumour, regardless of the initial conditions. Conversely, the level of 'pseudo-randomness' greatly affected the size, shape and location of the tumour. Fixed algorithm simulations produced a more-circular shape, while partially and completely random algorithm simulations resulted in larger, more abstract, square-like shapes. These simulations reveal that more information about tumour growth is required through comparative analysis among actual tumours to determine to what degree tumour growth and diffusion is deterministic.

Ultimately, it appears as though the most-influential factor on tumour growth is the manner in which cancerous cells diffuse. As most mathematical models focus on the avascular stages of tumour growth, the effects of diffusion can be crucial [3, 5, 14-16]. If used to predict the ontogeny of a tumour in a given time frame, these differences could prove to be fundamental in determination of tumour size and growth rate. While the two simulations focusing on the number of diffusional neighbours elicit similar growth curves, the pattern and the speed at which the tumour evolved differed (Figure 7). A doubling in the number of neighbours caused the time at which the tumour consumes the entire tissue area to halve ($T \approx 300$ using a von Neumann neighbourhood, data not shown, versus

$T \approx 150$ using a Moore neighbourhood). Additionally, if the model were to be expanded to three dimensions, the number of surrounding nodes in von Neumann and Moore neighbourhoods would increase to 6 and 26, respectively. The effects of this added dimension, and corresponding neighbours, most likely would exert a more-noticeable difference in pattern and speed. In addition, if the quantity and direction of cancer cells migrating were undetermined, then this added complexity also may exert an effect on growth curve characteristics.

Despite limiting simulations to alterations to values for individual parameters, the potential impact that simultaneous changes to values for multiple parameters could exert on the ability for a computational model to emulate accurately a biological process such as cancer growth is evident. Additional simulations using a variety of combinations of parameter values and grid size would be beneficial in ultimately helping to identify the most-accurate scenario for emulating cancer growth. Given that most biological processes are non-linear, such changes in parameters and testing their corresponding effects using a parallel programming platform is vital for the substantiation of any computational model.

We anticipate ultimately incorporating virtual chemotherapeutic agents into the model. For example, Fe-chelators have been studied as anti-proliferative agents [17]. Using our computational model, the effects of Fe-chelators could be

modelled. Furthermore, the use of oncolytic viruses as potential cancer therapies is becoming increasingly promising [18]. Modelling viral therapies also may be incorporated into our model to simulate the interaction between a virus and cancer cells. Such modelling would enable researchers to predict optimal timing and dosages for therapies needed to prevent cancer metastasis while preventing patient toxicity.

ACKNOWLEDGEMENTS

We acknowledge and thank M. Jordana, D. Harnish, and M. Abou Chakra from McMaster University, P. Diamandis from the University of Toronto, S. Dascalu from University of Nevada Reno, and M. Scalerandi from The Politecnico di Torino, as well as the Shared Hierarchical Academic Research Computing Network, and Natural Sciences and Engineering Research Council of Canada Discovery Grant 261590 for funding and support.

REFERENCES

- [1] R. A. Weinberg, "How cancer arises", *Sci Am*, 275(3): pp. 62-70, Sep, 1996.
- [2] D. W. Ross, *Introduction to Oncogenes and Molecular Cancer Medicine* Springer, 1998.
- [3] A. R. A. Anderson, "A hybrid mathematical model of solid tumour invasion: the importance of cell adhesions", *Mathematical Medicine and Biology*, 22(pp. 163-186, 2005, 2005.
- [4] M. de Sousa, "Lymphocyte traffic and positioning in vivo: an expanded role for the ECM, the VLA proteins and the cytokines", *Pathol Res Pract*, 190(9-10): pp. 840-850, Oct, 1994.
- [5] G. P. Pescarmona, M. Scalerandi, P. P. Delsanto and C. A. Condat, "Non-linear model of cancer growth and metastasis: a limiting nutrient as a major determinant of tumor shape and diffusion", *Med Hypotheses*, 53(6): pp. 497-503, Dec, 1999.
- [6] P. P. Delsanto, A. Romano, M. Scalerandi and G. P. Pescarmona, "Analysis of a "phase transition" from tumor growth to latency", *Phys Rev E Stat Phys Plasmas Fluids Relat Interdiscip Topics*, 62(2 Pt B): pp. 2547-2554, Aug, 2000.
- [7] M. Scalerandi, V. Agostini, P. P. Delsanto, K. Van Den Abeele and P. A. Johnson, "Local interaction simulation approach to modelling nonclassical, nonlinear elastic behavior in solids", *J Acoust Soc Am*, 113(6): pp. 3049-3059, Jun, 2003.

- [8] M. Scalerandi, G. P. Pescarmona, P. P. Delsanto and B. Capogrosso Sansone, "Local interaction simulation approach for the response of the vascular system to metabolic changes of cell behavior", *Phys Rev E Stat Nonlin Soft Matter Phys*, 63(1 Pt 1): pp. 011901, Jan, 2001.
- [9] J. E. Cohen, "Mathematics is Biology's Next Microscope, Only Better; Biology is Mathematics' Next Physics, Only Better", *PLoS Biol*, 2(12): pp. e439, 2004.
- [10] D. Gavaghan, A. Garny, P. K. Maini and P. Kohl, "Mathematical models in physiology", *Philos Transact A Math Phys Eng Sci*, 364(1842): pp. 1099-1106, May 15, 2006.
- [11] L. Gray, "A Mathematician Looks at Wolfram's New Kind of Science", *Not. Amer. Math. Soc.*, 50(pp. 200-211, 2003.
- [12] M. Colangelo, P. Diamandis and J. Stone, "A Complex Dynamic Model for Cancer Growth and Metastasis", *Proceedings of the 18th International Conference on Computer Applications in Industry and Engineering*, 1-880843-57-9, 2005.
- [13] M. Colangelo, M. Lovric, D. Harnish and J. Stone, "Modelling Diffusional Neighbourhoods", *Proceedings of the 22nd International Conference on Computers and Their Applications* 978-1-880843-62-8, 2007.
- [14] V. Cristini, J. Lowengrub and Q. Nie, "Nonlinear simulation of tumor growth", *J Math Biol*, 46(3): pp. 191-224, Mar, 2003.
- [15] A. Friedman and F. Reitich, "Analysis of a mathematical model for the growth of tumors", *J Math Biol*, 38(3): pp. 262-284, Mar, 1999.

[16] J. A. Sherratt and M. A. Chaplain, "A new mathematical model for avascular tumour growth", *J Math Biol*, 43(4): pp. 291-312, Oct, 2001.

[17] D. R. Richardson, "Potential of iron chelators as effective antiproliferative agents", *Can J Physiol Pharmacol*, 75(10-11): pp. 1164-1180, Oct-Nov, 1997.

[18] E. A. Chiocca, "Oncolytic viruses", *Nat Rev Cancer*, 2(12): pp. 938-950, Dec, 2002.

TABLES & FIGURES

i	j	C_I	C_J	C_0	α	β	γ	λ	P_D	Q_D	Q_M	ρ_d	ρ_m	ρ_D
101	101	51	51	0.2	0.2	0.05	0.1	0.1	0.7	0.12	0.3	0	0	0

Table 1: Default parameter values used for baseline simulations.

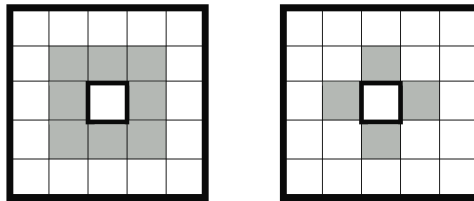


Figure 1: Potential directions for cancer cell diffusion in two-dimensional space in a Moore neighbourhood (8 possible directions) and a von Neumann neighbourhood (with 4 possible directions).

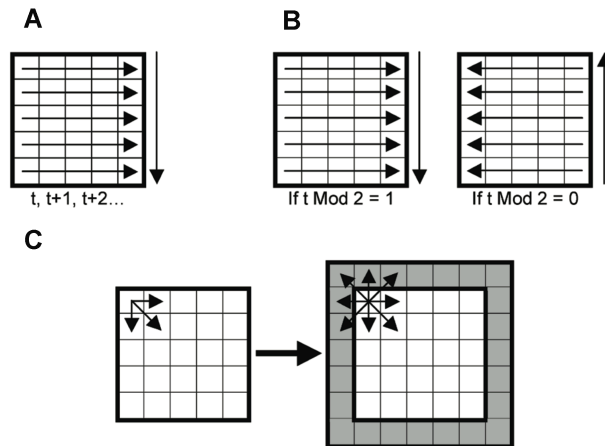


Figure 2: Various methods used in the cancer cell diffusion process.

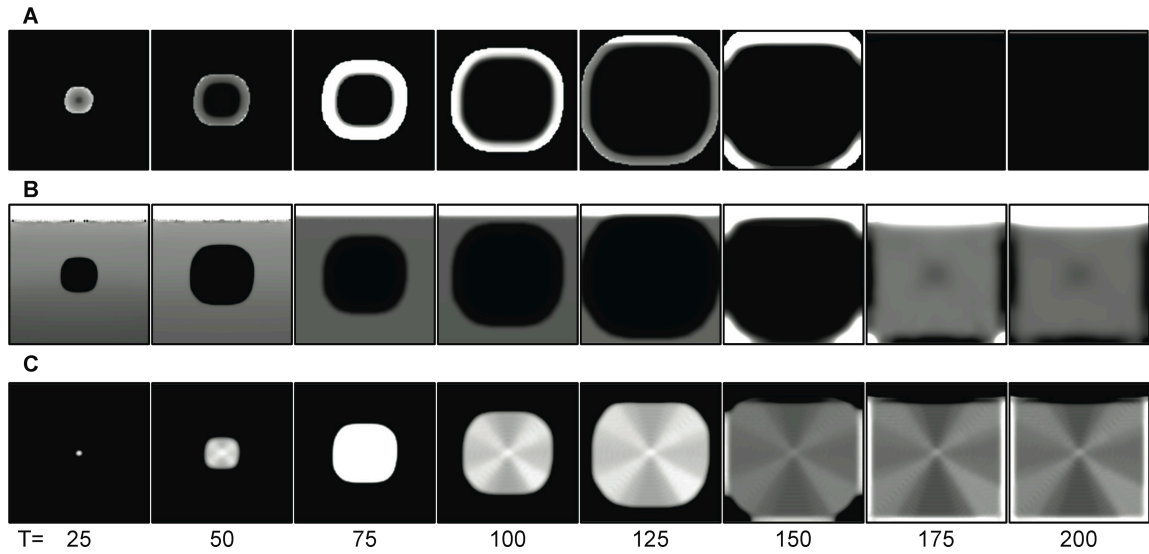


Figure 3: Simulated tumour growth over time showing A) Cancer cell distribution, B) nutrient distribution and C) dead cell distribution, using baseline parameters (Table 1).

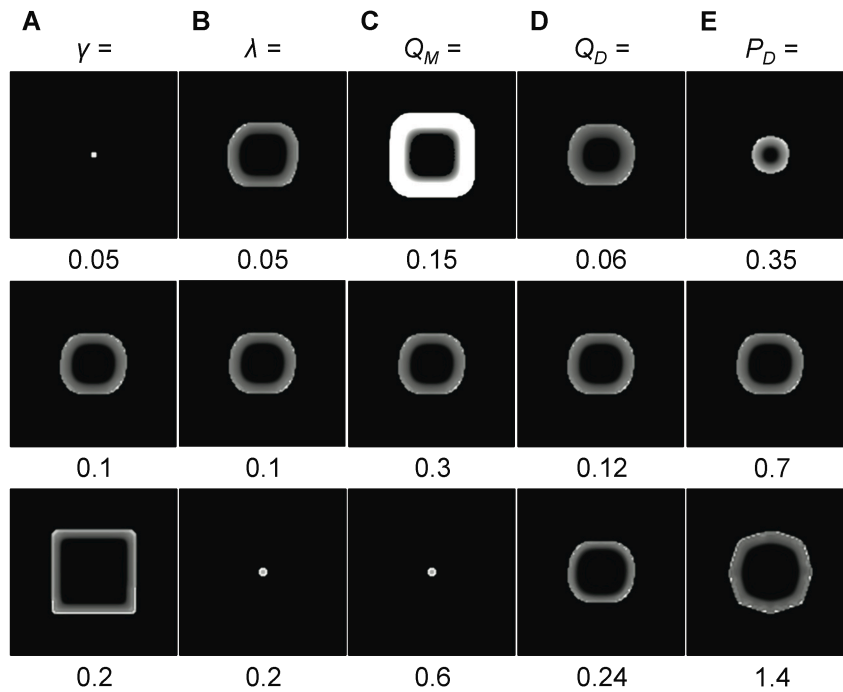


Figure 4: Effects of variation in model parameters on tumour growth at T = 50, with all other baseline parameters used (Table 1).

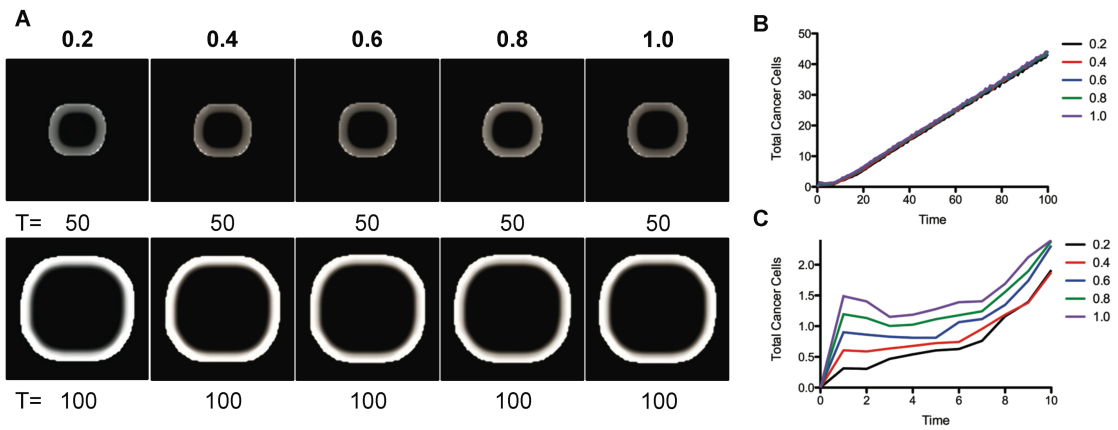


Figure 5: A) Simulated tumour growth over time with varying seed sizes. Growth curves for varying seed sizes over the first B) 100 iterations and C) 10 iterations.

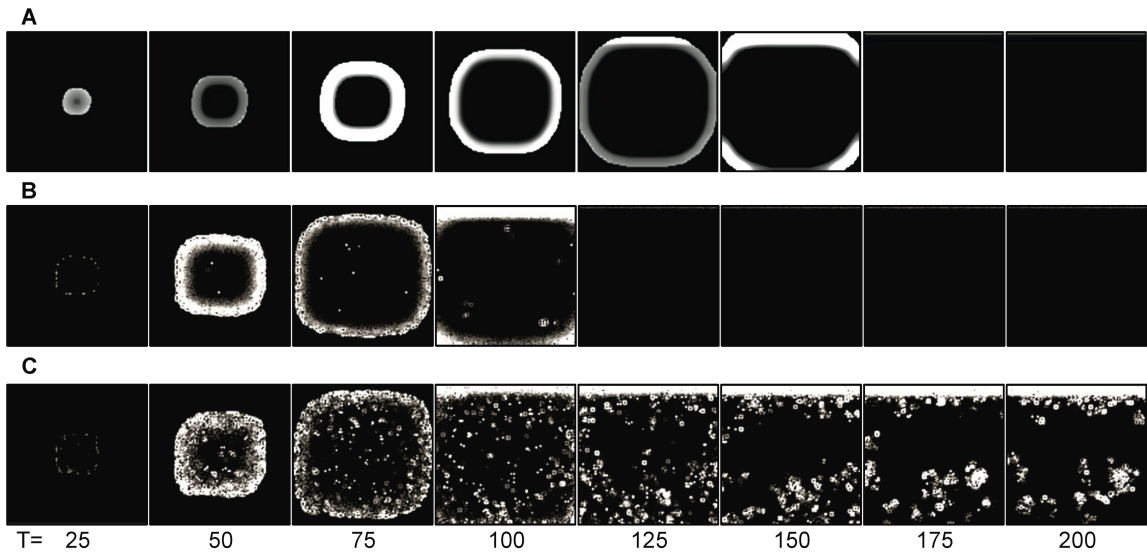


Figure 6: Simulated tumour growth over time for A) deterministic algorithms ($\rho_m = \rho_d = \rho_D = 0$), B) mixed algorithms ($\rho_m = \rho_d = \rho_D = 0.5$), and C) pseudorandom algorithms ($\rho_m = \rho_d = \rho_D = 1$). Simulations were run using baseline parameters in Table 1.

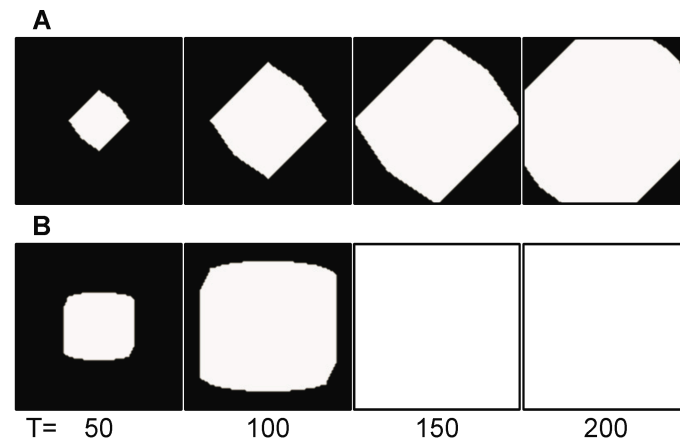


Figure 7: Simulated cancer cell distribution using A) a von Neumann neighbourhood and B) a Moore neighbourhood.

CHAPTER 5
DISCUSSION

CHAPTER 5

DISCUSSION

The intent in this chapter is to identify and recapitulate what was revealed in each project, and to then explain limitations and prospective next steps. The key results and discoveries have been discussed in each individual manuscript included in this thesis. Consequently, it seems appropriate to elaborate on the overall implications of the research contained herein, as well as potential areas for improvement.

WHAT DID MODELLING REVEAL?

The process of creating a model characteristically involves a constant cycle of development, refinement, prediction, and validation. During this process, knowledge is gained about the methodology and the system being modelled. Through the development and application of *in silico* models, we were not only able to learn more about each system that was studied in this work, but we also learned how to refine our modelling process and conduct our research more efficiently. Overall, the goals of each model were to reveal and describe specific characteristics of the respective systems. Using mathematical techniques, further goals were elaborated that were specific to each system.

For the HDM exposure model, presented in Chapter 2, the initial goal was to establish a tool to predict the response of various measures of airway

inflammation and sensitization over a broad range of doses of allergen over time. As a result, we were able to visualize how the system responded to different changes to initial conditions in a manner that would otherwise have been both costly and time-consuming using *in vivo* experimentation. Importantly, we established that the system is non-linear. More specifically, although the initial dose of allergen determines the responsiveness of both the inflammatory and sensitization variables, these responses do not increase proportionally to increases in the dose of allergen. Throughout the entire spectrum of simulated responses, the distribution is also non-linear with respect to both dose of allergen and time. Furthermore, we observed maximal responses in the range of 10 to 15 μg of HDM. The implication of these findings was that the behaviour of the system changes at some point during the experimental protocol. Correspondingly, we were able to identify properties of the system where the behaviour changed, namely threshold doses of allergen for both the eosinophil and immunoglobulin responses (2.0 μg and 0.5 μg of HDM, respectively). Collectively, as we identified the non-linearity among allergen exposure and both inflammation and sensitization, we were able to surmise that the inflammation-sensitization relationship is also non-linear. This premise could be extrapolated in order to distinguish the differences among atopic and asthmatic patients.

Additionally, an important lesson learned through the completion of this project was the recognition of the limitations of our methodology. Given the empirical methods used, the model equations were representative of the trends

exhibited by the experimental data, however they were not unique to the system. In other words, the mathematical properties (model equations) of the system did not encapsulate or correlate to specific immunological properties of allergic asthma. Despite this shortcoming, the model was a fundamental step in our pursuit of studying allergic asthma from a mathematical standpoint as it ultimately shaped the manner in which future projects were designed both experimentally, in terms of dose of allergen and time-points used, and mathematically, in terms of the methodology used.

The model of eosinophil trafficking, presented in Chapter 3, was specifically designed to incorporate mechanistic modelling techniques. In addition, the goals of this model were to identify the relative contribution of various eosinophil trafficking processes to airway eosinophilia. Upon identification of eosinophil production, survival and death as the key processes that had the greatest relative impact on airway eosinophilia, the model was also able to simulate how airway eosinophilia is affected when minimizing and reducing these processes, meant to represent *in vivo* experimentation using knockout models or antibodies. We observed that although changes in eosinophil production, survival and death exhibited non-linear reductions to varying extents, values in airway eosinophilia were similar at 14 weeks, suggesting an attraction point for the complex system. The significance of these observations was the identification of these processes for further *in vivo* investigation, a sharp contrast to experimentation focusing on impairing eosinophil migration.

Furthermore, eosinophil production appeared to be the most sensitive to changes, implying that production via IL-5 is best suited for therapeutic intervention. Although experimental data were used with respect to the various eosinophilic compartments, the processes of production, migration, death, and survival were theorized and used the limited experimental data available to solve for their values. A limitation of this model was the absence of a comparison of simulations to experimental data outside of the protocol (i.e. data not previously used in the modelling process).

Chapter 4 describes the development of the cancer model. The goal was to create a simulation program that would emulate tumour growth and metastasis in two dimensions. As anticipated, our simulation program was able to mimic a tumour evolving in tissue, growing in the direction of the nutrient source and developing a necrotic core. Through various simulations, we were able to test the effects of changing a number of model parameters, including growth and death rates, the level of randomness for calculations, and particularly the manner in which cancer cells diffuse. We observed that the processes of cancer growth and death, when altered, would correspond to increases and decreases, respectively, in the tumour size. Interestingly, when using deterministic methods in the model, the tumour exhibited a dense, circular shape, whereas stochastic methods yielded a scattered, square shape. These simulations imply that tumour growth in the body is a combination of both random and deliberate calculations. The process of diffusion, and the manner in which it is calculated, proved to be the

most influential parameter in the model. Using different neighbourhoods corresponding to the number of directions in which cancer cells can move (4 or 8 directions), both the speed and size at which the tumour grows is affected. These findings not only have implications on previously established and future models of tumour growth in two-dimensional space, but also models in three-dimensional space, as the predicted size and shape may be grossly over or under-estimated. One of major assumptions previously included in the cancer growth model was the premise that cancer growth, death and diffusion were determined by the availability and quantity of an individual nutrient. Previously, this nutrient was considered to be iron [80,86,97]. The model presented in Chapter 4 took a more general approach, without the identification of a specific nutrient, given the lack of data to support the mathematical characteristics of iron diffusion. Regardless of the type of nutrient, the initial diffusion across the grid has the ability to affect all of the processes in the model, both directly and indirectly, and ultimately the shape and size of the simulated tumour.

FUTURE DIRECTIONS OF THE MODELS

Models, whether experimental or mathematical, are inherently limited. That is, there are always more variables that could potentially be included in a model. The conundrum with models, however, is that the *quantity* of information that is incorporated into the development of a model does not necessarily equate to the *quality* of the knowledge that can be extracted in return. For example, in

the TCN model presented in Chapter 2, the accuracy of the model was evaluated via linear regression at various stages throughout the modelling process when additional data was added. When adding an additional dose to the model, corresponding to 8 additional time-points, the R^2 value remained unchanged (at 0.987). Furthermore, the inclusion of 20-week data (5 additional time-points) increased the R^2 value only slightly (0.990) [100]. Collectively, from the initial to the final model, a 140% increase in the number of total data-points only corresponded to a 0.003 increase in the R^2 value, and consequently, no additional information about the system was gained.

The essence of a *model* is the ability to describe and predict behaviours through the simplification of a system. As part of this simplification, important variables and parameters are initially identified that are considered to be crucial to the system. In deciding how detailed a model should be, there cannot be any specific standards. However, it has been recently recommended that a model should encompass a set of criteria to render it useful to biologists, that it embraces the inclusion of actual data, the ability to account for the dynamics of the system, the option to perform simulated experiments, and a need to be as realistic as possible [25]. The researcher has autonomy to determine what is appropriate and necessary to include. Nevertheless, much like to the questions of suitability and methodology that arise when assessing the applicability of *in vivo* models to humans, there are many questions that are raised with *in silico* models that pertain to future directions and improvements that could be made.

FUTURE DIRECTIONS OF THE HOUSE DUST MITE MODELS

HDM EXPOSURE MODEL

We acknowledge the experimental limitations of using only one allergen, but we elected to use HDM because it is the most pervasive aeroallergen worldwide [101]. Furthermore, HDM allows for the investigation of a process that is initiated in the respiratory mucosa and does not require the use of exogenous adjuvants, in contrast to the typically used antigen OVA (ovalbumin), which is introduced along with a chemical adjuvant (aluminium hydroxide) intraperitoneally [102,103]. However, we are also aware that HDM is not the only allergen that elicits airway eosinophilia when mucosally delivered. In addition, we only used one strain (BALB/C) and age (6-8 week old) of mice. While we recognize that other models using different aeroallergens or different strains of mice may have different kinetics, it is likely that not only do they share similar dynamics and compartmentalization, but are also subject to regulation by the same processes that we have investigated in Chapters 2 and 3. To add all of strain, age, and allergen variables would further increase the intricacy of the research, but it would make it less manageable without any concomitant advantages to learning more about the system.

In Chapter 2, separate models were focused specifically on the total cell number, eosinophils alone, as well as HDM-specific IgE and IgG₁. As this was the first attempt to mathematically model allergic asthma, we chose to develop

an empirical model. In doing so, we based our mathematical construct purely on the patterns exhibited by the data themselves. Given the vast amount of experimental data that was collected, there are different approaches that could have been taken in the modelling process.

If the model were to be developed again using empirical methods, the total cell number could be modelled as the summation of each encompassing cell type, eosinophils, mononuclear cells, and neutrophils:

$$TCN = EOS + MNC + NT$$

In mathematical terms, the total cell number could be expressed as a function of all three different cell types:

$$TCN = f(EOS, MNC, NT)$$

Or, similarly, as a sum of the functions of each individual cell type:

$$TCN = f(EOS) + f(MNC) + f(NT)$$

Furthermore, the quantity of each cell type could be modelled as a function based on both dose of allergen and time. The advantage of this approach is that experimental data would have only been used to model eosinophils, mononuclear cells and neutrophils, allowing for the model predictions to be tested against the total cell numbers calculated during the collection of data. This disadvantage of using empirical methods, as with the methodology used in Chapter 2, is that the function f would not be attributed to any distinguishing

immunological properties of HDM, but rather it would be an arbitrary mathematical function only describing the pattern exhibited by the dose-response curves.

If the model were created using mechanistic methods, then equations could be used to model the change in each cell type with respect to time. In doing so, however, each function for each cell type would have to be based upon some additional factors, not purely dose and time as it currently stands, that would make the equations unique to allergic asthma. The system could be modelled as a series of differential equations:

$$\frac{dTCN}{dt} = f\left(\frac{dEOS}{dt}, \frac{dMNC}{dt}, \frac{dNT}{dt}\right)$$

$$\frac{dEOS}{dt} = f_1(EOS(t), E, t)$$

$$\frac{dMNC}{dt} = f_2(MNC(t), E, t)$$

$$\frac{dNT}{dt} = f_3(NT(t), E, t)$$

where the change in the total cell number over time is expressed as a function, f , of the sum changes of various cell categories. Furthermore, changes in each individual cell type over time would be modelled as separate functions based on dose (or exposure, E) and time (t). These functions (f_1 , f_2 , and f_3) would be expanded to include additional factors that are unique to the system and

attributed directly to immunological principles, either based on discrete data or theory.

EOSINOPHIL TRAFFICKING MODEL

In the model presented in Chapter 3, seven different rates were considered, each representing various processes that ultimately would determine the level of eosinophils in each compartment. Given that one of the main goals of the model was to make use of a limited data set, the model was restricted to using only data pertaining to eosinophils in the bone marrow, blood and lungs. Taking the model one step further, each rate of change included in the model could be modelled as a stand-alone function. The construct of the model could be presented as a larger set of equations. For instance, each eosinophil compartment would be expressed as:

$$\frac{dB(E,t)}{dt} = \frac{dk_P}{dt} - \frac{dk_E}{dt} BM(E,t) - \frac{dk_A}{dt} BM(E,t)$$

$$\frac{dB(E,t)}{dt} = \frac{dk_E}{dt} BM(E,t) - \frac{dk_I}{dt} B(E,t) - \frac{dk_B}{dt} B(E,t)$$

$$\frac{dL(E,t)}{dt} = \frac{dk_I}{dt} B(E,t) - \frac{dk_D}{dt} L(E,t) + \frac{dk_S}{dt} L(E,t)$$

where each process in the model would then be represented as separate equations:

$$\frac{dk_P}{dt} = f_P(k_P(t), E, t)$$

$$\frac{dk_E}{dt} = f_E(k_E(t), E, t)$$

$$\frac{dk_A}{dt} = f_A(k_A(t), E, t)$$

$$\frac{dk_I}{dt} = f_I(k_I(t), E, t)$$

$$\frac{dk_B}{dt} = f_B(k_B(t), E, t)$$

$$\frac{dk_D}{dt} = f_D(k_D(t), E, t)$$

$$\frac{dk_S}{dt} = f_S(k_S(t), E, t)$$

The caveats to this approach would be two-fold. First, the key components contributing to a particular process would have to be identified, or hypothesized. Currently, each rate is calculated as a static value at a particular dose and time-point. In a revised model, for example, the function for eosinophil production (k_P) would have to encompass the effects of IL-5, IL-3, and GM-CSF, or be assumed to be limited to one individual cytokine, IL-5 [104-107]. Second, experimental data, as it pertains to each individual process, would be needed.

APPLICABILITY AND IMPLICATIONS

In summary, the models in both Chapters 2 and 3 take into account different aspects of airway inflammation, a fundamental hallmark in allergic

asthma. With the understanding that mathematical models can (or rather, should) be modular in nature (i.e. have the ability to be sub-divided into smaller discrete parts), the models we have presented are complete and may stand alone. However, they may also be used as parts to larger and, correspondingly, more complex models. Similarly, other modules could be constructed to function in parallel to the existing models.

The overall applicability and goal would be to create a global, algorithm-based, construct that connects allergen exposure, allergic sensitization and allergic disease to obtain qualitative and quantitative knowledge of the relationships between these processes. In this case, we consider *allergic disease* to encompass all of the phenotypic conditions associated with exposure to an allergen, not solely airway inflammation. This research would have the ability to furnish a novel computational visualization of allergen-host interactions and clarify conditions under which allergic asthma emerges and evolves.

Both the emergence and evolution of allergic disease, we hypothesize, is primarily attributed to the interaction between the exposure to allergen (in this case, the amount and duration of HDM exposure) and the status of the lung at the time of exposure or, host susceptibility which in this case, the ability of the lung to respond to said exposure. Given that allergic disease is not easy to define experimentally, as mice do not exhibit the typical clinical features of human asthma, a mathematical approach may be beneficial.

Allergic asthma can be considered a complex disease (D). For this reason, we would model the disease as a mathematical system using differential equations. We postulate that the evolution over time (t) of the disease depends mainly on dose of allergen exposure (E) and host susceptibility (h). Thus:

$$D'(t) = \frac{dD}{dt} = f(D(t), E(t), h)$$

We would assume that host susceptibility is constant over time. However, allergen would be administered daily and this would likely result in cumulative effects. Even though defined doses of HDM would be used, exposure would also be based on time.

In order to mathematically define “disease”, we would utilize lung function, or rather dysfunction, (F), as the closest surrogate of asthma. We propose that “disease”, or lung dysfunction, depends on the present state of dysfunction (F), as well as the extent of sensitization (S), inflammation (I), and airway remodelling (R). Thus:

$$D'(t) = F'_{E,h}(t) = f(F_{E,h}(t), S_{E,h}(t), I_{E,h}(t), R_{E,h}(t))$$

where $I_{E,h}(t)$, $S_{E,h}(t)$ and $R_{E,h}(t)$ are functions dependent on allergen exposure and host susceptibility. Here, allergen exposure would be fixed, while susceptibility would be held constant. Our goal would be to determine the function f to establish mathematical rules that could elucidate biological principles in the system.

For brevity, the first step would be to empirically model the various individual processes, each of which is comprised of several variables, to generate equations based on dose of allergen and time for each variable.

The second step would be to collectively model S , I , R , and F by gathering information acquired in the previous phase. As each variable is expressed in different units, it would be necessary to normalize the values. To do so, the maximal response for each variable would be determined and individual measurements will be expressed as a percentage of that maximal response. The third step would employ an additional method of analysis to define the patterns in S , I and R as they change between doses and over time. The change for each process, at a given dose would be determined by calculating the ratio of the change in one given process to the sum of the absolute change in all processes, over a specified time interval (i.e. from t to $t+1$). The resulting values of S , I , R , and F for each time interval and dose would be simplified as a set. Using these sets, a matrix would be constructed with the relative change in each variable at all doses and time intervals:

	E_1	E_2	E_3	E_n
t_1	$\{S_{11}, I_{11}, R_{11}, F_{11}\}$	$\{S_{12}, I_{12}, R_{12}, F_{12}\}$	$\{S_{13}, I_{13}, R_{13}, F_{13}\}$.
t_2	$\{S_{21}, I_{21}, R_{21}, F_{21}\}$	$\{S_{22}, I_{22}, R_{22}, F_{22}\}$	$\{S_{23}, I_{23}, R_{23}, F_{23}\}$.
t_3	$\{S_{31}, I_{31}, R_{31}, F_{31}\}$	$\{S_{32}, I_{32}, R_{32}, F_{32}\}$	$\{S_{33}, I_{33}, R_{33}, F_{33}\}$.
t_m	.	.	.	$\{S_{mn}, I_{mn}, R_{mn}, F_{mn}\}$

Analysis of the pattern of change for each variable, as well as the overall response, would provide insight into the relative contribution of each individual process (S , I , and R) to the functional outcome (F). The system is dynamic and dose-dependent, implying that the contribution of each process on dysfunction would likely vary with exposure and time. Using these observations, we would be able to identify properties of the system, and the doses and times at which these changes happen. As a result of this analysis, a complete mathematical of allergic asthma from a system's perspective could be achieved.

FUTURE DIRECTIONS OF THE CANCER MODEL

The model of cancer growth and metastasis presented in Chapter 4 was initially designed to build upon a previously established model [80]. One of the distinguishing features of the model we created was the inclusion of elements previously unaccounted for, namely the methods used to calculate the diffusion of cancer cells and the combination of deterministic and pseudorandom processes. Through the creation of a computer simulation tool, various simulations were performed in order to highlight both the methodology used within the model, as well as the effects of individual variables on overall tumour shape and size.

Although the range of simulations demonstrates these effects, there are areas for improvement that could expand the range. For instance, all simulations were performed using the same initial seed location, as well as the same location

of the nutrient supply. It would be interesting to examine the overall effects that changes in these parameters would elicit, both individually and in combination with other parameter modifications. Furthermore, each of the simulations was performed using a 100 by 100 grid. This size was chosen for two main reasons. First, we believed this size was able to demonstrate the global effects when changing parameters. Second, results were generated in a timely manner, due to the amount of time needed to run these simulations. A grid that has dimensions of 100 by 100 nodes and runs for a single iteration results in 10,000 calculations. This number is increased exponentially given the various calculations of processes occurring within each node and the number of iterations. Future simulations using larger grid sizes would be beneficial in order to see the long-term behaviour of the system, and to investigate limitations of the different processes previously identified in the model, such as space and nutrient limitations.

In addition, one of the apparent limitations of the model is the premise of tumour growth in a two-dimensional space. In order to make the model and ensuing simulation results more realistic, it would be valuable to add an additional dimension to allow for simulations in three-dimensional space, albeit adding further complexities in the process. In order to add a spatial dimension to the model, the information within each node, along with each process, would be expanded to include a third coordinate. The process of diffusion would have the greatest impact, as cancer cells would now have the option to diffuse in more

directions. In two-dimensions, using a Moore neighbourhood, a cancer cell has 8 potential directions in which to diffuse. In three-dimensions, however, this value is increased to twenty-six. With respect to calculations, the default grid size would be 100 by 100 by 100 nodes. For a single iteration, the number of calculations would rise to 1,000,000. Over multiple iterations, a third dimension would significantly affect the simulation time.

APPLICABILITY AND IMPLICATIONS

The overall applicability and goal of mathematically modelling cancer would ultimately be to mimic what is actually happening to a tumour in the body, and apply this tool to test various therapeutic interventions. As such, the model presented in Chapter 4 could be considered as a module to a larger, more encompassing model that would capture additional elements involved in cancer growth and metastasis. Other areas to consider would include a more refined method of nutrient diffusion, the incorporation of angiogenesis, and the addition of a therapeutic application.

For simplicity, the cancer model used a simple method for the initial nutrient diffusion, whereby the grid was divided approximately into quarters. The first quarter of the grid (closest to the location of the blood vessel) was initialized with a nutrient value of 1, and each successive quarter decreased by a value of 0.25. Most published models on cancer growth do not mention or explain how, if at all, a nutrient is distributed [74,90,91,108,109]. The use of a linear distribution

starting from the origin can be found in some models [110]. While this linear method can provide a reasonable representation of the distribution of a nutrient, it remains to be seen if this is biologically plausible.

The diffusion of the nutrient across the grid could have been considered synonymous to an ice cube tray (Figure 1). Assuming nutrient is diffused from one end of the grid where the blood supply is located, each successive “opening” in the tray continues to fill. The openings closest to the source would then contain the highest concentration of nutrient, with concentrations decreasing as the distance from the blood source increases.

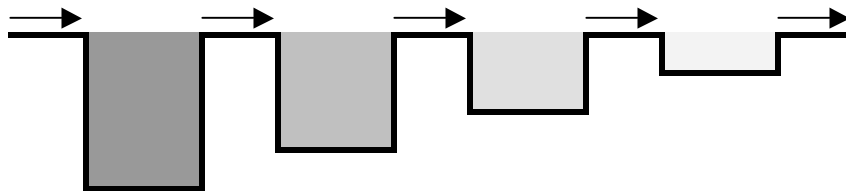


Figure 1: A graphical representation of iron diffusion. Similar to an ice cube tray. As the iron diffuses from the left (or top of the grid) the nodes closest to the nutrient source contain higher concentration of iron, with each successive node containing a lower concentration as the distance from the nutrient source increases.

In order to describe a new method of nutrient diffusion, we would consider the equation:

$$N = A(1 - e^{-kt})$$

where N is the amount of nutrient at a given node, A is the theoretical maximum amount of nutrient that a node could contain and the rate $k > 0$ is taken to be constant. The equation above describes how the nutrient level in one individual

node in the grid would continue to increase in the absence of any other process. Since the amount of nutrient is dependent on the distance from the blood vessel, either of the row or column coordinates can be disregarded, depending on the location of the blood supply. If, for example, the blood vessel is located at the top of the grid, we could ignore the column in which a node is in, concentrating solely on the row. In order to model the amount of nutrient in each of the nodes in a particular row, we reformulate the equation:

$$N = Ae^{-kt}$$

The highest level of nutrient would begin at the row closest to the blood supply, decreasing as the distance from the blood supply increases. Note that the variable x replaces the time variable, to denote the row (or column) number, and A has been normalized to 1. The amount of nutrient in subsequent iterations would be determined by:

$$N_{t+1} = N_t + \frac{1 - N_t}{d}$$

where $1/d$ is the speed at which a node can fill with free nutrient. This method creates a thorough distribution both initially over the grid and for all ensuing iterations.

By modelling the growth of a tumour in an avascular environment, we have assumed that nutrients are provided to the grid by a single blood source. In reality, angiogenesis may ensue, resulting in the creation of new blood vessels

that would provide the tumour with continuous resources to continue growing and sustain itself [111]. While there are numerous established models of angiogenesis, each modelling individual or multiple components contained within the cancer model presented herein, none of the models take all of these aspects into consideration [112-116].

In one instance, Chaplain (2000) presents a model based solely upon the development of new capillaries as opposed to incorporating cancer cell growth as well [112]. The equations used to model the angiogenic process in this model contain only the endothelial cell density, angiogenic factor and cell adhesion molecule, all of which alter in time and position in space. Plank and Sleeman (2003) use a circular random walk to describe the movement of endothelial cells as they move towards a growing tumour [113]. In this model, Heaviside's function (essentially a function returning only two outcomes) is used to determine whether a cell will turn clockwise or counter-clockwise at a given angle, or whether it will remain in the same direction. The incorporation of random and deterministic processes allows for the possibility of a capillary to undergo anastomosis, creating a loop within the new blood vessel. Based primarily on the concentrations of fibronectin and chemotactic growth factor (CGF) to describe the conditions leading to capillary formation, Sun *et al.* (2005) constructed an additional model, combining elements from the aforementioned models [116].

Most models of angiogenesis do not take into account the concentration of cancer cells, which would ultimately lead to higher concentrations of tumour angiogenic factors (TAF) [112-116]. The location of these cancer cells in relation to the blood source would alter the speed and location in which new blood vessels are formed. To model angiogenesis within our model, the model would be expanded to include TAFs at cancerous nodes. As the tumour begins to grow and spread within the tissue, cancer cells would release TAFs that would diffuse outward towards the blood supply, similar to the diffusion exhibited by cancer cells. As these factors reach the blood supply, the development of new blood vessels would be initiated and continue to spread throughout the tissue (Figure 2). Essentially, during this process, a node would be replaced by a blood vessel, with the existing contents displaced to neighbouring nodes.

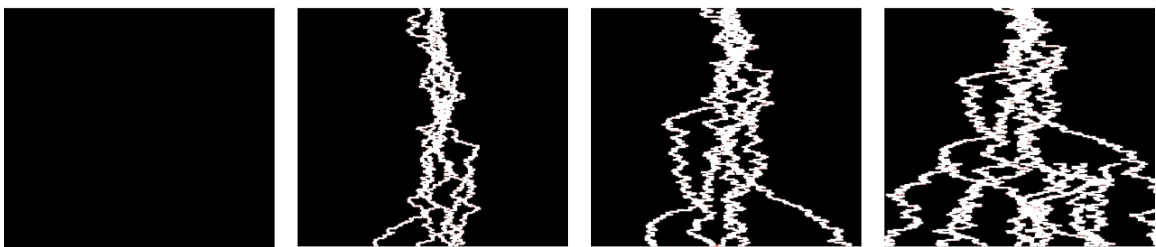


Figure 2: A simple model of angiogenesis. Using a random-walk function originating from the top of the grid where the blood supply is located, this simulated angiogenesis would initiate new blood vessels in order to vascularize the tissue.

Upon completing the model in Chapter 4, we considered inclusion of an oncolytic virus as a possible therapeutic intervention for the growing tumour. A virus was thought to be appropriate given that viruses have been previously studied from a mathematical perspective, as well as the potential benefits of the

virus from a clinical perspective. Oncolytic viruses have been shown to selectively infect cancer cells [117,118]. Furthermore, they have been shown to have no toxic effects in clinical testing, thus maintaining healthy tissue [119]. Although oncolytic viruses are replication-competent in only cancer cells, as the virus binds to healthy cells an immune response ensues, which can affect not only the concentration of virus, but also a potential indirect effect on the cancer cell themselves [120].

To incorporate an oncolytic virus into the model, a comparable approach would be taken in constructing the framework to that of the aforementioned cancer model. Using a similar two-dimensional grid (with dimensions i and j) as before, each node would additionally include the virus in five potential states: free (V_{ij}), bound to cancer cells (B_{ij}^C), bound to healthy cells (B_{ij}^H), replicating (R_{ij}) and cleared (E_{ij}). Similarly, each process would be modelled anywhere in the spectrum of stochastic to deterministic. In this addition to the model, the parameter ε would also be introduced to represent the relative efficiency of each of the viral processes, ranging from 0 to 1, representing completely inefficient to completely efficient processes respectively. In addition to the processes established in the cancer model, all nodes in the grid would be subject to seven major viral processes that may be potentially carried out during each iteration: infection, binding, entry, replication, clearance, diffusion and apoptosis.

The initial infection of the virus (V_0) would be user-defined in placement, quantity and timing, and can be comparable to the cancer 'seed' outlined in the cancer model. In accordance to the properties of oncolytic viruses and the assumptions of the model, it could be assumed that the free virus can potentially bind to both healthy and cancerous cells that are available at a given node. Whether the virus is binding to a healthy or cancerous cell, the amount of free virus that becomes bound would be proportional to both the amount of the cells present in a node, and the amount of free virus. Although oncolytic viruses may bind to both healthy and cancerous cells, they are assumed to only enter cancer cells [121]. As a result, the amount of virus that enters the available cancer cells at a node and becomes replication-competent would be proportional to the amount of virus that was previously bound as well as the amount of cancer cells currently in the node.

Once the virus has entered the cancer cells and becomes replication-competent, it would replicate accordingly. It is assumed that viral replication would be strictly based on the efficiency of the replication process for simplicity. Further refinement of the replication process could be calculated based upon the multiplicity of infection (MOI), the ratio of virus to target cells. Given that virus infections follow a Poisson distribution [122], the MOI could be used together with this distribution to render the total number of cells that would become infected. This would allow for the calculation of the start and end points of infection.

Following replication, a relative amount of the virus may be cleared from the system. Similar to replication, it is assumed that this process would be determined by its efficiency. Viral diffusion would be considered to act in a similar manner as cancer cell diffusion. The model would allow for free virus to diffuse according to a Moore neighbourhood (in 8 directions), proportional to the amount of free virus that is present in the neighbouring nodes.

With the incorporation of additional processes, the overall model becomes a network of intricate relationships among all of the parameters involved:

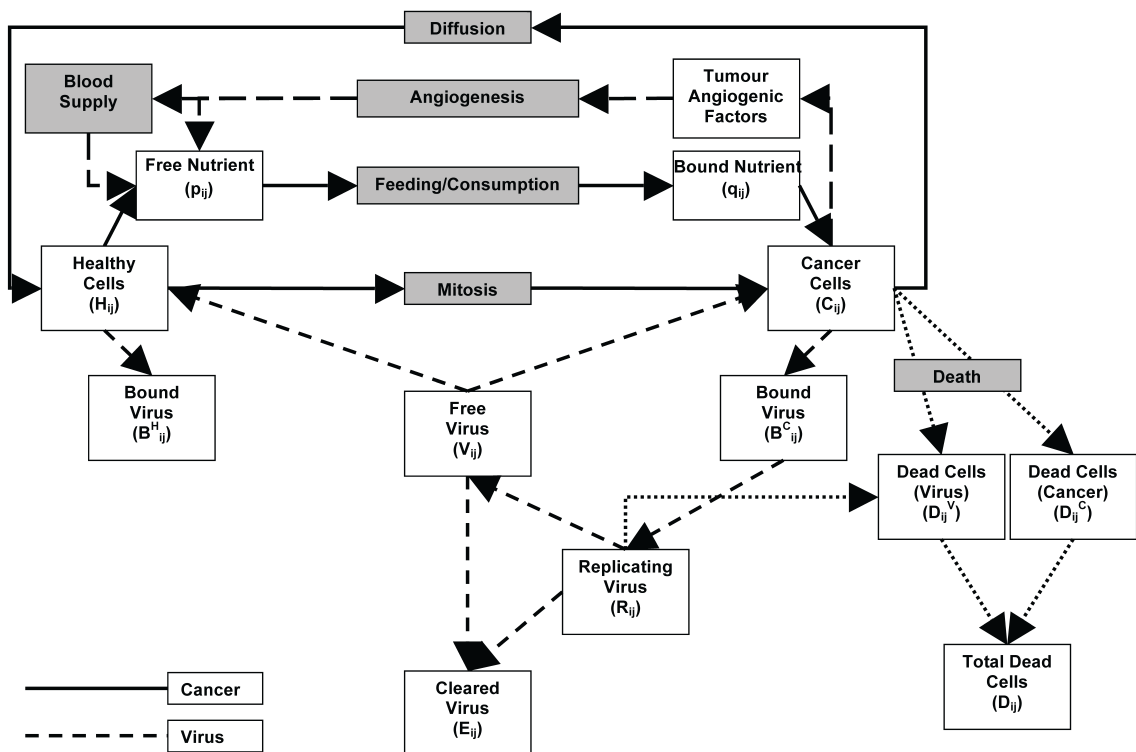


Figure 3: The major variables and processes in an expanded cancer model. A conceptual outline of the complete model would include cancer growth and metastasis, nutrient diffusion, angiogenesis and the use of an oncolytic virus as a therapeutic intervention.

CONCLUDING REMARKS

Collectively, through the models presented in this thesis, we have affirmed that both allergic asthma and cancer growth are complex processes. We have learned that there are alternative ways of studying these systems with models and that these models may reveal the advantages of incorporating mathematical and computational techniques into biological and immunological research, by means of the identification of system properties and the ability to simulate a wide range of scenarios.

In the context of allergic asthma, the models described in this thesis have provided two separate tools to investigate the inflammatory effects in response to HDM exposure. With respect to cancer growth and metastasis, a two-dimensional model was constructed to simulate patterns of growth, as well as various methods of diffusion. In addition to experimental data and/or theory, our models were formulated on assumptions, either explicit or generally understood. Each model contained conceptual platforms that were deemed appropriate, in our opinion, given the nature of the model and the information available at the time.

Aside from the apparent similarity of using mathematical and computational methods to develop models for both biological systems studied in this thesis, perhaps they may also be connected through the conceptual properties that are revealed in the modelling process. From a two-dimensional

modelling perspective, allergic asthma and tumour growth could be considered as having inverse structural properties. The narrowing and constricting of the airways, as a result of airway inflammation, can be considered as a circular area growing inward as inflammation accrues. Conversely, an avascular tumour could be considered to be relatively circular in nature as well, however the growth is outward. In both instances, the system is evolving over time with respect to initial parameters and changing variables.

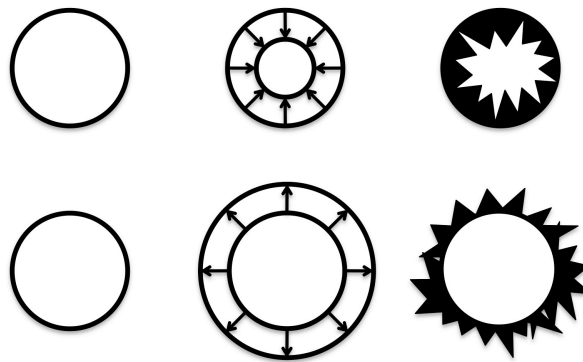


Figure 4: Conceptual similarities between allergic asthma and tumour growth. In two dimensions, the two systems studied in this thesis, allergic asthma and tumour growth, have converse patterns. Allergic asthma (top row), from an inflammation perspective, narrows in space, while tumour growth (bottom row) expands.

While any potential similarities between the two systems may not contribute in any way to each respective individual model, it does highlight the perspective and conceptualization that is possible via mathematical and computational modelling.

Simply stated, modelling in any environment allows for understanding, predicting and learning. In particular, *in silico* modelling does so from mathematical and computational points of view. The benefits of such modelling lie in its prospective applications to the overall scope of the research process. Our models are not meant to extrapolate experimental data directly to human data. Rather, the intent is to incorporate them seamlessly into biological research as an effective complement to *in vivo* experimentation. With these premises in mind, there is no limit to how prolific and valuable mathematical and computational models may be when applied to complex biological processes.

REFERENCES

(FOR CHAPTERS 1 AND 5)

REFERENCES

1. Aderem A, Hood L (2001) Immunology in the post-genomic era. *Nat Immunol* 2: 373-375.
2. Rew DA (1999) Tumour biology, chaos and non-linear dynamics. *Eur J Surg Oncol* 25: 86-89.
3. Goel G, Chou I-C, Voit EO (2006) Biological systems modeling and analysis: a biomolecular technique of the twenty-first century. *J Biomol Tech* 17: 252-269.
4. Higgins J (2002) Nonlinear systems in medicine. *The Yale Journal of Biology and Medicine* 75: 247.
5. Kitano H (2002) Computational systems biology. *Nature* 420: 206-210.
6. Ulrich C, Nijhout H, Reed M (2006) Mathematical modeling: epidemiology meets systems biology. *Cancer Epidemiology Biomarkers & Prevention* 15: 827.
7. Liu E (2005) Systems Biology, Integrative Biology, Predictive Biology. *Cell* 121: 505-506.
8. Rickles D, Hawe P, Shiell A (2007) A simple guide to chaos and complexity. *J Epidemiol Community Health* 61: 933-937.
9. Aderem A (2005) Systems Biology: its practice and challenges. *Cell* 121: 511-513.
10. Moore J (1997) Dynamical systems, optimization, and chaos. *Control and Chaos*: 197.

11. McDaniel RR, Jr., Lanham HJ, Anderson RA (2009) Implications of complex adaptive systems theory for the design of research on health care organizations. *Health Care Management Review* 34: 191-199.
12. Shapira Y, Kenett DY, Ben-Jacob E (2009) The Index cohesive effect on stock market correlations. *Eur Phys J B* 72: 657-669.
13. Mennin S (2007) Small-group problem-based learning as a complex adaptive system. *Teaching and Teacher Education* 23: 303-313.
14. Theise ND, d'Inverno M (2004) Understanding cell lineages as complex adaptive systems. *Blood Cells Mol Dis* 32: 17-20.
15. Dosenbach NUF, Fair DA, Miezin FM, Cohen AL, Wenger KK, et al. (2007) Distinct brain networks for adaptive and stable task control in humans. *Proceedings of the National Academy of Sciences* 104: 11073-11078.
16. Zheng Y, Sriram G (2010) Mathematical modeling: bridging the gap between concept and realization in synthetic biology. *Journal of Biomedicine and Biotechnology* 2010: 541609.
17. Scheiner SM (2010) Toward a conceptual framework for biology. *Q Rev Biol* 85: 293-318.
18. Wiley RE (2004) Investigation of immunomodulatory concepts in a { urine model of airway mucosal sensitization to innocuous antigen. Hamilton: McMaster University. 139 p.
19. Otto SP, Day T (2007) A biologist's guide to mathematical modelling in ecology and evolution Woodstock: Princeton University Press.

20. Cohen JE (2004) Mathematics is biology's microscope, [nly better; biology is { mathematics' } ext] physics, [nly better. PLoS Biol 2: e439.
21. Kirkland MA (2004) A phase space model of hemopoiesis and the concept of stem cell renewal. Exp Hematol 32: 511-519.
22. Greenspan NS (2001) You can't have it all. Nature 409: 137.
23. May RM (2004) Uses and abuses of { mathematics in biology. Science 303: 790-793.
24. Rosenbaum DA (1998) Is dynamical systems modeling just curve fitting? Motor Control 2: 101-104.
25. Cohen IR (2007) Modeling immune behavior for experimentalists. Immunol Rev 216: 232-236.
26. Srivastava R, You L, Summers J, Yin J (2002) Stochastic vs. deterministic modeling of intracellular viral kinetics. J Theor Biol 218: 309-321.
27. Bruggeman FJ, Westerhoff HV (2007) The nature of systems biology. Trends Microbiol 15: 45-50.
28. Asthma Society of Canada. (2005) Asthma Facts & Stats.
29. Agrawal DK, Shao Z (2010) Pathogenesis of allergic airway inflammation. Current Allergy and Asthma Reports 10: 39-48.
30. Broide DH (2009) Immunomodulation of allergic disease. Annu Rev Med 60: 279-291.
31. Hamid Q, Tulic M (2009) Immunobiology of asthma. Physiology 71: 489-507.

32. Suarez CJ, Parker NJ, Finn PW (2008) Innate immune mechanism in allergic asthma. *Current Allergy and Asthma Reports* 8: 451-459.
33. Averbeck M, Gebhardt C, Emmrich F, Treudler R, Simon JC (2007) Immunologic principles of allergic disease. *J Dtsch Dermatol Ges* 5: 1015-1028.
34. Anderson GP (2008) Endotyping asthma: new insights into key pathogenic mechanisms in a complex, heterogeneous disease. *The Lancet* 372: 1107-1119.
35. Holgate Stephen T, Arshad Hasan S, Roberts Graham C, Howarth Peter H, Thurner P, et al. (2009) A new look at the pathogenesis of asthma. *Clin Sci* 118: 439-450.
36. Nials AT, Uddin S (2008) Mouse models of allergic asthma: acute and chronic allergen challenge. *Disease Models & Mechanisms* 1: 213-220.
37. Shapiro SD (2006) Animal models of asthma: role of allergic avoidance of animal (models) of an infection. *American Journal of Respiratory and Critical Care Medicine* 174: 1171-1173.
38. Takeda K, Gelfand EW (2009) Mouse models of allergic diseases. *Curr Opin Immunol* 21: 660-665.
39. Zosky GR, Sly PD (2007) Animal models of asthma. *Clinical & Experimental Allergy* 37: 973-988.

40. Chakraborty A, Dustin M, Shaw A (2003) In silico models for cellular and molecular immunology: successes, promises and challenges. *Nature Immunology* 4: 933-936.
41. Chavali A, Gianchandani E, Tung K, Lawrence M, Peirce S, et al. (2008) Characterizing emergent properties of immunological systems with multi-cellular rule-based computational modeling. *Trends in Immunology* 29: 589-599.
42. Merrill SJ (1998) Computational models in immunological methods: an historical review. *J Immunol Methods* 216: 69-92.
43. Andrew S, Baker C, Bocharov G (2007) Rival approaches to mathematical modelling in immunology. *Journal of Computational and Applied Mathematics* 205: 669-686.
44. Chan C, Kepler TB (2007) Computational immunology--from bench to virtual reality. *Ann Acad Med Singap* 36: 123-127.
45. DeLisi C (1983) Mathematical modeling in immunology. *Annu Rev Biophys Bioeng* 12: 117-138.
46. Forrest S, Beauchemin C (2007) Computer immunology. *Immunol Rev* 216: 176-197.
47. Mohler R, Bruni C, Gandolfi A (2005) A systems approach to immunology. *Proceedings of the IEEE* 68: 964-990.
48. Yates A, Chan CC, Callard RE, George AJ, Stark J (2001) An approach to modelling in immunology. *Brief Bioinformatics* 2: 245-257.

49. Mayer H, Zaenker KS, An Der Heiden U (1995) A basic mathematical model of the immune response. *Chaos* 5: 155-161.
50. Matzavinos A, Chaplain MAJ, Kuznetsov VA (2004) Mathematical modelling of the spatio-temporal response of cytotoxic T-lymphocytes to a solid tumour. *Math Med Biol* 21: 1-34.
51. Perelson AS (2002) Modelling viral and immune system dynamics. *Nat Rev Immunol* 2: 28-36.
52. Handel A, Antia R (2008) A simple mathematical model helps to explain the immunodominance of CD8 T cells in influenza A virus infections. *Journal of Virology* 82: 7768-7772.
53. Wodarz D (2003) Mathematical models of HIV and the immune system. *Novartis Found Symp* 254: 193-207; discussion 207-122, 250-192.
54. Funk GA, Jansen VA, Bonhoeffer S, Killingback T (2005) Spatial models of virus-immune dynamics. *J Theor Biol* 233: 221-236.
55. Goldstein B, Faeder J, Hlavacek W (2004) Mathematical and computational models of immune-receptor signalling. *Nature Reviews Immunology* 4: 445-456.
56. Cohn M, Mata J (2007) Quantitative modeling of immune responses. *Immunol Rev* 216: 5-8.
57. Epstein M (2004) Modeling allergic asthma: from assays to virtual patients. *Drug Discovery Today: Disease Models* 1: 387-394.

58. Brusic V, Petrovsky N, Gendel S, Millot M, Gigonzac O, et al. (2003) Computational tools for the study of allergens. *Allergy* 58: 1083-1092.
59. Lewis A, Paterson T, Leong C, Defranoux N, Holgate S, et al. (2001) The roles of cells and mediators in a computer model of chronic asthma. *International Archives of Allergy and Immunology* 124: 282-286.
60. Stokes C, Lewis A, Paterson T, Leong C, Defranoux N, et al. (2002) Asthma PhysioLab: a dynamic, computer-based mathematical model of acute and chronic asthma. *BMES/EMBS Conference, 1999 Proceedings of the First Joint 2*: 1208.
61. Frey U (2007) Predicting asthma control and exacerbations: chronic asthma as a complex dynamic model. *Curr Opin Allergy Clin Immunol* 7: 223-230.
62. Frey U (2008) Asthma as a nonlinear complex dynamic system: a novel approach to understand the temporal behaviour of chronic asthma and its response to β -agonists. *European Respiratory Review* 17: 67-69.
63. Frey U, Suki B (2008) Complexity of chronic asthma and chronic obstructive pulmonary disease: implications for risk assessment, and disease progression and control. *Lancet* 372: 1088-1099.
64. Amin SD, Majumdar A, Frey U, Suki B (2010) Modeling the dynamics of airway constriction: effects of agonist transport and binding. *Journal of Applied Physiology* 109: 553-563.

65. Wagers S (2004) The allergic mouse model of asthma: normal smooth muscle in an abnormal lung? *Journal of Applied Physiology* 96: 2019-2027.
66. Frey U, Brodbeck T, Majumdar A, Robin Taylor D, Ian Town G, et al. (2005) Risk of severe asthma episodes predicted from fluctuation analysis of airway function. *Nature* 438: 667-670.
67. Ross DW (1998) *Introduction to oncogenes and molecular cancer medicine*. New York: Springer.
68. Macdonald F, Ford CHJ, Casson AG (2004) *Molecular biology of cancer*. London ; New York, N.Y.: Taylor & Francis. 269 p.
69. Weinberg RA (1996) How cancer arises. *Sci Am* 275: 62-70.
70. Frank SA, Iwasa Y, Nowak MA (2003) Patterns of cell division and the risk of cancer. *Genetics* 163: 1527-1532.
71. Tomlinson IP, Novelli MR, Bodmer WF (1996) The mutation rate and cancer. *Proc Natl Acad Sci USA* 93: 14800-14803.
72. Bagi CM (2002) Cancer cell metastases. *J Musculoskelet Neuronal Interact* 2: 565-566.
73. Van't Veer L, Weigelt B (2003) Road map to metastasis. *Nature Medicine* 9: 999-1000.
74. Anderson ARA (2005) A hybrid mathematical model of solid tumour invasion: the importance of cell adhesions. *Mathematical Medicine and Biology* 22: 163-186.

75. Guiot C, Degiorgis PG, Delsanto PP, Gabriele P, Deisboeck TS (2003) Does tumor growth follow a "universal law"? *J Theor Biol* 225: 147-151.
76. Rasnick D (2002) Aneuploidy theory explains tumor formation, the absence of immune surveillance, and the failure of chemotherapy. *Cancer Genet Cytogenet* 136: 66-72.
77. Dalglish A (1999) The relevance of non-linear mathematics (chaos theory) to the treatment of cancer, the role of the immune response and the potential for vaccines. *QJM* 92: 347-359.
78. Delsanto PP, Condat CA, Pugno N, Gliozzi AS, Griffa M (2008) A multilevel approach to cancer growth modeling. *Journal of theoretical biology* 250: 16-24.
79. Delsanto PP, Romano A, Scalerandi M, Pescarmona GP (2000) Analysis of a "phase transition" from tumor growth to latency. *Phys Rev E Stat Phys Plasmas Fluids Relat Interdiscip Topics* 62: 2547-2554.
80. Pescarmona GP, Scalerandi M, Delsanto PP, Condat CA (1999) Non-linear model of cancer growth and metastasis: a limiting nutrient as a major determinant of tumor shape and diffusion. *Med Hypotheses* 53: 497-503.
81. Thomlinson RH, Gray LH (1955) The histological structure of some human lung cancers and the possible implications for radiotherapy. *Br J Cancer* 9: 539-549.
82. Burton AC (1966) Rate of growth of solid tumours as a problem of diffusion. *Growth* 30: 157-176.

83. Iyer KS, Saksena VN (1970) A stochastic model for the growth of cells in cancer. *Biometrics* 26: 401-410.
84. Deakin AS (1975) Model for the growth of a solid in vitro tumor. *Growth* 39: 159-165.
85. Byrne H, Matthews P (2002) Asymmetric growth of models of avascular solid tumours: exploiting symmetries. *IMA J Math Appl Med Biol* 19: 1-29.
86. Colangelo M, Diamandis P, Stone J. (2005) A complex dynamic model for cancer growth and metastasis. in 18th International Conference on Computer Applications in Industry and Engineering. Honolulu, Hawaii.
87. Scalerandi M, Capogrosso Sansone B, Benati C, Condat CA (2002) Competition effects in the dynamics of tumor cords. *Phys Rev E Stat Nonlin Soft Matter Phys* 65: 051918.
88. Wu JT, Kirn DH, Wein LM (2004) Analysis of a three-way race between tumor growth, a replication-competent virus and an immune response. *Bull Math Biol* 66: 605-625.
89. Cristini V, Lowengrub J, Nie Q (2003) Nonlinear simulation of tumor growth. *J Math Biol* 46: 191-224.
90. Sherratt JA, Chaplain MA (2001) A new mathematical model for avascular tumour growth. *J Math Biol* 43: 291-312.
91. Friedman A, Reitich F (1999) Analysis of a mathematical model for the growth of tumors. *J Math Biol* 38: 262-284.

92. Rygaard K, Spang-Thomsen M (1997) Quantitation and gompertzian analysis of tumor growth. *Breast Cancer Res Treat* 46: 303-312.
93. Galatzer-Levy RM (2009) Finding our way through chaos, fractals, and the exotic mathematical subjects: a guide for the perplexed. *Journal of the American Psychoanalytic Association* 57: 1227-1249.
94. Wodarz D, Komarova NL (2005) *Computational biology of cancer : lecture notes and mathematical modeling*. Hackensack, NJ: World Scientific. 250 p.
95. Gibbs WW (2004) Untangling the roots of cancer. *Sci Am* 289: 56-65.
96. Scalerandi M, Romano A, Pescarmona G, Delsanto P, Condat C (1999) Nutrient competition as a determinant for cancer growth. *Physical Review E* 59: 2206-2217.
97. Colangelo M, Lovric M, Harnish D, Stone J. (2007) Modelling diffusional neighbourhoods. in 22nd International Conference on Computers and Their Applications Honolulu, Hawaii.
98. Deisboeck TS, Mansury Y, Guiot C, Degiorgis PG, Delsanto PP (2005) Insights from a novel tumor model: indications for a quantitative link between tumor growth and invasion. *Med Hypotheses* 65: 785-790.
99. Friedman A, Tao Y (2003) Analysis of a model of a virus that replicates selectively in tumor cells. *J Math Biol* 47: 391-423.

100. Llop-Guevara A, Colangelo M, Chu DK, Moore CL, Stieber NA, et al. (2008) In vivo-to-in silico iterations to investigate aeroallergen-host interactions. PLoS ONE 3: e2426.
101. Cates EC, Fattouh R, Johnson JR, Llop-Guevara A, Jordana M (2007) Modeling responses to respiratory house dust mite exposure. Contrib Microbiol 14: 42-67.
102. Fuchs B, Braun A (2008) Improved mouse models of allergy and allergic asthma - chances beyond ovalbumin. Curr Drug Targets 9: 495-502.
103. Kumar RK, Herbert C, Foster PS (2008) The "classical" ovalbumin challenge model of asthma in mice. Curr Drug Targets 9: 485-494.
104. Kariyawasam HH, Robinson DS (2006) The eosinophil: the cell and its weapons, the cytokines, its locations. Semin Respir Crit Care Med 27: 117-127.
105. Kay AB (2005) The role of eosinophils in the pathogenesis of asthma. Trends Mol Med 11: 148-152.
106. Radinger M, Lotvall J (2009) Eosinophil progenitors in allergy and asthma - do they matter? Pharmacol Ther 121: 174-184.
107. Rothenberg ME, Hogan SP (2006) The eosinophil. Annu Rev Immunol 24: 147-174.
108. Breward CJ, Byrne HM, Lewis CE (2003) A multiphase model describing vascular tumour growth. Bull Math Biol 65: 609-640.

109. Kansal AR, Torquato S, Harsh IG, Chiocca EA, Deisboeck TS (2000) Cellular automaton of idealized brain tumor growth dynamics. *Biosystems* 55: 119-127.
110. Nandakumaran M, Dashti HM, Al-Saleh E, Al-Zaid NS (2003) Transport kinetics of zinc, copper, selenium, and iron in perfused human placental lobule in vitro. *Mol Cell Biochem* 252: 91-96.
111. Risau W (1997) Mechanisms of angiogenesis. *Nature* 386: 671-674.
112. Chaplain MA (2000) Mathematical modelling of angiogenesis. *J Neurooncol* 50: 37-51.
113. Plank MJ, Sleeman BD (2003) A reinforced random walk model of tumour angiogenesis and anti-angiogenic strategies. *Math Med Biol* 20: 135-181.
114. Plank MJ, Sleeman BD (2004) Lattice and non-lattice models of tumour angiogenesis. *Bull Math Biol* 66: 1785-1819.
115. Plank MJ, Sleeman BD, Jones PF (2004) A mathematical model of tumour angiogenesis, regulated by vascular endothelial growth factor and the angiopoietins. *J Theor Biol* 229: 435-454.
116. Sun S, Wheeler MF, Obeyesekere M, Patrick CW, Jr. (2005) A deterministic model of growth factor-induced angiogenesis. *Bull Math Biol* 67: 313-337.
117. Chiocca EA (2002) Oncolytic viruses. *Nat Rev Cancer* 2: 938-950.
118. Mullen JT, Tanabe KK (2002) Viral oncolysis. *Oncologist* 7: 106-119.
119. Nemunaitis J, Ganly I, Khuri F, Arseneau J, Kuhn J, et al. (2000) Selective replication and oncolysis in p53 mutant tumors with ONYX-015, an E1B-

55kD gene-deleted adenovirus, in patients with advanced head and neck cancer: a phase II trial. *Cancer Res* 60: 6359-6366.

120. Biederer C, Ries S, Brandts CH, McCormick F (2002) Replication-selective viruses for cancer therapy. *J Mol Med* 80: 163-175.

121. Everts B, van der Poel HG (2004) Replication-selective oncolytic viruses in the treatment of cancer. *Cancer Gene Ther* 12: 141-161.

122. Gart JJ (1964) The analysis of poisson regression with an application in virology. *Biometrika* 51: 517-521.

APPENDIX I

PERMISSION TO REPRINT PUBLISHED MANUSCRIPTS

Open-Access License


No Permission Required

The Public Library of Science (PLOS) applies the Creative Commons Attribution License (CCAL) to all works we publish (read the [human-readable summary](#) or the [full license legal code](#)). Under the CCAL, authors retain ownership of the copyright for their article, but authors allow anyone to download, reuse, reprint, modify, distribute, and/or copy articles in PLOS journals, so long as the original authors and source are cited. **No permission is required from the authors or the publishers.**



In most cases, appropriate attribution can be provided by simply citing the original article (e.g., Kaltenbach LS et al. (2007) Huntingtin Interacting Proteins Are Genetic Modifiers of Neurodegeneration. *PLoS Genet* 3(5): e82. doi:10.1371/journal.pgen.0030082). If the item you plan to reuse is not part of a published article (e.g., a featured issue image), then please indicate the originator of the work, and the volume, issue, and date of the journal in which the item appeared. For any reuse or redistribution of a work, you must also make clear the license terms under which the work was published.

This broad license was developed to facilitate open access to, and free use of, original works of all types. Applying this standard license to your own work will ensure your right to make your work freely and openly available. Learn more about [open access](#). For queries about the license, please [contact us](#).

 All site content, except where otherwise noted, is licensed under a Creative Commons Attribution License.

ISCA JOURNAL COPYRIGHT FORM

This form is intended for original, previously unpublished manuscripts submitted to the International Journal for Computers and Their Applications. The completed and signed form is necessary as a prerequisite for publication. Please send it with the final version of your paper. No other form or wording modifications are allowed.

Title of Paper: *A Mathematical and Computational Model for Simulating Complex Dynamic Cancer Growth and Metastasis*

Author(s): *M. Colangelo, M. Lovric & J. R. Stone*

Part A: Copyright Transfer Form

The undersigned hereby transfer any and all rights in and to the paper including without limitation all copyrights to The International Society for Computers and Their Applications, Inc., known as ISCA. The undersigned hereby represents and warrants that the paper is original and that he/she is the author of the paper, except for material that is clearly identified as to its original source, with permission notices from the copyright owners where required. The undersigned represents that he/she has the power and authority to make and execute this assignment.

In return, ISCA agrees to the following:

1. Employers/authors retain all proprietary rights in any process, procedure, or article of manufacture described in the paper.
2. Employers/authors may copy, or authorize the copy of, the paper, or derivative portions of the paper for company/personal use, provided the copies are not offered for sale, that the source of the material is indicated, and that ISCA's endorsement is not implied by the use.
3. Employers/authors must request permission from ISCA for copy privileges not covered by items 1,2 above (such as third party requests for reprinting, republishing, etc.).
4. ISCA recognizes that the U.S. government has royalty free permission to copy, or authorize the copy of, all/portions of the paper for official U.S. government purposes only, when the contained work was done under a U.S. government grant/contract and the grant/contract so requires.

If the paper is not accepted and published by ISCA, or is withdrawn by the author(s) before acceptance, this agreement becomes null and void.



Authorized Signature Title

McMaster University, Hamilton, Ontario, Canada

Employer (for whom the work was performed) Date **December 3, 2010**

Part B: U.S. Government Employee Certification

This certifies that all authors of the paper are employees of the U.S. government and performed this work as part of their official duties, and that therefore the paper is not subject to U.S. copyright protection.

Authorized Signature and Title

Government Organization/ Date

Part C: Crown Copyright (ISCA recognizes and will honor the Crown Copyright (British Commonwealth) as it does U.S. Government work)

This certifies that all authors of the paper are subject to Crown Copyright.

Authorized Signature Title

Government Organization Date

Information for Employers/Authors

It is the policy of ISCA to own the copyrights to all copyrightable material in its publications, and to the individual contributions therein, in order to protect the interests of ISCA, its authors and their employers. ISCA will make every reasonable effort to act in the interests of employers/authors as well as in its own interests. For all third party republication requests, ISCA requires that:

- The consent of the first-named author be sought as a condition in granting republication rights.
- The consent of the employer be obtained as a condition in granting permission for reuse of a paper or portion thereof for promotion/marketing purposes.

If you are employed and you prepared your paper as a part of your job, the rights to your paper initially rest with your employer. In that case, when you sign the copyright transfer form, we assume you are authorized to do so by your employer and that your employer has consented to all the terms and conditions of this form. If not, it should be signed by someone so authorized.

For jointly-authored papers, either all the authors should sign, or one may sign as an agent for all. For U.S. government-sponsored work where not all authors are government employees, any non government author-participants should sign part A; authors who are government employees need not sign.

All questions regarding ISCA copyright policy should be directed to: ISCA Headquarters, 975 Walnut Street, Suite 132, Cary, NC 27511, (919) 467-5559.

BioMed Central copyright and license agreement

In submitting a research article ('article') to any of the journals published by BioMed Central Ltd ('BioMed Central') I certify that:

1. I am authorized by my co-authors to enter into these arrangements.
2. I warrant, on behalf of myself and my co-authors, that:
 - a. the article is original, has not been formally published in any other peer-reviewed journal, is not under consideration by any other journal and does not infringe any existing copyright or any other third party rights;
 - b. I am/we are the sole author(s) of the article and have full authority to enter into this agreement and in granting rights to BioMed Central are not in breach of any other obligation. If the law requires that the article be published in the public domain, I/we will notify BioMed Central at the time of submission upon which clauses 3 through 6 inclusive do not apply;
 - c. the article contains nothing that is unlawful, libellous, or which would, if published, constitute a breach of contract or of confidence or of commitment given to secrecy;
 - d. I/we have taken due care to ensure the integrity of the article. To my/our - and currently accepted scientific - knowledge all statements contained in it purporting to be facts are true and any formula or instruction contained in the article will not, if followed accurately, cause any injury, illness or damage to the user.

And I agree to the following license agreement:

■ BioMed Central Open Access license agreement

Brief summary of the agreement

Anyone is free:

- to copy, distribute, and display the work;
- to make derivative works;
- to make commercial use of the work;

Under the following conditions: Attribution

- the original author must be given credit;
- for any reuse or distribution, it must be made clear to others what the license terms of this work are;
- any of these conditions can be waived if the authors gives permission.

Statutory fair use and other rights are in no way affected by the above.

Full BioMed Central Open Access license agreement

(Identical to the [Creative Commons Attribution License](#))